Faculdade de Engenharia da Universidade do Porto









A multimodal therapeutic alginate-based platform for customized medical application in chronic wound healing

João Pedro Tavares Soares Brum da Silveira

Dissertation for the Degree of Master of Science

in Bioengineering

Supervisor: Marco Araújo, PhD

Co-Supervisor: Aureliana Filipa Sousa, PhD

Co-Supervisor: Cristina Barrias, PhD

June 2019

© João Silveira, 2019

Resumo

A cicatrização de feridas consiste num processo extremamente complexo de reparação de tecidos que envolve uma interatuação dinâmica de vários tipos de células, enzimas, citoquinas e fatores de crescimento. Qualquer desregulação nesta cascata de sinalização complexa pode conduzir ao desenvolvimento de uma ferida crónica que não cicatriza, impedindo, assim, que se desenrole o curso normal das fases de reparação e de regeneração tecidular.

O comprometimento da cicatrização de feridas representa um encargo significativo em termos económicos e humanísticos quer para os sistemas de cuidados de saúde quer para a sociedade, sendo responsável por elevados custos de cuidados de saúde, assim como por uma menor qualidade de vida em termos de bem-estar nos indivíduos afetados. Atualmente, as opções terapêuticas disponíveis são incapazes de fazer face ao conjunto de requisitos impostos pelo ambiente dessas feridas. Assim, existe uma grande necessidade médica e social de novas abordagens terapêuticas.

O desenvolvimento e caracterização de um biomaterial inovador que constitua uma abordagem diferente à cicatrização de feridas, focado na regulação do microambiente da ferida crónica, e com o intuito de promover a regeneração dos tecidos, é o objetivo primordial deste projeto.

Assim, apresenta-se neste trabalho uma plataforma multimodal avançada para a cicatrização de feridas crónicas, e que consiste num patch único de um hidrogel de alginato biologicamente funcionalizado.

A conceção do biomaterial desenvolvido assenta numa estratégia de fotopolimerização UV que permite a produção de hidrogéis de alginato fotoreticulados. Estes hidrogéis encontram-se funcionalizados com sinais bioquímicos específicos como, por exemplo, pequenos péptidos contendo a sequência de aminoácidos RGD, a fim de aumentar as interações que se estabelecem entre as células e o biomaterial, ou uma sequência clivável por metaloproteinases da matriz (MMPs) que permita uma remodelação da estrutura mediada por enzimas celulares. Assim, o hidrogel de alginato desenvolvido pode proporcionar uma potencial capacidade de regeneração tecidular, uma vez que a suprarregulação de MMPs é uma característica típica de ambientes em que a cicatrização de feridas se encontra comprometida. Para além disso, a presença de cisteína em ambos os extremos da sequência peptídica clivável por MMPs permitirá a produção de hidrogéis com propriedades bioquímicas e mecânicas ajustáveis.

A principal inovação do presente estudo reside na incorporação de nanopartículas biopoliméricas de melanina na estrutura do hidrogel, de forma a criar uma plataforma com uma maior capacidade de remover radicais livres. Tal valência iria ter como alvo o excesso de espécies reativas de oxigénio que estão presentes em ambientes típicos de feridas crónicas.

A finalidade primordial de uma maior captura destas espécies radicalares é a sua potencial contribuição para a regulação dos processos imunológicos associados à inflamação crónica.

Desta forma, o objetivo principal deste projeto assenta no desenvolvimento de uma plataforma terapêutica multimodal capaz de atenuar o severo microambiente inflamatório e, simultaneamente, estimular a regeneração dos tecidos.

A incorporação de nanopartículas de melanina no sistema do hidrogel de alginato providenciou ao biomaterial uma maior capacidade em captura de radicais, o que constitui um resultado promissor no que diz respeito à regulação dos ambientes de inflamação crónica.

Por outro lado, a plataforma apresentou propriedades viscoelásticas ajustáveis de acordo com a formulação do hidrogel, nomeadamente do conteúdo de melanina e da concentração de péptido clivável por MMPs. Este facto pode ser importante dado que as propriedades mecânicas do biomaterial desenvolvido devem correlacionar-se com os requisitos biomecânicos do tecido alvo.

O sistema desenvolvido pode ser aplicado em feridas crónicas de duas formas distintas: como um scaffold baseado num hidrogel de alginato, que permitirá ao sistema desenvolver otimizações para se constituir um hidrogel capaz de direcionar o comportamento das células, e como um hidrogel liofilizado. Nesta última configuração, os aspetos proregenerativos inerentes ao biomaterial podem até ser potencialmente melhorados por um modo facilitado de aplicação no local da ferida e uma validade prolongada, do ponto de vista da comercialização e da aplicabilidade clínica.

Uma aprofundada avaliação biológica e validação da plataforma em modelos bem estabelecidos de cicatrização de feridas é requerida para testar a eficácia do biomaterial num meio que se assemelhe às condições que se verificam *in vivo*.

Espera-se que este projeto possa proporcionar uma melhor perspetiva no que diz respeito ao desenvolvimento de novas terapêuticas-alvo, capazes de influenciar positivamente as feridas crónicas, contribuindo para a reparação e a regeneração do tecido, assim como o encerramento de feridas, garantindo deste modo a qualidade de vida dos pacientes afetados.

Abstract

Wound healing consists in an extremely complex process of tissue repair that relies on a dynamic interplay of several types of cells, enzymes, cytokines, and growth factors. A deregulation in this complex signaling cascade can lead to the development of a non-healing chronic wound, thus preventing the normal tissue repair and regeneration course of events to take place. Impaired wound healing presents a significant economic and humanistic burden to healthcare systems and societies, being responsible for major healthcare expenses and a decreased health-related quality of life for those affected. Currently existing treatment options are unable to meet the challenging requirements set by the wound environment. Therefore, there is a great medical and social need for new therapeutic approaches.

The development and characterization of a novel biomaterial that constitutes a different wound healing approach, focused on the regulation of the chronic wound microenvironment, in order to promote tissue regeneration, is a primary goal of this project.

Herein, an advanced multimodal platform for chronic wound healing, consisting on a biofunctionalized alginate-based hydrogel single patch, is presented.

The manufacturing of the developed biomaterial relies on a UV photopolymerization strategy that allows the production of photocrosslinked alginate hydrogels. Such hydrogels are functionalized with specific biochemical cues, such as small peptides containing the RGD motif, in order to increase cell-biomaterial interactions, and a matrix-metalloproteinase (MMP) cleavable sequence to allow an enzymatically mediated remodelling of the structure to occur in a "cell-demanded" fashion. Thus, the designed alginate hydrogel may provide a potential tissue regeneration ability, since upregulated MMPs are a hallmark of impaired wound healing environments. Furthermore, the presence of cysteine on both ends of the MMP-cleavable peptide will allow the production of hydrogels with tunable biochemical and mechanical properties.

The main novelty of the current study relies on the incorporation of biopolymeric melanin nanoparticles within the hydrogel, in order to create a platform with an enhanced free radical scavenging ability. This would allow to target excessive reactive oxygen species (ROS) that are present in chronic non-healing wounds environments. The primary objective of such approach is that the capture of these radical species may potentially contribute for the regulation of immune processes associated with chronic inflammation.

Thus, the main goal of the current project relies on the development of a multimodal therapeutic platform capable of attenuating the harsh inflammation microenvironment, while stimulating tissue regeneration.

The incorporation of melanin nanoparticles to the alginate-based hydrogel system granted a higher radical scavenging ability to the biomaterial, which constitute promising results towards the regulation of chronic inflammation environments. Moreover, the platform presented tailored viscoelastic properties by varying the hydrogel formulation, namely the melanin content and the MMP-sensitive peptide concentration. This may be important since the mechanical properties of the developed biomaterial should match the biomechanical requirements of the target tissue.

The developed system may be applied to chronic wounds in two distinctive manners: as a native hydrogel scaffold, which will allow the system to be further optimized as a cell-instructive hydrogel, and as a lyophilized hydrogel construct. In this latter approach, the full inherent pro-regenerative features of the biomaterial may even be potentially enhanced due to the easier delivery to the wound site and increased shelf life in a commercialization and clinical applicability point of view.

Further biological assessment and validation of the platform in well-established wound healing models is required to test the biomaterial efficacy in an environment that may closely resemble actual in vivo *conditions.*

Hopefully, this project might provide a better insight into the development of new targeted therapies that are able to positively influence chronic wounds, promoting tissue repair and regeneration, as well as wound closure, thus granting quality of life to patients affected.

Acknowledgements

O meu primeiro reconhecimento vai para o meu orientador Dr Marco Araújo, por ter sido o responsável por este projeto, por toda a paciência demonstrada ao longo dos últimos meses, e por todo o trabalho que diariamente desenvolve no instituto onde trabalha, de manhã à noite.

Devo também agradecer às minhas duas co-orientadoras, Dra Aureliana Filipa e Dra Cristina Barrias, por me terem acolhido no vosso laboratório e grupo de trabalho e por me terem dado dicas indispensáveis ao trabalho desenvolvido.

Dedico este trabalho aos meus companheiros de lab, Mariana "Lurdes", Francisco "Cabeças", Sara, Margarida, Rafaela e Filipa, bem como a todos os outros que comigo conviveram, tornando mais fácil o trabalho de cada dia.

Aos meus pais, pela educação que me transmitiram e por todos os sábios conselhos que me foram dando ao longo da vida, bem como pelo apoio incondicional, mesmo aqui ou ali não concordando com uma ou outra decisão, abrindo espaço para o erro e, consequentemente, para o crescimento e maturação pessoal. Sou hoje uma pessoa melhor devido a vocês os dois. Quero que saibam que são os meus dois maiores exemplos de vida, de gente trabalhadora, humilde e que teve de subir a pulso na vida.

Às minhas irmãs, Maria João e Sofia, por todo o amor, carinho e convivência. No meio de tantas brigas e poucas demonstrações de afeto, continuam a aturar-me como ninguém.

A toda a minha família, que eu amo muito, por todas as vivências.

Ao meu gato, Poirot, por toda a companhia.

Aos amigos que a faculdade me deu, por toda a partilha de experiências e pela amizade. Ao meu mano Hugo, um verdadeiro amigo que nunca me falhou. Ao Alexandre e ao Renato, por tantas aventuras, jantares e loucuras. E a todos os outros colegas de Bioengenharia.

Ao Eduardo Reyes Blancas, sigues siendo el puto amo!! Por me mostrar a relativização das coisas que pensamos serem importantes, mas que na verdade não o são, de forma a ter uma vida mais leve e despreocupada, focada só no essencial. Aos mis compañeros de piso, Nicolas e Rafa, pelos exemplos de humildade e pela forte amizade, ajudando-me a sobreviver a Pelotas.

Ao Adriel, el crack de cracks, pela amizade sincera e sabedoria, por sempre saber quando transmitir a palavra certa na altura adequada e por todas as noites de loucura.

Ao Hugo Pinto, “El Profesor”, por todo o companheirismo ao longo dos últimos anos e por uma amizade forte e inquebrável.

Ao Cadu e Petri, dois amigos verdadeiros com os quais posso contar sempre.

Ao Chousa, meu indiano favorito, por todas as aventuras sem noções e sem medo das consequências. Tenho saudades das nossas noites de Miss Burn.

Ao Antonio Lins, pela amizade verdadeira e por todo o apoio nos últimos meses, tens sido um pilar muito importante. Por saber bem o equilíbrio entre o trabalho e a diversão e por alinhar em qualquer plano sem pensar duas vezes. Tu é o cara, pivete!!

Ao Dr Evandro Piva, pela oportunidade maravilhosa que me concedeu, pela inspiração e por ser um modelo a seguir, pessoal e profissionalmente. O respeito que todos os que trabalham consigo têm por si e a forma como o admiram é reveladora da sua integridade e qualidade humana.

Ao Dr Carlos Enrique “Speedy González” Suárez, por ser um exemplo de humildade, trabalho e simpatia, sumamente reconhecido por todos como uma pessoa maravilhosa. Obrigado por toda a orientação e paciência, foi um enorme prazer trabalhar contigo.

À Dra Adriana Piva, por todo o apoio durante o desenvolvimento do meu trabalho em Pelotas, e por todos os ensinamentos que me concedeu.

E a todos os que, de uma forma positiva ou negativa, passaram pela minha vida e contribuíram, direta ou indiretamente, para a realização deste trabalho.

The research described in this thesis was financially supported by:

Project Biotherapies (NORTE-01-0145-FEDER-000012) funded by North Portugal Regional Operational Program (Norte2020) under PORTUGAL2020 Partnership Agreement through Regional Development Fund (FEDER).

Table of Contents

Resumo i

Abstract iii

Acknowledgements v

Table of Contents vii

List of Figures ix

List of Abbreviations and Symbols xi

Chapter 1 1

Purpose of the thesis 1

1. Introduction 2

1.1 **Non-healing wounds** 2
1.1.1 Chronic wound healing 3
1.1.2 Internal chronic wounds in the gut: Inflammatory Bowel Disease (IBD) 5

1.2 **Therapeutic platforms for treatment of chronic wounds in the gut** 7
1.2.1 Hydrogels 8
1.2.2 Alginate – chemical structure, properties and applications 8
1.2.3 Alginate functionalization 10
1.2.3.1 Covalently crosslinked alginate hydrogels through photopolymerization . 10
1.2.3.2 Functionalization of alginate with biochemical cues 11
1.2.3.3 Chemical strategies for alginate biofunctionalization 13
1.2.4 Melanin – structure, biosynthesis and general properties 15

Chapter 2 19

2. Materials and Methods 19

2.1 **Synthesis and characterization of methacrylated alginate (AlgMa)** 19
2.1.1 Nuclear magnetic resonance (^{1}H-NMR) 20
2.1.2 Attenuated total reflectance – fourier-transform infrared spectroscopy (ATR-FTIR) 20

2.2 **Functionalization of AlgMa with cell-adhesion motifs (AlgMaRGD)** 20
2.2.1 Quantification of incorporated cell-adhesive peptide (AlgMaRGD) 21

2.3 **Development and characterization of the multi-functional alginate-based patch** 21
2.3.1 Preparation of photocrosslinked alginate hydrogels 21
2.3.2 Coupling efficiency of the MMP-cleavable peptide 22

2.3.3 Free-radical scavenging activity 22
2.3.4 Rheological properties 23
2.3.5 Swelling ratio 23

Chapter 3 24

3. Results 24

3.1 Synthesis and characterization of methacrylated alginate (AlgMa) 24

3.2 Conjugation of cell-adhesive peptide to methacrylated alginate (AlgMaRGD) 25

3.3 Characterization of melanin particles 28

3.4 Development and characterization of the multi-functional alginate-based patch 29
3.4.1 Preparation of photocrosslinked alginate hydrogels 29
3.4.2 Coupling efficiency of the MMP-cleavable peptide 35
3.4.3 Free-radical scavenging activity 37
3.4.4 Rheological properties 41
3.4.5 Swelling Ratio 44

Chapter 4 46

4. Discussion 46

Chapter 5 56

5. Conclusion and Future Perspectives 56

References 61

List of Figures

Figure 1 – Normal wound healing overlapping stages and their main characteristics 3

Figure 2 - IBD location along the gastrointestinal tract 5

Figure 3 - Upregulated ROS production may lead to oxidative stress due to an imbalance between ROS formation and the antioxidant activity 6

Figure 4 – Chemical structure of alginate, representing the G-blocks, M-blocks and alternating blocks 9

Figure 5 – Scheme of the physical gelation process that generates alginate hydrogels by ionic crosslinking with divalent cations – "egg-box model" 9

Figure 6 - Schematic illustration of the photocrosslinking of a polymer via radical polymerization of the methacrylated polymer 10

Figure 7 – Cell-biomaterial interactions – Different types of cell behavior may be developed when the cells are in contact with the hydrogel functionalized with cell-adhesion and MMP-cleavable motifs 13

Figure 8 – The hydrothiolation of a carbon-carbon double bond (C=C) 14

Figure 9 - Schematic illustration of the hydrothiolation of a carbon-carbon double bond (C=C) under exposure to UV or visible light and in the presence of the adequate photoinitiator 14

Figure 10 - Schematic illustration of the formation of the photocrosslinked biofunctionalized alginate hydrogel through sequential chemical reactions 15

Figure 11 - Biosynthesis of eumelanin 16

Figure 12 - Chemical reaction of native alginate (G-block) with methacrylic anhydride, yielding methacrylated alginate as a product 24

Figure 13 - ^{1}H-NMR spectrum of methacrylated alginate 25

Figure 14 - Synthesis of RGD-modified methacrylated alginate (AlgMaRGD) 26

Figure 15 - ^{1}H-NMR spectrum of methacrylated alginate functionalized with the cell-adhesive peptide (AlgMaRGD) 26

Figure 16 - ATR/FTIR spectra of high molecular weight alginate (AlgHMW), methacrylated alginate (AlgMa), RGD-modified methacrylated alginate (AlgMaRGD), and the RGD-containing peptide (RGD) 27

Figure 17 - ATR/FTIR spectrum of melanin particles 28

Figure 18 - TEM images of melanin particles 28

Figure 19 - ATR/FTIR spectra of the MMP-cleavable peptide and hydrogels with different composition 30

Figure 20 - Hydrogels formed after 300 s of photopolymerization, with varying concentrations of melanin and peptide crosslinker 31

Figure 21 - Mel0.3Pep4 hydrogels were photocrosslinked for different time periods (70 s, 80 s, 100 s, 140 s and 300 s) to study the structural stability of the newly formed gel network 32

Figure 22 - Blank, Pep4 and Mel0.3Pep4 hydrogels before (left) and after (right) the freeze-drying process 33

Figure 23 - Blank, Pep4 and Mel0.3Pep4 freeze-dried hydrogels 34

Figure 24 - Freeze-dried Mel0.3Pep4 hydrogels before (left) and after rehydration (right) 35

Figure 25 - Chemical reaction between the Ellman's reagent (DTNB) and free thiols in the DTNB assay 35

Figure 26 - Coupling Efficiency of the MMP-Sensitive Peptide was determined through a DTNB assay. 36

Figure 27 - Reaction mechanism of DPPH with an antioxidant 37

Figure 28 - Free-radical scavenging ability of the hydrogels through different time points, namely 2h, 3h, 6h, 9h and overnight (OT) was determined via the DPPH assay. All hydrogel samples present different composition and were photocrosslinked after 300 s. 38

Figure 29 - Free-radical scavenging ability was assessed through different time points, namely 2h, 3h, 6h, 9h and overnight (OT). Hydrogels were prepared with a varying concentration of melanin (0 wt%; 0.3 wt% (Mel 0.3); 0.45 wt% (Mel 0.45)). All hydrogel samples contain a MMP-cleavable peptide molar concentration of 4 mM (Pep4) 39

Figure 30 - Free-radical scavenging ability of hydrogels. All hydrogel samples present different composition and were photocrosslinked after 300 s. All samples contain a MMP-cleavable peptide molar concentration of 8 mM (Pep8) 40

Figure 31 - Free-radical scavenging ability of the hydrogels. All hydrogel samples present the same composition (Mel0.3Pep4) 41

Figure 32 - Influence of crosslinking time on the rheological properties of Mel0.3Pep4 hydrogels 42

Figure 33 - Influence of a varying content of melanin on the rheological properties of hydrogels with a MMP-cleavable peptide molar concentration of 4 mM 43

Figure 34 - Influence of the MMP-cleavable peptide concentration on the rheological properties of hydrogels with a melanin content of 0.3 wt% 44

Figure 35 - Swelling ratio of hydrogels produced under different conditions 45

Figure 36 – Mechanism of the H_2DCFDA/DCFDA assay 58

List of Abbreviations and Symbols

List of Abbreviations

$^{\bullet}NO$	Nitric oxide
$^{\bullet}OH$	Hydroxyl radical
^{1}H-NMR	^{1}H-Nuclear magnetic resonance
3D	Three-dimensional
ATR-FTIR	Attenuated total reflectance/Fourier transform infrared spectroscopy
CD	Crohn's disease
CGGGGRGDSP	Amino Acid Sequence of the Cell-Adhesive Peptide (Cysteine-Glycine-Glycine-Glycine-Glycine-Arginine-Glycine-Aspartic Acid-Serine-Proline)
CGPQGIWGQC	Amino Acid Sequence of the MMP-Cleavable Peptide (Cysteine-Glycine-Proline-Glutamine-Glycine-Isoleucine-Tryptophan-Glycine-Glutamine-Cysteine)
CT	Computed tomography
DA	Dopamine
DHI	5,6-dihydroxyindole
DHICA	5,6-dihydroxyindole-2-carboxylic acid
diH_2O	Deionized water
DMEM	Dulbecco's modified Eagle's medium
DNA	Deoxyribonucleic acid
DOPA	3,4-dihydroxyphenylalanine
DPPH	1,1-diphenyl-2-picrylhydrazyl
DTNB	5,5′-dithiobis-(2-nitrobenzoic) acid
ECM	Extracellular matrix
FEUP	Faculdade de Engenharia da Universidade do Porto
FTIR	Fourier transform infrared spectroscopy
G'	Elastic component of shear modulus
G''	Viscous component of shear modulus
GPXs	Glutathione peroxidases
H_2O_2	Hydrogen peroxide
HEPES	4-(2-hydroxyethyl)-1-piperazineethanesulfonic acid

HMW-ALG	High-molecular weight alginate
IBD	Inflammatory bowel disease
IL	Interleukin
IQ	Indolequinone
LVR	Linear viscoelastic region
MA	Methacrylic anhydride
MCP-1	Monocyte chemoattractant protein-1
MIP-1β	Macrophage inflammatory protein-1 beta
MMP	Matrix metalloproteinase
MRI	Magnetic resonance imaging
Na_2HPO_4	Sodium phosphate dibasic
NaCl	Sodium chloride
NaOH	Sodium hydroxide
NPs	Nanoparticles
O_2^-	Superoxide
$ONOO^-$	Peroxynitrite
OT	Overnight
PAI	Photoacoustic imaging
PDA	Polydopamine
PEG	Polyethylene glycol
PET	Positron emission tomography
PMNs	Polymorphonuclear neutrophils
PTT	Photothermal therapy
q	Swelling ratio
QI	Quinone-imine
RGD	Amino acid sequence Arginine-Glycine-Aspartic Acid
RONS	Reactive oxygen and nitrogen species
ROS	Reactive oxygen species
SOD	Superoxide dismutase
TBS	Tris buffered saline
TIMPs	Tissue inhibitors of matrix metalloproteinases
TNB	5-thio-2-nitrobenzoic acid
TNF-α	Tumor necrosis factor-α
UC	Ulcerative colitis
UV	Ultraviolet
W_{ID}	Initial dry weight
W_S	Swollen weight

List of Symbols

ω	Radial frequency

Chapter 1

Purpose of the thesis

Prolonged wound healing and chronic wounds present challenging issues to the healthcare system and a significantly decreased health-related quality of life for those affected [1]. The economic burden and human health complications related to poor wound healing are likely to increase, as the number of patients suffering from impaired healing conditions and chronic wounds is reaching larger proportions worldwide [2,3].

Although a normal and successful wound healing usually occurs in small injuries, this may not be the case when it comes to larger wounds or in the presence of a set of typical physiological or clinical conditions such as infection, age, obesity, diabetes, vascular disease and even cancer [2]. These factors may negatively influence the healing process and lead to an incomplete tissue repair, even though the underlying explanation at a cellular and molecular level is not yet fully understood [4]. The lack of knowledge regarding the abnormal healing mechanisms, as well as the scarcity of preclinical animal models that may more closely resemble human conditions [5], end up determining the reduced availability and poor efficiency of the treatment alternatives provided to patients with wound-healing pathologies.

Therefore, there is a great and urgent medical and social need to develop new therapeutic approaches improving the endogenous tissue regenerative capacity [5].

Promote a faster and more efficient healing of these injuries and a maximal restoration of tissue function, allowing tissues to regain their structural and functional integrity, becomes then a top priority of medical care [5].

As currently existing therapies for treating non-healing chronic wounds fail to provide the desired clinical outcomes, the challenge relies on developing multimodal therapeutic platforms that could target the inflammation process and promote tissue repair or regeneration.

Moreover, as wound healing is an extremely complex process with several different factors involved, multi-targeted therapies are nowadays essential to promote efficient and fast regeneration

of chronic wounds [6]. New therapeutic strategies should present a broad range of applications and act rapidly, without giving rise to significant side effects, which always constitutes a challenging task.

The main goal of this project is to develop a novel advanced multi therapeutic platform aimed at targeting general typical conditions within the chronic wound healing niche. In order to obtain the best possible solution, one needs to clarify what are the central biological features related to a non-healing wound that might be addressed through the developed strategy. Among these characteristics, prolonged inflammation and tissue regeneration constitute fundamental aspects of wound healing that should be targeted in a preliminary phase [7].

Therefore, a multi-therapeutic patch that attenuates the harsh conditions of non-healing wounds and ultimately leads to a reverse of their chronicity, while simultaneously stimulating new tissue formation, would be an ideal outcome of this project.

1. Introduction

1.1 Non-healing wounds

Impaired wound healing following trauma, surgery, acute illness, or chronic disease conditions may be the result of the deregulation of essential parts of the normal tissue repair response, such as inflammation, matrix deposition, angiogenesis, and cell recruitment [5]. The active pursuit of novel clinical approaches that might lead to a more effective wound healing relies on a deeper understanding of the underlying biological basics of repair and regeneration [5].

Therefore, in this section, the hallmarks of non-healing wounds are presented in order to grant a better insight on how the developed platform may positively affect the course of events during the healing process of chronic wounds. First, general characteristics regarding typical chronic wounds environments are described. Later, since inflammatory bowel disease (IBD) consists in a specific type of chronic disease that is associated to the development of chronic wounds, classic features of IBD are also presented.

1.1.1 Chronic wound healing

Upon tissue injury, normal wound healing comprises four main overlapping stages, namely hemostasis, inflammation, proliferation (the repair phase) and neo-tissue formation (the remodeling phase) [5] (Figure 1).

During hemostasis, the blood clotting system aims at forming a stable clot in order to stop the bleeding through a coagulation process. Afterwards, in the inflammatory phase, its main goal is to destroy bacteria and remove debris to allow the growth of new tissue, as it will be explained later in detail. The proliferative phase is characterized by the formation of new blood vessels and extracellular matrix synthesis. Finally, in the neo-tissue formation stage, the local tissue is remodeled and increases its tensile strength [8].

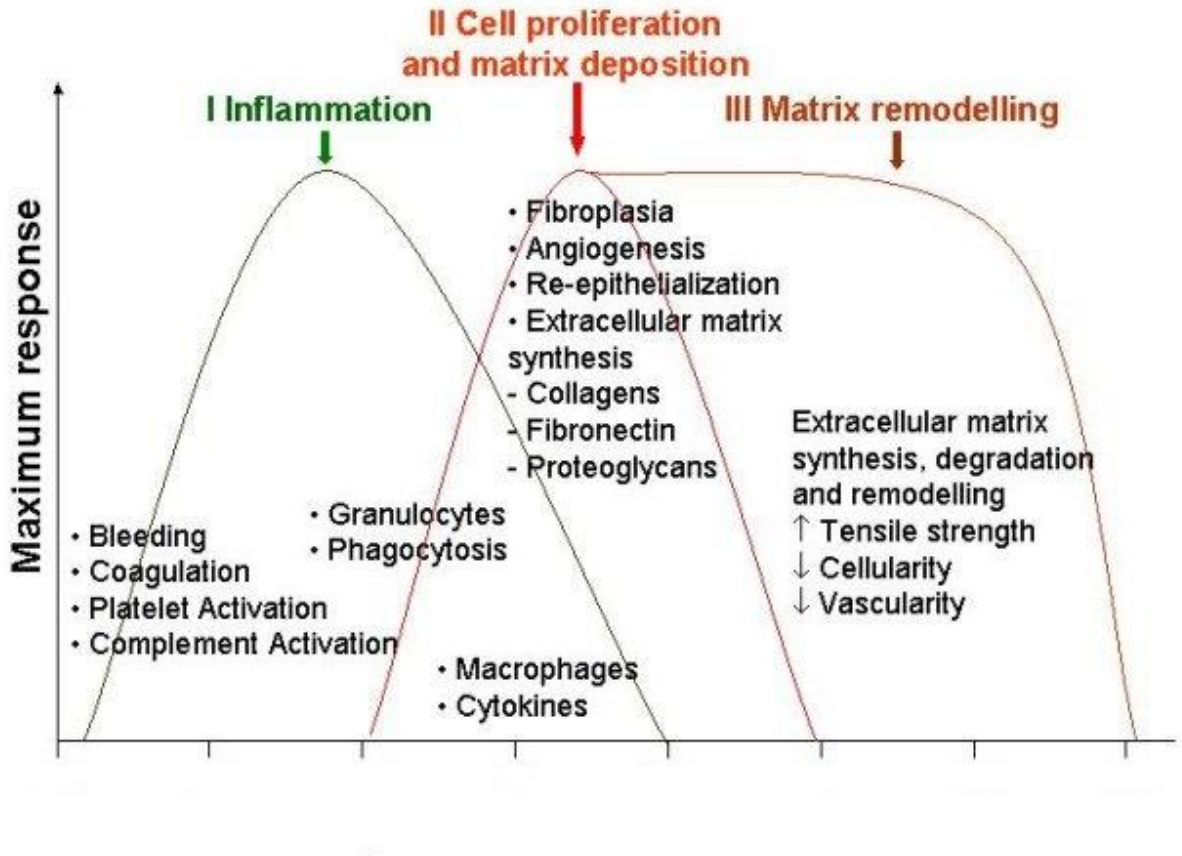


Figure 1 - Normal wound healing overlapping stages and their main characteristics. Retrieved from [9].

However, following an acute wound such as trauma or surgery, if other pathologic factors, including an underlying disease state as diabetes, are present, and depending on the nature of the wound, an acute wound may become a chronic wound, examples being diabetic foot ulcers, venous leg ulcers and pressure ulcers [10] [11]. In these cases, the healing process stalls in the inflammatory phase, thus resulting in chronic inflammation, which may lately evolve to cancer [12].

Regarding the inflammatory phase of wound healing, removal of pathogens, such as bacteria, and nonviable tissue by neutrophils and monocytes that arrive to the wound site takes place [10]. Complex interactions generated by proinflammatory cytokines regulate this stage, ultimately leading to the differentiation of monocytes into macrophages [10], [13]. Due to their ability to change their physiology, macrophages may present two possible phenotypes: a pro-inflammatory (M1) and an anti-inflammatory one (M2). Therefore, macrophages play an extremely important role in wound healing (M1) and tissue repair or remodeling (M2) [14]–[18], two coexisting processes in this type of inflammation as destruction and healing of the local tissue can be observed [19]. As a result, the most important cells at this point are phagocytic cells like neutrophils and macrophages that, besides phagocytosis, are responsible for other functions. Neutrophils release proteases, such as matrix metalloproteinases (MMPs) like gelatinases (MMP-2 and MMP-9), collagenases (MMP-1, MMP-8) and membrane-type MMPs (MMP-14) [20], and reactive oxygen species (ROS) to cleanse the wound and induce cell migration. Macrophages also secrete ROS and several growth factors and cytokines, such as tumor necrosis factor-α (TNF-α), interleukins (IL)-8 and IL-1β, monocyte chemoattractant protein-1 (MCP-1) and macrophage inflammatory protein-1 beta (MIP-1β), thus promoting tissue proliferation and cell migration by recruiting fibroblasts and endothelial cells to restore the damaged blood vessels [11].

While in acute wounds, proteases are well-regulated by their inhibitors, namely tissue inhibitors of matrix metalloproteinases (TIMPs) [21], in chronic wounds, protease levels exceed the ones of their corresponding inhibitors, resulting in extracellular matrix (ECM) degradation. Constant tissue injury results in an increased level of proteases at the wound site, promoting the recruitment of more immune cells, amplifying the proinflammatory cytokine cascade [11] and preventing the wound healing process to proceed to the proliferative phase.

In an attempt to remove injured tissue, polymorphonuclear neutrophils (PMNs) produce high amounts of ROS, causing endothelial dysfunction and allowing the migration of inflammatory cells through the endothelial barrier due to the opening of inter-endothelial junctions, destroying the tissue and creating a persistent inflammation [22]. Destroyed tissue and apoptotic cells may trigger an immune response, and as the inflammatory stimulus is persistent, recruitment of monocytes and proliferation of macrophages is continuously induced [23]. This results in an endless sequence of inflammatory events, which hampers the healing process to proceed to the next stage.

In conclusion, overproduction of ROS is a hallmark of chronic wounds. Upregulation of ROS production may promote oxidative stress, inducing damage in cells and biomolecules as DNA, lipids, ECM or cellular proteins and, thus, to local tissue [24]. Such oxidative stress may stall the normal wound healing process, as well as lead to more complicated pathological conditions and, eventually, cancer [23].

1.1.2 Internal chronic wounds in the gut: Inflammatory Bowel Disease (IBD)

Inflammatory bowel disease (IBD) consists in a chronic inflammatory disorder associated to an immunological imbalance of the intestinal mucosa, comprising two main forms, Crohn's disease (CD) and ulcerative colitis (UC) [25]. While CD can involve each part of the gastrointestinal tract, UC only affects rectum and colon (Figure 2) [26].

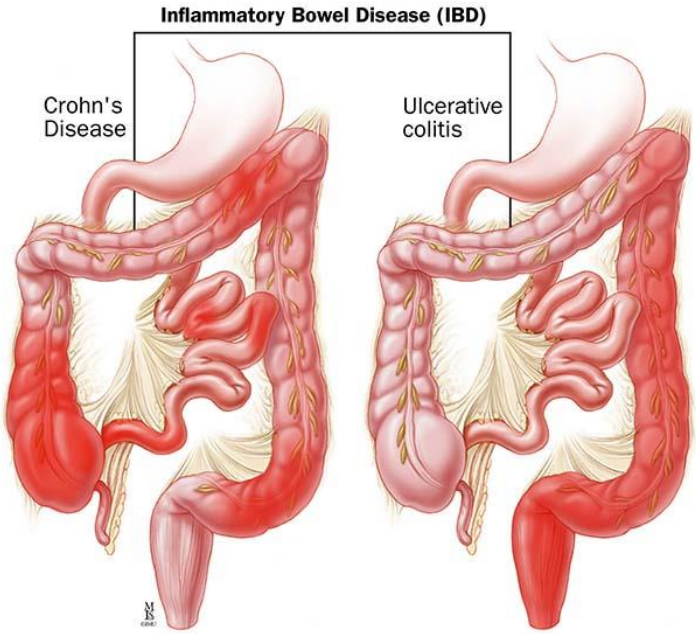


Figure 2 - IBD location along the gastrointestinal tract - Crohn's disease may affect any part of the gastrointestinal tract, most commonly the end of the small intestine (the ileum) and the colon, while ulcerative colitis only affects rectum and colon. Retrieved from [27]

Currently, there is a lack of knowledge regarding the etiology of IBD and full comprehension of its pathophysiology has not yet been achieved [25]. However, it is well established that chronic intestinal inflammation presents similar features to the majority of chronic wounds, namely the overproduction of both reactive oxygen and nitrogen species (RONS). Therefore, oxidative and nitrosative stress may play an important role in the IBD development [28].

ROS production is tightly regulated by the antioxidant system, consisting of several enzymes such as superoxide dismutase (SOD), catalase, and glutathione peroxidases (GPXs) and their antioxidant substrates (like glutathione and α-tocopherol) [29]. The production of ROS leads to a condition of oxidative stress, which is counterbalanced by the production of antioxidants in the tissue. However, in a condition of persistent oxidative stress, the antioxidant resources of the body may be considerably depleted, generating an imbalance between ROS and antioxidant activity [26]. It has been suggested that IBD might be linked to an imbalance between ROS generation and antioxidant activity, which

could explain, to some extent, clinical pathophysiological features, such as inflammation and damage of the mucosal layer in the gastrointestinal tract [30] of both disease cases [31].

Moreover, the activation of neutrophils through the cytokines produced by macrophages in a chronic inflammation situation generates high levels of ROS as an inflammatory response. Upregulated ROS production by both neutrophils and macrophages can then be correlated with the harsh inflammatory changes in the colonic mucosa that are reported in UC [32], which may lead to mucosal barrier depletion [33]. On the other hand, CD patients show decreased SOD and GPX activities in intestinal mucosa [34]. Therefore, monitoring the activity of these cellular antioxidant enzymes may allow the regulation of the levels of oxidative stress and tissue damage in a chronic wound environment [34].

Significant oxidative stress may lead to oxidative injury by inducing lipid peroxidation, cellular oxidative damage, enzymatic disfunction and eventual tissue destruction in IBD [35]. Abnormal expressions of pro-inflammatory and anti-inflammatory molecules, which are implicated in the innate and adaptive immunity [36], may also enhance the deleterious effects of oxidative stress.

One critical issue in IBD is that inflammation can be prolonged due to the opening of the intestinal epithelial barrier and increased bowel permeability [26]. This barrier is mainly composed by epithelium cells, that are specialized in absorption and secretion functions [37]. These cells are connected through different types of cellular junctions, which can be affected by upregulated cytokines and interleukins [38], eventually leading to the disruption of such junctions. Therefore, epithelial permeability increases, generating a greater immune response followed by increased intestinal inflammation [39]. Intestinal homeostasis will then be compromised, triggering the inflammatory cascade and leading to a persistent inflammation, which is a hallmark of IBD [40].

The influence of ROS in IBD is summarized in the scheme of Figure 3.

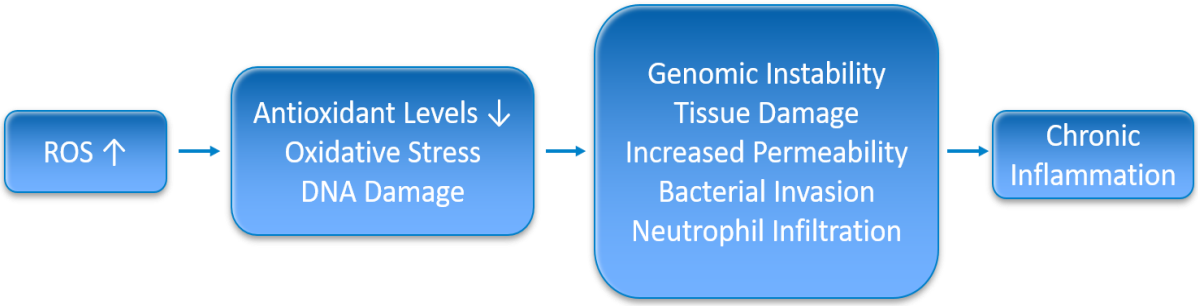


Figure 3 - Upregulated ROS production may lead to oxidative stress due to an imbalance between ROS formation and the antioxidant activity. Oxidative stress may then have deleterious effects on cells (DNA, lipids and proteins damage) and tissue (increased epithelial permeability and loss of intestinal homeostasis), which can induce chronic inflammation, a typical feature of IBD

Another important feature regarding IBD, is the upregulation of matrix metalloproteinases (MMPs) [41], which can be produced by immune and stromal cells in response to inflammatory cytokines and growth factors [41]. Since MMPs promote the digestion of the extracellular matrix (ECM), it is believed

that these proteases may regulate epithelial barrier function, immune response and even wound healing, which turns them into potential biomarkers for disease activity in IBD [41].

Therefore, it would be of high interest to develop a multi-therapeutic strategy that could simultaneously promote the scavenging of ROS and the remodeling of the intestinal mucosal barrier.

1.2 Therapeutic platforms for treatment of chronic wounds in the gut

In recent years, treat-to-target approaches have gathered much attention regarding IBD. Novel therapeutic targets include proinflammatory pathways in the intestine, since achieving control of the chronic inflammation that is present in gastrointestinal tissue in IBD may be critical towards efficient treatment of the disease [42]. Pro-inflammatory cytokine tumor necrosis factor-alfa (TNF-α) may contribute decisively to the most studied inflammatory pathway in IBD, thus playing a pivotal role in the pathogenesis of the disease [43]. Anti-cytokine therapies focused on TNF-α were clinically effective in a segment of patients with IBD, showing promising results concerning this pathway-based anti-inflammatory approach. However, only a subgroup of patients may benefit from this therapy [44].

Apart from regulating the underlying chronic inflammation, mucosal healing may also be regarded as a priority in the treatment of patients with IBD, as it is associated with lower hospitalization and relapse rates [45],[46], [47].

Moreover, there is growing interest in therapeutic approaches based on inflammation-targeting biomaterials, which can act as a drug delivery system to the inflamed gut. Zhang et al. [48] reported the delivery of an anti-inflammatory drug at the local level, in order to enhance therapeutic outcomes and minimize systemic toxicity. The developed biomaterial demonstrated preferential adhesion to inflamed epithelial surfaces and released the drug only upon enzymatic digestion.

A multi-therapeutic patch was then designed in order to achieve the main goal of this project: the development of a multifunctional biomaterial able to attenuate the severe conditions that are typically featured in a chronic wound environment.

As seen in the previous section, oxidative stress and high levels of proteases are hallmarks of non-healing wounds. In this work, it was hypothesized that the development of a platform that is able to specifically target oxidative stress through the scavenging of ROS might be able to attenuate the harsh inflammatory conditions related to chronic wounds. Moreover, higher levels of proteases may be exploited through the manufacturing of a protease-sensitive construct.

Herein, a description of the general structure and single components of the multifunctional patch developed is presented.

Beyond critical characteristics, the biomaterial to be developed needed to fulfill some important requirements: 1) be adaptable, 2) easy to produce and ready-to-use, 3) present adequate mechanical

properties, 4) easy to store and to handle. Therefore, it was decided that the patch should consist of a lyophilized hydrogel that could be applied onto the chronic wound and rehydrated *in situ*.

1.2.1 Hydrogels

Hydrogels, also known as aqua gels, are three-dimensional (3D) polymeric networks formed via crosslinking of either natural or synthetic water-soluble polymers, thus generating a water-insoluble hydrophilic material that is able to absorb and retain substantial amounts of water [49], [50]. Hydrogels present extremely attractive physicochemical properties that can be tunable, making them suitable for a wide range of biomedical applications, such as their use as scaffolds in tissue engineering or as constructs for sustained-release drug delivery [51], [52]. Hydrogels derived from natural polymers such as alginate, collagen, chitosan, dextran and hyaluronic acid are frequently used in tissue regeneration approaches due to their ability to mimic natural ECM [53]. ECM is a 3-D network of extracellular macromolecules, such as collagen, enzymes and glycoproteins, that provides structural and biochemical support of surrounding cells. Common functions of ECM include cell adhesion, cell-to-cell communication and cell differentiation [54]. Besides their inherent biocompatibility, naturally derived polymers may be designed in order to better mimic such features [55]–[57]. Hydrogels based on natural polymers constitute a versatile platform that may resemble native ECM, granting spatial support and access to bioactive motifs such as RGD, protect cellular functions and promote tissue formation, which is of the utmost importance in wound healing [58]–[60] [61].

To design a tailored ECM-mimicking biomaterial, bioinert polymers that do not interact with cells are typically preferred starting materials.

1.2.2 Alginate – chemical structure, properties and applications

Alginate is one of the most well-known polysaccharidic polymers, being widely used among the fields of wound healing, drug delivery and tissue engineering [53]. This biopolymer may be found in seaweed or in some types of bacteria, either as structural components of marine brown algae, or as capsular polysaccharides in some soil bacteria, respectively [53]. Alginate is an anionic, naturally derived polysaccharide block copolymer composed of regions of either (1,4)-linked sequential ß-D-mannuronic acid monomers (M-blocks) or sequential α-L-guluronic acid (G blocks) monomers, as well as regions of (1,4)-linked alternating M and G residues (Figure 4) [53], [62]. Depending on the alginate source, the length of the consecutive M (MMMMM) or G (GGGGG) residues and its sequential distribution throughout the polymer chain may vary [53].

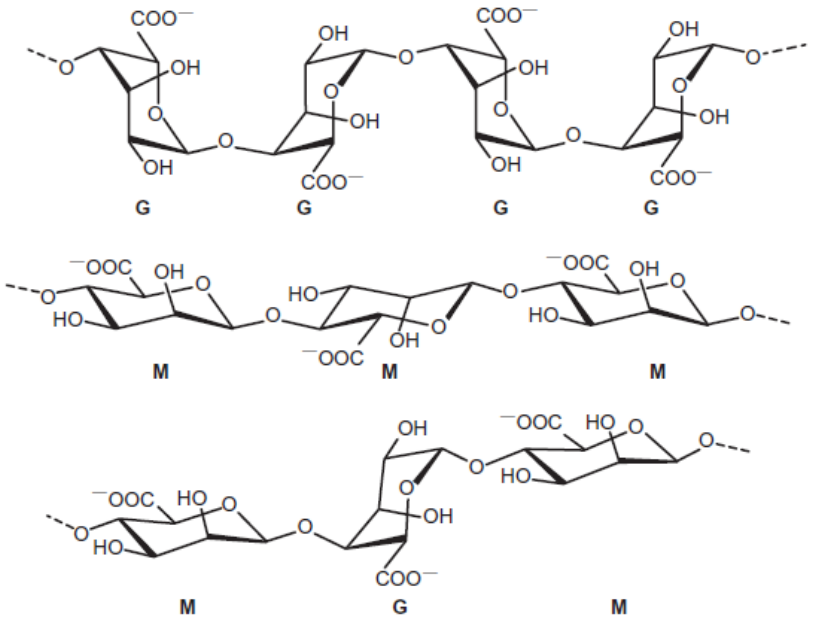


Figure 4 - Chemical structure of alginate, representing the G-blocks, M-blocks and alternating blocks. Retrieved from [63]

Alginate is biocompatible, biodegradable in some extent, nontoxic, pH sensitive and easy to modify chemically due to the presence of reactive carboxyl and hydroxyl groups in the polymer backbone (Figure 4) [64], [65]. More importantly, alginate is bioinert and can be functionalized with biochemical cues in order to build a cell-instructive material with tailored properties [66]–[68]. Additionally, alginate is considered a good mucoadhesive agent [63] due to its carboxyl end groups, as it has been reported that polymers with increased charge density and, particularly, polyanion polymers, are efficient bioadhesive polymers [69], [70].

Alginate may easily form gels through ionic crosslinking of carboxylate groups from adjacent guluronate monomers on the polymer backbone (G-blocks), in the presence of divalent cations, such as Ca^{2+}, Ba^{2+}, Sr^{2+} [53], [63], [64]. This leads to the formation of a three dimensional network of alginate fibers, typically described by the "egg-box model" (Figure 5) [63].

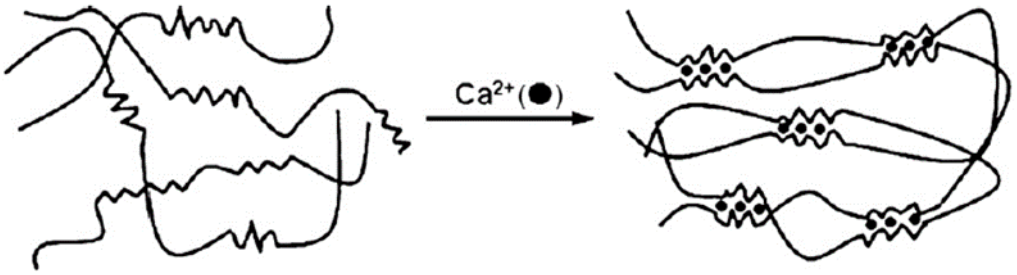


Figure 5 - Scheme of the physical gelation process that generates alginate hydrogels by ionic crosslinking with divalent cations – "egg-box model". Retrieved from [63]

The frequency and length of guluronic acid residues (G residues) and the ionic cross-linker can affect the resultant overall strength of the network. Gels derived from alginate with a high content of G residues in its structure usually present higher stiffness and lower porosity, maintaining their structural integrity for longer periods of time [71]. As physical gelation is an easy and reversible process that can occur under mild conditions in aqueous solution, it has contributed to the wide use of alginate polymers as wound dressings and cell transportation vehicles to promote tissue regeneration [53]. However, in physiological conditions, the ionically crosslinked alginate hydrogels present a limited long-term stability, representing a crucial drawback in this gel formation mechanism. These hydrogels can be dissolved due to the release of divalent ions into the surrounding environment by exchange reactions with monovalent cations [72].

Concerning wound dressing and tissue regeneration applications, the uncontrollable degradation kinetics of ionically crosslinked alginate hydrogels is considered a disadvantage, since the hydrogel may degrade faster than the time required to achieve complete wound healing. Bearing this in mind, a better control of the hydrogel performance is required to overcome general limitations of physically crosslinked gels. Thus, in the case of using alginate hydrogels as scaffolds for tissue engineering, chemically crosslinked hydrogels are advantageous since they provide long-term stability and allow a more specific control of degradation kinetics [62], [64].

1.2.3 Alginate functionalization

1.2.3.1 Covalently crosslinked alginate hydrogels through photopolymerization

Among the strategies that are used to induce the covalent crosslinking of polymers, photocrosslinking is a well-established, rapid and extremely efficient method, granting a high crosslinking reaction rate [50], [63]. Photopolymerization can occur under ultraviolet (UV) or visible light and in the presence of photoinitiators, which generate free radicals that trigger the polymerization process [73]. The free radicals generated upon irradiation of the photoinitiator will react with the active end group on the methacrylated polymer, promoting the formation of covalent crosslinked bonds in the polymer through free radical photopolymerization (Figure 6) [74], [75].

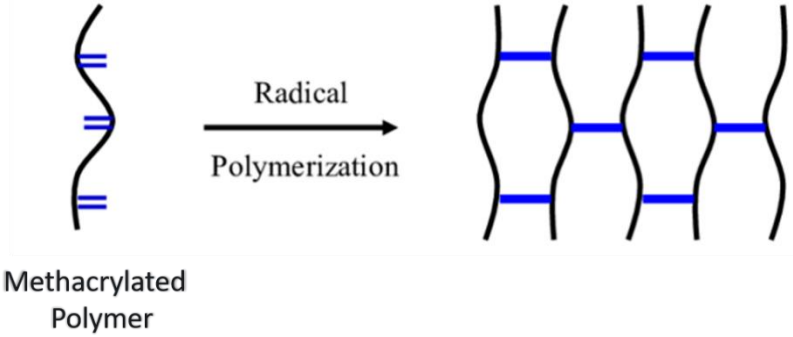


Figure 6 - Schematic illustration of the photocrosslinking of a polymer via radical polymerization of the methacrylated polymer. Adapted from [82]

The adequate choice of a photoinitiator system and short exposure to low-intensity light promote the occurrence of the radical polymerization mechanism with reduced damaging effects to cells and bioactive molecules [76]. Varying the photo-curable moiety may also provide a tight control of the mechanical properties, degradation rates and swelling behavior of hydrogels formed by photocrosslinking [74], [77].

Photocrosslinkable biocompatible polymers are of great interest in the field of tissue engineering, since they may be injected into a target defect site in a minimally invasive approach and, following brief exposure to ultraviolet (UV) or visible light, rapidly form hydrogels *in situ* under physiological conditions [50]. Consequently, aqueous macromer solutions incorporating cells and drugs, such as bioactive factors, may be delivered in a less invasive manner by photocrosslinking [62], [78], [79]. Jeon et al. [74] reported an example of methacrylated alginate macromers forming hydrogels with tunable biodegradation rates and mechanical properties, through photopolymerization. The photocrosslinked alginate hydrogels exhibited good cytocompatibility, and constitute an exciting approach as cell carriers for tissue engineering applications [50].

In this project, the multimodal hydrogel matrix was obtained through UV photopolymerization of alginate modified with methacrylic moieties, in the presence of 2-hydroxy-1-[4-(2-hydroxyethoxy) phenyl]-2-methyl-1-propanone (Irgacure® 2959). The biocompatibility of this photoinitiator, as well as its low cytotoxicity over a wide range of mammalian cell types and species, has been well demonstrated in previous studies [80], [81].

1.2.3.2 Functionalization of alginate with biochemical cues

As mentioned in section 1.2.2, alginate is a bioinert polymer, meaning that it does not interact with cells. Furthermore, as alginate hydrogels are inherently hydrophilic, this leads to a low adsorption of ECM proteins onto the hydrogel surface and, subsequently, to reduced cell adhesion [64].

However, the absence of bioactive cues in the native composition of alginate allows the design of tailored cell-instructive biomaterials, since this biopolymer can act as a "blank slate" for further functionalization [82]. Bioactive cues can then be attached to alginate as required in order to fabricate customized cell-instructive hydrogels. The grafting of such biochemical cues may trigger and control specific cell responses and, therefore, regulate cell behavior in some extent to mimic native ECM environments [83]. As a result, cell-instructive hydrogels may resemble a synthetic ECM, allowing cell culture to occur under near-physiological microenvironments with real three-dimensional conditions, which constitute an attractive approach for mechanical models regarding *in vitro* studies [84]. The mechanical, biological and physicochemical properties of such hydrogels can be independently tailored to promote specific cell-biomaterial interactions and cellular responses [82].

Among the bioactive cues that can be incorporated in native alginate, cell-adhesive peptides containing the amino acid sequence arginine-glycine-aspartic acid (RGD) have been widely used as model adhesion ligands, due to the extensive presence of integrin receptors, for example, $\alpha_v\beta_3$ and $\alpha_5\beta_1$, for this ligand in the cytoplasmic membrane of several cell types [85], [86]. Consequently, the attachment of peptides containing this cell-adhesion motif will enhance cell-biomaterial interactions through integrin-mediated cell attachment, generating a biomaterial that more closely mimics the cell-adhesion ability of native ECM [87]. Cell-matrix interactions may then be regulated according to the concentration of cell-adhesive peptide that is incorporated in the hydrogel structure. This allows the design and engineering of a chemically well-defined biomaterial with tunable physicochemical and biological properties.

Furthermore, other functions of native ECM may be reproduced, for example, the stimulation of cellular responses such as proliferation and differentiation [88]. In fact, a previous study developed in our work group reported that bone cells within RGD-modified alginate microspheres established improved cell-biomaterial interactions and showed a higher level of differentiation when compared to cells immobilized within unmodified alginate microspheres [89].

Besides cell adhesion ligands, it is also possible to modify alginate with protease-labile crosslinking peptides, in order to obtain hydrogels with triggered degradation kinetics [68]. Matrix metalloproteinases (MMPs) may be a good target, since they are well-known enzymes capable of cleaving several components of the ECM, and thus playing a crucial role in morphogenesis, wound healing and tissue remodeling [83], [90]. Furthermore, as higher levels of MMPs are a hallmark of chronic wounds, these enzymes can be exploited to facilitate the hydrogel remodeling and the release of any added substance to the hydrogel. Sun et al. [68] reported the development of a MMP-sensitive photocrosslinkable alginate-based hydrogel system that showed a substantially higher degradation by MMPs secreted by the cells. Furthermore, the biomaterial promoted cell spreading, proliferation and enhanced functional expression.

Another possible strategy for obtaining MMP-sensitive hydrogels relies on the partial crosslinking of the hydrogel with MMP-degradable amino acid sequences such as CGPQG↓IWGQC, as reported in a study conducted by Pereira et al. [91] based on pectin hydrogels. The arrow indicates the MMP-cleavage site, which is located in the peptide bond between the amino acid glycine (G) and the amino acid isoleucine (I) [91]. The addition of MMP-cleavable moieties allows the hydrogel matrix to be partially degradable by cell-driven local proteolysis [91], providing cell-mediated control over the hydrogel degradation. Figure 7 provides an overview of cell behavior in a hydrogel functionalized with cell-adhesion and MMP-sensitive motifs.

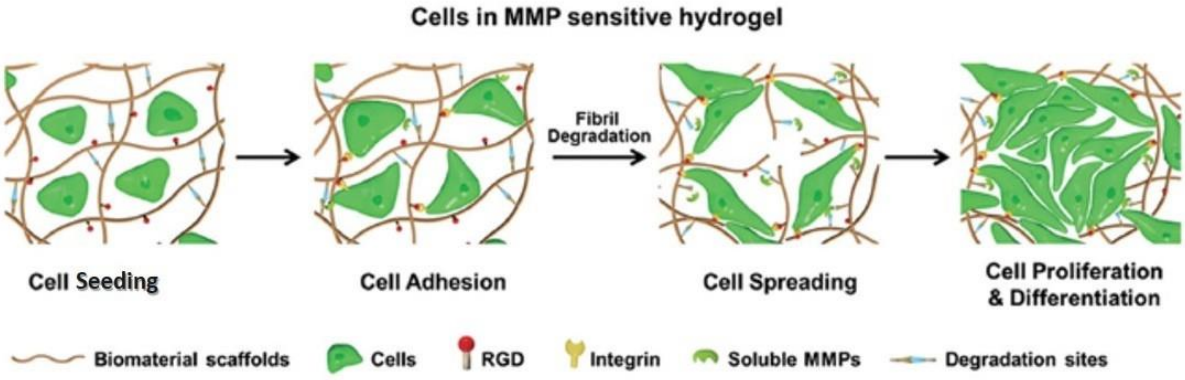


Figure 7 – Cell-biomaterial interactions – Different types of cell behavior may be developed when the cells are in contact with the hydrogel functionalized with cell-adhesion and MMP-cleavable motifs. Adapted from [68].

The possibility of manufacturing alginate hydrogels with tunable degradation rates through the incorporation of different densities of MMP-cleavable peptides is extremely important regarding tissue engineering. The degradation rate of the hydrogel should match cell growth and proliferation cycles, as well as the rate at which new tissue structure is formed in chronic wound healing [68]. Besides its degradation profile, the variation of the amount of MMP-degradable peptide that is incorporated into the hydrogel network may modulate the mechanical properties of the matrix [92]. Since a continuous cell-mediated degradation process will take place, the hydrogel must be designed with an adequate initial mechanical strength in order to allow the development of a construct that closely mimics native ECM [68].

In conclusion, by functionalizing alginate with appropriate biochemical cues in adequate amounts, tunable cell-instructive hydrogels may be obtained, which is of the utmost importance in the design of a multimodal platform that can be applied onto chronic wounds located in different types of tissues and, thus, with different requirements according to the specific cell types of the local tissue.

1.2.3.3 Chemical strategies for alginate biofunctionalization

The selection of adequate chemical strategies for grafting of such biochemical cues is of crucial importance. Polymer biofunctionalization can be achieved through different chemical approaches such as carbodiimide chemistry, reductive amination, “click” chemistry [93]. Although carbodiimide is the most used strategy to achieve the attachment of amine-terminated peptides to carboxylic groups of alginate, through the formation of an amide bond, “click” chemistry has started to emerge as an attractive approach due to its higher yields in aqueous medium and inherent biocompatibility [94], [95]. According to the definition of Sharpless and Finn, a “click” reaction can be described as a selective, high-yield reaction carried under mild water-tolerant conditions and with no by-products [96]. Due to their safety and non-toxic nature, where no metal catalysts are used, thiol-based

reactions, as thiol-ene and thiol-yne reactions, have been widely used to produce functional biomaterials for both tissue engineering and regenerative medicine [97], [98].

In the current work, the functional cysteine-terminated integrin-binding peptide containing the amino acid RGD motif was covalently coupled to the alginate backbone through base-catalyzed thiol-Michael addition click reaction [99]. This reaction exploited the reactivity between activated carbon double bonds (C=C) of methacrylated alginate and the thiolate anion of the cysteine terminated cell-adhesive peptide, which acts as a nucleophile [100]. In thiolene click chemistry, sulfhydryl-containing linkers (e.g., biscysteine peptides, dithiothreitol), may react with molecules presenting alkene groups through a hydrothiolation (Figure 8).

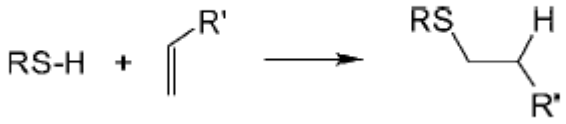


Figure 8 - The hydrothiolation of a carbon-carbon double bond (C=C). Retrieved from [98]

The bisfunctional cysteine-containing MMP-sensitive peptide with amino acid sequence CGPQGIWGQC was introduced during hydrogel formation, acting as a crosslinker. It contributed to hydrogel formation through a thiolene-based photoclick approach, after exposure to UV or visible light in the presence of an adequate photoinitiator (Figure 9) [101]. This reaction mechanism involves step growth reactions and polymer chain growth reactions. The thiol-ene click reaction is triggered by the presence of photoinitiators, which, upon exposure to UV radiation, generate free radicals that will deprotonate the thiol group, originating thiyl radicals. Such thiyl radicals will then react with the alkene or alkyne bonds forming covalent carbon-sulfur bonds (Figure 9) [102].

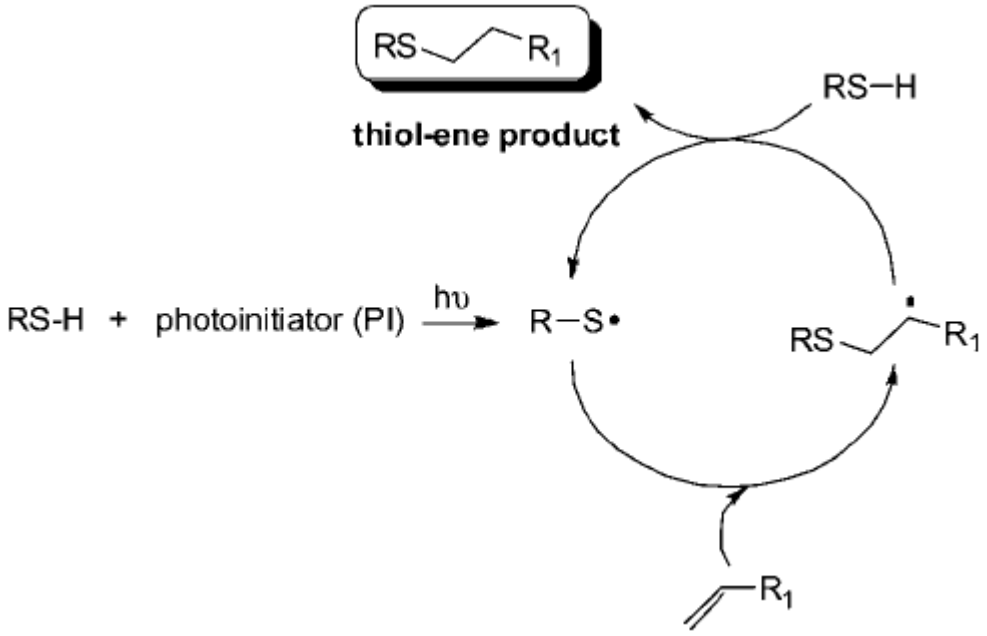


Figure 9 - Schematic illustration of the hydrothiolation of a carbon-carbon double bond (C=C) under exposure to UV or visible light and in the presence of the adequate photoinitiator. Retrieved from [98].

This thiol-ene based click chemistry may provide simple, fast, reproducible, versatile and highly efficient chemical reactions, presenting high reaction rates, high yield, oxygen and water insensitivity, high selectivity and biocompatibility, allowing the formation of orthogonal networks [94], [103], [104]. In a work conducted by Polizzotti et al. [102], the thiolene photoclick reaction was explored in order to develop polyethylene glycol (PEG) hydrogels with enhanced mechanical properties and controlled network structure. It is important to highlight that both thiol-ene photocoupling reactions and radical polymerization between methacrylate moieties may occur simultaneously, thus resulting in the fabrication of hydrogels through a dual crosslinking strategy.

A brief summary of the reactions carried out to obtain the biofunctionalized hydrogel matrix is presented (Figure 10).

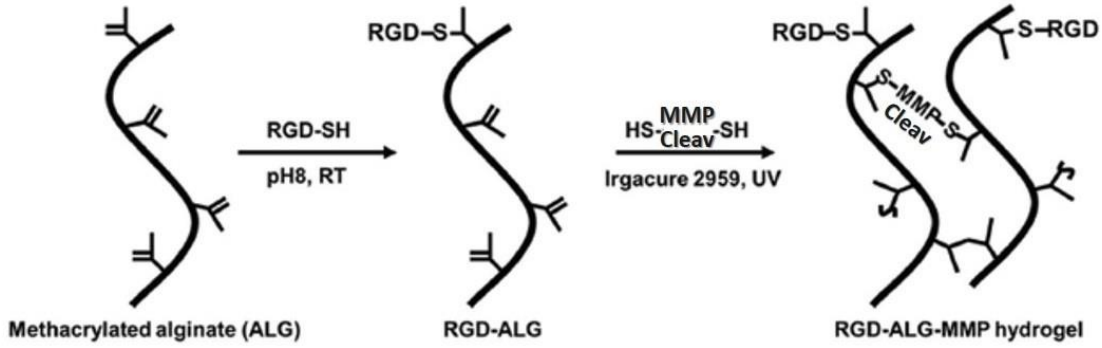


Figure 10 - Schematic illustration of the formation of the photocrosslinked biofunctionalized alginate hydrogel through sequential chemical reactions. Adapted from [68]

It should also be noticed that although the hydrogel may undergo enzymatically mediated degradation, the bonds that are cleaved are related to the newly formed covalent bonds between the methacrylated alginate and the MMP-cleavable moiety. Remarkably, considering the degradation is cell-mediated, the MMP-sensitive hydrogels are suitable for a wide variety of cells [68], which generates a vast series of applications to different body tissues and their particular chronic wounds.

1.2.4 Melanin - structure, biosynthesis and general properties

Natural melanin is one of the most abundant biological pigments in nature, being widespread distributed among living organisms, such as plants, microorganisms and animals, including in a rather high quantity in humans, being responsible for skin pigmentation [105], [106]. It is a hydrophobic, negatively charged, high molecular weight biopolymer, which essentially exists in three forms, namely eumelanin, pheomelanin and neuromelanin, and can be extracted from several organisms such as bacteria, fungi, plants and animals [107]–[110]. The most common type is eumelanin, which is widely present in cephalopods [111].

The biosynthesis of this pigment in animal cells occurs in melanosomes, starting from the conversion of tyrosine to dopaquinone in the presence of the enzyme tyrosinase (Figure 11) [112]. As this intermediate compound is relatively unstable, it can rapidly lead to the formation of dopachrome through an intramolecular cyclization reaction [112]. Then, depending on the presence of dopachrome tautomerasis, dopachrome can be converted either in 5,6-dihydroxyindole (DHI) or 5,6-dihydroxyindole-2-carboxylic acid (DHICA) [112]. Currently, it is strongly believed that melanins are formed through oxidative polymerization of phenolic and/or indolic compounds [107]. For example, it is reported that eumelanin may result from the oxidative polymerization of DHI and/or DHICA [113]. Consequently, among these redox forms of DHI and DHICA, quinone-imine (QI) and indolequinone (IQ) species can be found in the composition of eumelanin [114]. Due to the presence of these units, melanins are classified as paramagnetic biopolymers, which present reducing and oxidizing sites within their structure, and are not typically soluble either in water or in organic solvents [115].

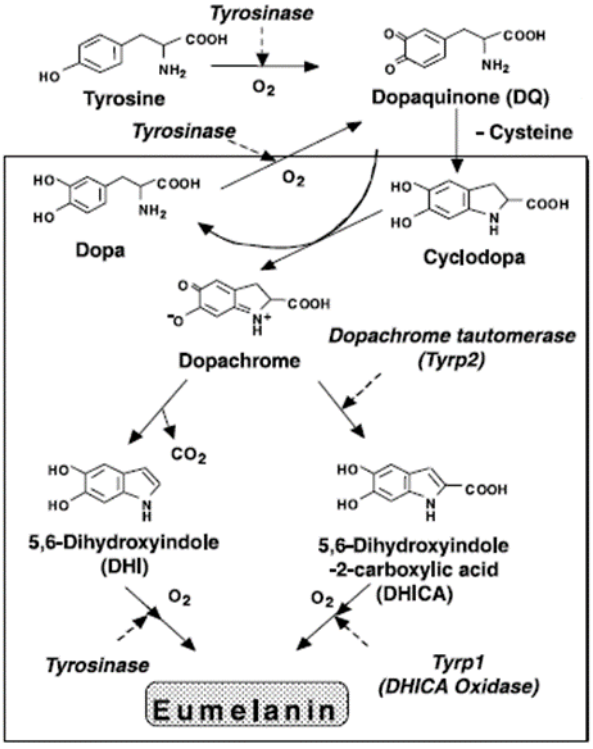


Figure 11 - Biosynthesis of eumelanin. Adapted from [112]

Araújo *et al.* reported that eumelanin can be obtained from cephalopod ink [111] through an easy extraction method that is based on successive ink dilutions and washings with distilled water [116]. This process is then economically advantageous as the biopolymer is obtained ready-to-use, without requiring additional structure modification. Synthetic eumelanin, usually known as polydopamine (PDA), presents identical chemical composition to naturally derived melanin, although some physicochemical and morphological properties might be substantially different [105]. PDA may be produced through the spontaneous oxidation and polymerization of 5,6-dihydroxyindole (DHI), 5,6-

dihydroxyindole-2-carboxylic acid (DHICA), 3,4-dihydroxyphenylalanine (DOPA) or dopamine (DA) in alkaline environments [105], [108], [117], [118].

Although the structure of melanin is not fully understood, it is characterized for being highly disordered and heterogeneous, generating a considerable diversity of structures, depending on its source and metabolic or synthetic pathway [119]. Natural melanin performs a great variety of biological functions, such as structural coloration, photosensitization, photoprotection from UV and visible radiation, free-radical scavenging, antioxidant activity, metal ion chelation and neuroprotection. It also plays an important role in the regulation of a large range of metabolic processes and molecular interactions [120]–[126]. As a result of these properties, together with the polymer inherent biocompatibility and high photothermal conversion efficiency, there has been growing interest in the use of both natural and synthetic melanin as a new type of versatile biomolecules that can find a wide range of applications in the biomedical field [105]. Melanin has been used as a naturally active multifunctional nanoplatform for tumour photoacoustic imaging (PAI) and photothermal therapy (PTT) [127]–[130], as well as in the development of multifunctional bioprobes for multimodal molecular imaging, including positron emission tomography (PET), magnetic resonance imaging (MRI), PAI and computed tomography (CT) [131]–[134]. Araújo et al. [116] reported the use of melanin nanoparticles as nanocarriers in formulations for colon and intestine targeted drug delivery, due to the strong pH dependency exhibited by the drug release activity from melanin.

Due to their free-radical scavenging ability and high antioxidant activity, melanin and PDA nanoparticles (NPs) have also been used as a novel nanoplatform for antioxidative therapy through scavenging excessive reactive oxygen and nitrogen species (RONS) [105]. Liu et al. [122] studied the effect of the activities of melanin NPs against toxic RONS (such as superoxide ($O_2^{\bullet-}$), hydrogen peroxide (H_2O_2), hydroxyl radical ($^{\bullet}OH$), nitric oxide ($^{\bullet}NO$) and peroxynitrite ($ONOO^-$)), and further assessed the potential of melanin nanoparticles for antioxidative therapy *in vitro* and in a rat model of ischemic stroke. The results obtained demonstrated that melanin nanoparticles present an extensive defense against multiple RONS. They were also able to attenuate the RONS-triggered inflammatory responses by repressing the expression of cytokines and inflammatory mediators [122], which allows for a more controlled regulation of chronic inflammation environments. In another study, Bao et al. [135] developed a powerful antioxidant defense PDA-based platform for ROS elimination in oxidative stress-induced periodontal disease.

In the present work, melanin nanoparticles have been entrapped during hydrogel formation. It was hypothesized that the incorporation of these nanoparticles in the hydrogel patch may allow a better control of the chronic wound environment by scavenging the increased amount of ROS that is typically present in non-healing wounds. This would help to attenuate the harsh conditions of chronic inflammation environments and, eventually, reverse the chronicity of such events, leading to tissue repair and restoration.

Chapter 2

2. Materials and Methods

Ultrapure sodium alginate (High-molecular weight alginate (AlgHMW), Pronova UP LVG, G/M ratio: ≥ 1.5, Viscosity: 20-200 mPa*s; Mw= 75-200 kDa) was purchased from Novamatrix (FMC Biopolymers). Methacrylic anhydride was purchased from Sigma-Aldrich and used as received. Naturally derived melanin nanoparticles obtained from cuttlefish ink were kindly provided by Dr. Marco Araújo and used without further modification [136]. The RGD cell-adhesive CGGGGRGDSP (MW = 861.88) peptide and the MMP-cleavable CGPQG↓IWGQC (MW = 1048.2, arrow indicates the cleavage site) peptide were custom-synthesized and obtained from GenScript. Dulbecco's modified Eagle's medium (DMEM) was purchased from Gibco. Photoinitiator Irgacure 2959, 4-(2-hydroxyethyl)-1-piperazineethanesulfonic acid (HEPES), Tris buffered saline (TBS), 5,5′-dithiobis-(2-nitrobenzoic) acid (DTNB, Ellman's reagent), L-cysteine and 2,2-Diphenyl-1-picryl-hydrazyl (DPPH) were obtained from Sigma-Aldrich.

2.1 Synthesis and characterization of methacrylated alginate (AlgMa)

A 1 wt% solution of AlgHMW (0.4 g; 2.02 mmol) in Tris buffered saline (TBS, 50 mM Tris, 150 mM NaCl, pH= 8) was treated with methacrylic anhydride (8.13 g; 52.76 mmol; 7.86 mL) at 0 °C, under vigorous stirring. The methacrylic anhydride was added into two portions distributed by intervals of 5h, and the pH continuously adjusted to pH = 8 with a 5M NaOH solution. After vigorous stirring for 10h at room temperature (rt), ethanol (150 mL) was added and the precipitated solid centrifuged at 4000 rpm (Eppendorf centrifuge 5810R, rotor A-4-62) for 8 min. The pellet was further washed twice with ethanol and allowed to dry on air overnight. The obtained solid was rehydrated and purified through dialysis against decreasing concentrations of NaCl for three days. The resultant solution was passed through a 0.45 μm filter and lyophilized to give the product, methacrylated alginate (AlgMa), as a white foam (0.370 g). ^{1}H NMR (D_2O, 400 MHz): δ (ppm) 6.25 (br, s), 5.82 (br, s), 5.25 (br, s), 4.23-

3.77 (br, m), 1.97 (br, s). FTIR (cm^{-1}): 3264, 2933, 1711, 1596, 1407, 1297, 1160, 1123, 1088, 1027, 949, 811, 727, 620, 556, 419.

2.1.1 Nuclear magnetic resonance (^{1}H-NMR)

^{1}H NMR spectra were recorded using a 400 MHz spectrometer AVANCE III (Bruker). Polymers were dissolved (13.3 mg/mL) in deuterated water (D_2O, Euriso-top) and transferred to NMR tubes.

2.1.2 Attenuated total reflectance - fourier-transform infrared spectroscopy (ATR-FTIR)

Attenuated total reflectance/Fourier transform infrared spectroscopy (ATR-FTIR) spectra were recorded using a Frontier FT-IR spectrometer (PerkinElmer, USA) and FTIR spectra were recorded over a range of 4000-400 cm^{-1} at a resolution of 4 cm^{-1}.

2.2 Functionalization of AlgMa with cell-adhesion motifs (AlgMaRGD)

Before any functionalization, methacrylated alginate (AlgMa) was dissolved in a 0.5 M Na_2HPO_4 buffer solution, at rt, to obtain a 1 wt% final solution. pH level was adjusted to 9.5 by adding 0.1 M NaOH dropwise.

The cell-adhesive peptide (CGGGGRGDSP) was then added to the AlgMa solution at a weight ratio of 200 mg/g AlgMa, to promote the coupling of the integrin-binding peptide. The obtained solution was protected from light and allowed to react overnight under stirring and inert atmosphere. The RGD-modified polymer (AlgMaRGD) was then purified through dialysis against decreasing concentrations of NaCl for three days using a MWCO 3500 membrane (Spectra/Por®, SpectrumLabs). Then, the final solution was frozen, lyophilized, and stored at -20 ºC until further use. Control AlgMa was prepared through the same method, although without the addition of peptide (Blank).

^{1}H NMR and FTIR spectra were also recorded.

^{1}H NMR (D_2O, 400 MHz): δ (ppm) 6.23 (br, s), 5.79 (br, s), 5.05 (br, s), 4.48 (br, s), 4.39 (br, s), 4.29 (br, m), 4.04-3.91 (br, m), 3.75 (br, m), 3.23 (br, t), 2.70 (br, m), 2.25 (br, m) 1.96 (br, s), 1.67 (br, m). FTIR (cm^{-1}): 3230, 2932, 1600, 1408, 1318, 1161, 1124, 1088, 1027, 948, 811, 724, 620, 559, 408.

2.2.1 Quantification of incorporated cell-adhesive peptide (AlgMaRGD)

The amount of incorporated cell-adhesive peptide onto the structure of AlgMa was assessed through the colorimetric DC protein assay (BIO-RAD). AlgMa (8 mg) was dissolved in ultrapure water (Millipore) to obtain a 2 wt% solution. 100 µL of this solution were mixed with 100 µL of 2 mg/mL peptide solution to obtain the highest peptide concentration standard for the calibration curve (named P7, 1 mg peptide/mL solution). The remaining standard solutions (0.5 mg/mL to 0.015 mg/mL) were prepared sequentially by successive dilutions with 1 wt% AlgMa solution. P0 was exclusively prepared with 1 wt% AlgMa, since it should not contain any cell-adhesive peptide. Afterwards, 5 µL of each sample containing the RGD-modified alginate or standard were transferred to a 96-well plate. To this sample, 25 µL of alkaline copper tartrate solution (Reagent A) and 200 µL of Folin reagent (Reagent B) were then added, and the mixture was allowed to react at room temperature for 15 minutes in complete darkness. Finally, the protein content was determined by measuring the absorbance at 750 nm using a micro-plate reader (Synergy Mx™ , BioTek, USA). The incorporated peptide concentration was determined from the performed calibration curve.

2.3 Development and characterization of the multi-functional alginate-based patch

2.3.1 Preparation of photocrosslinked alginate hydrogels

AlgMa and AlgMaRGD were separately dissolved in 0.9 wt% NaCl at 25 ºC (Eppendorf Thermomixer®, Germany) to obtain 4 wt% solutions.

Melanin nanoparticles were dissolved in 0.9 wt% NaCl at final concentrations of 1.5 wt%, 2.25 wt% and 3 wt% and the obtained solutions were sonicated during 20 minutes. Photoinitiator Irgacure 2959 was dissolved in 0.9 wt% NaCl at a final concentration of 0.235 wt%. The prepared solution was kept wrapped with aluminum foil to be protected from light. A MMP-sensitive peptide solution was prepared by dissolving 1.05 mg (final molar concentration in the hydrogel of 4 mM) or 2.10 mg (final molar concentration in the hydrogel of 8 mM) of MMP-cleavable peptide in 25 µL of 1M sodium acetate buffer (pH = 5).

To fabricate photocrosslinked MMP-sensitive alginate hydrogels, 4 wt% AlgMa and AlgMaRGD solutions were mixed in adequate proportions to obtain a 1.5 wt% precursor alginate solution containing 200 µM RGD [137].

The total volume of the precursor solution was then completed by adding melanin stock solution in the desired amounts, the intended volume of MMP-cleavable peptide stock and 0.9 wt% NaCl solutions, and the photoinitiator at 0.05 wt%. The final gel precursor solutions (14 µL) were placed

between two glass slides separated by 250 μm spacers. The samples were then irradiated (7 mW/cm^2, λ within the range 280-450 nm) using a BlueWave® 200 curing spot lamp (Dymax, USA) for the desired time periods (60-300 s). Photocrosslinked hydrogel discs were then placed in diH_2O or DMEM supplemented with HEPES until further analysis. Hydrogel discs with different melanin (0 wt%, 0.3 wt%, 0.45 wt%, 0.6 wt%) and MMP-sensitive peptide (0 mM, 4 mM, 8mM) concentrations were obtained. Some formulations were characterized either in the form of hydrogel or as a lyophilized scaffold. For obtaining a lyophilized scaffold, the manufactured hydrogel discs were transferred to a 48-well plate, frozen and freeze-dried overnight (FreeZone Plus 2.5 Liter Cascade Console Freeze Dry System, Labconco). ^{1}H NMR and FTIR spectra of different hydrogel samples were also recorded.

2.3.2 Coupling efficiency of the MMP-cleavable peptide

The amount of MMP-cleavable peptide incorporated onto the hydrogel network during photopolymerization was determined by performing the DTNB (Ellman's reagent) assay. Briefly, photocrosslinked hydrogel discs were transferred to a 48 well-plate and stirred overnight in diH_2O (200 μL) at 70 rpm, protected from light. 30 μL of the sample solution were then mixed with 150 μL of a DTNB solution at 0.03 wt% in sodium phosphate buffer.

Absorbance was measured at 410 nm in a microplate reader (Synergy Mx™ , BioTek, USA). The standards for the calibration curve were prepared with serially diluted L-cysteine solutions (concentrations ranging from 5.63 mM to 0.0718 mM) in sodium phosphate buffer (pH = 8). Sodium phosphate buffer was used as a blank. All measurements were made using at least three replicates.

The efficiency of the MMP-cleavable peptide incorporation (I_{eff}) can then be determined by equation 1:

$$I_{eff} = \frac{P_{ADD} - F_{SH}}{P_{ADD}} \times 100, \quad (1)$$

where F_{SH} indicates the amount of free sulfhydryl groups, corresponding to the amount of MMP-cleavable peptide that was not conjugated to alginate and P_{ADD} is the total amount of peptide that was added to alginate.

2.3.3 Free-radical scavenging activity

The free-radical scavenging ability of the developed hydrogel was evaluated through the DPPH antioxidant assay. Briefly, photocrosslinked hydrogel discs were transferred to a 48-well plate and 425 μL of a 0.1 mM DPPH solution in 95% Ethanol were added. The plate was protected from light and kept at rt, and 60 μL aliquots were taken at different time points, namely after 2 hours, 3 hours, 6 hours, 9 hours and overnight. Absorbance was read at λ = 517 nm using a UV-Vis spectrophotometer (Lambda 35, PerkinElmer, USA). A control containing a similar concentration of free melanin nanoparticles was also run, as well as a blank consisting of DPPH in ethanol solution. All measurements

were made using at least three replicates. Lower absorbance values were associated to a higher free radical scavenging activity.

2.3.4 Rheological properties

The linear-viscoelastic behavior of the alginate-based hydrogels was assessed through oscillatory shear experiments using Kinexus Pro rheometer (Malvern Instruments Ltd., UK).

Photocrosslinked hydrogel discs obtained by the abovementioned procedure (section **2.2.1**) were immersed in DMEM supplemented with HEPES and incubated overnight at 37 ºC in a CO_2 incubator. Then, a sample disc was cut using a 4 mm diameter biopsy punch and placed onto the bottom geometry plate. Afterwards, the top geometry was lowered in order to contact the hydrogel with a predefined gap, calculated based on 30% compression of their initial thickness, which was measured with a digital caliper (Duratool). All tests were carried out in a humidified environment at physiological temperature (37 ºC) to prevent hydrogel dehydration during analysis.

Amplitude sweep (strain sweep) tests were performed, by maintaining the frequency constant at 0.1 Hz and varying the amplitude of the shear strain from 0.1 to 100%. The linear viscoelastic region (LVR), which corresponds to the values of the shear storage modulus (the elastic component of shear modulus - G') and the shear loss modulus (the viscous component of shear modulus – G'') that display low dependence on amplitude, was determined. The mean of the selected values of G' and G'' was calculated. Moreover, frequency sweep tests were also conducted, by varying the radial frequency (ω) from 0.01 to 10 Hz, while the strain amplitude was held constant at a predefined value within the LVR of the amplitude sweep test. The values of G' and G'' that showed a low dependence on frequency, corresponding to the values within the LVR, were then selected and their mean was calculated. At least three replicates were used for each test.

2.3.5 Swelling ratio

The swelling ratio was determined by following a reported procedure [137]. Briefly, hydrogel samples (14 µL, n = 4) were lyophilized and weighted to obtain the initial dry weight (W_{ID}). Freeze-dried samples were then incubated in ultrapure water (1 mL) at 37 ºC for 24h. Afterwards, the hydrogel's superficial excess water was gently removed with a tissue paper, and the hydrated sample was weighted to determine the swollen weight (W_S). Swelling ratio (q) was then determined by dividing the weight after the hydration step of the hydrogel (W_S) by its initial dry weight (W_{ID}) (Eq. 2):

$$q = \frac{W_S}{W_{ID}}, \qquad (2)$$

Chapter 3

3. Results

3.1 Synthesis and characterization of methacrylated alginate (AlgMa)

Methacrylated alginate (AlgMa) was synthesized by replacing secondary hydroxyl groups (alcohols) on the alginate backbone with methacrylate groups, through a nucleophilic substitution reaction of AlgHMW with methacrylic anhydride (Figure 12), as reported in a previous study [138].

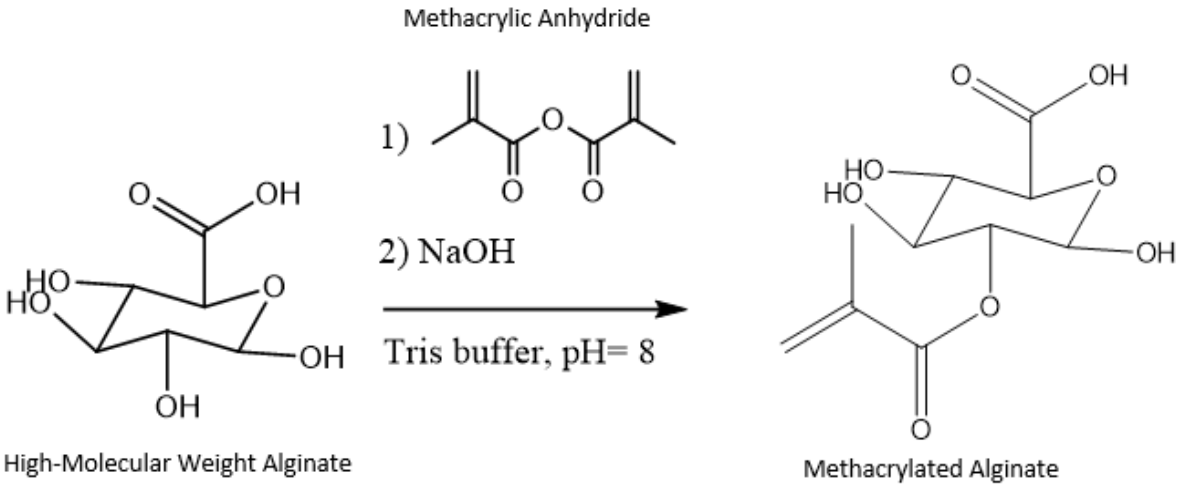


Figure 12 - Chemical reaction of native alginate (G-block) with methacrylic anhydride, yielding methacrylated alginate as a product

The success of functionalization was confirmed by the ^{1}H-NMR spectrum of AlgMa (Figure 13), which presents two characteristic peaks at 5.82 and 6.25 ppm (protons 13 and 14, respectively), belonging to the methylene group in the vinyl bonds. Moreover, a new sharp peak at 1.97 ppm can also be observed, which is related to the methyl group (proton 15) [137].

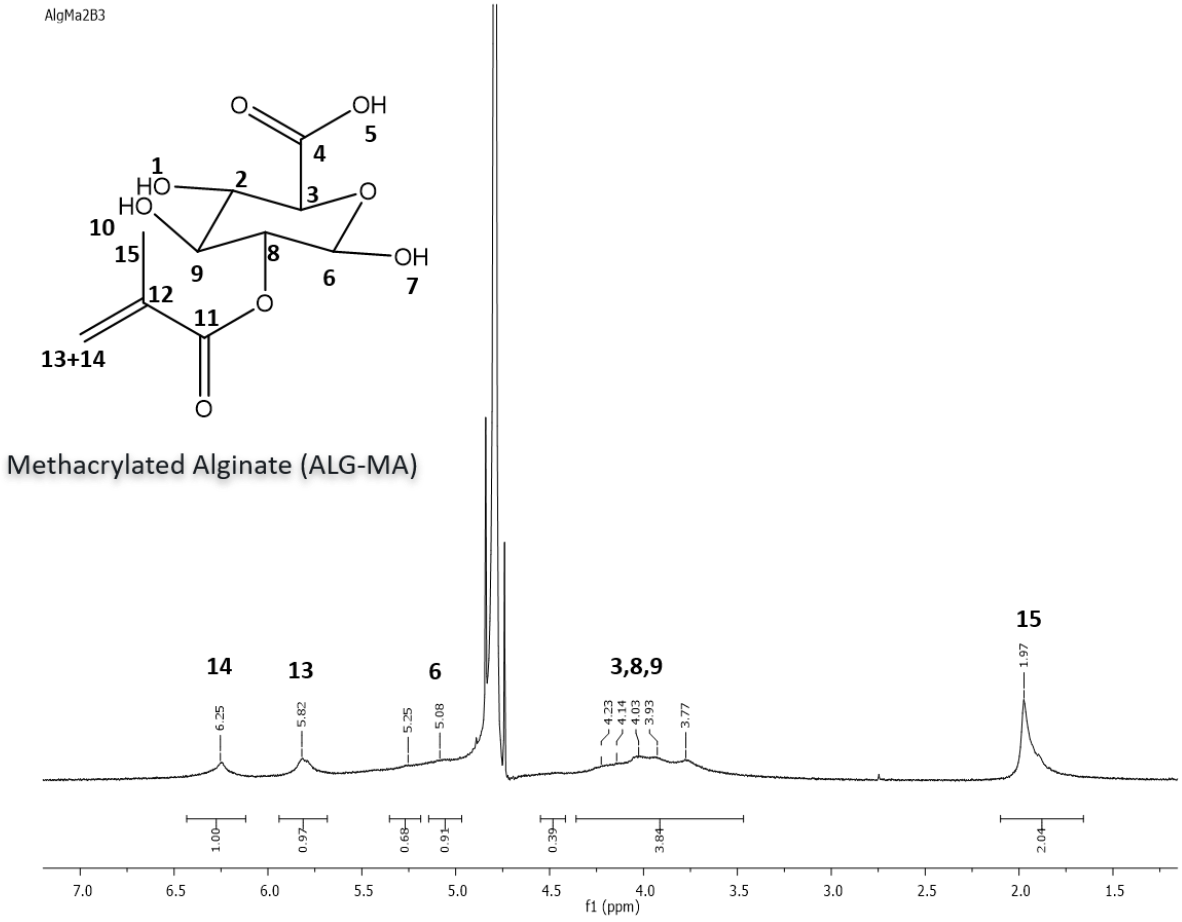


Figure 13 - ^{1}H-NMR spectrum of methacrylated alginate, showing the characteristic proton peaks of the modified polymer

The functionalization degree was determined through the ratio between the peak corresponding to the alginate proton 6 at δ = 5.08 ppm and the one at δ = 6.25 ppm corresponding to methylene protons of the methacrylate moiety, being approximately 52%. The obtained functionalization degree is in accordance with common methacrylation percentages regarding AlgMa, as reported in the literature [68].

3.2 Conjugation of cell-adhesive peptide to methacrylated alginate (AlgMaRGD)

Functionalization of methacrylated alginate (AlgMa) with a bioactive ligand containing a cell-adhesion motif (RGD) was accomplished via thiol-Michael addition reaction between the terminal thiol

group of the RGD-containing peptide and the methacrylate groups of the polymer (Figure 14), as previously reported [68]. The conjugation was achieved through a base catalyzed mechanism, where the thiol is deprotonated and reacts with the alkene moiety of the methacrylate functional group. This addition reaction can occur in water and under mild conditions with high yields, which were important characteristics that gave preference for this reaction over the traditional carbodiimide methodologies [94], [95].

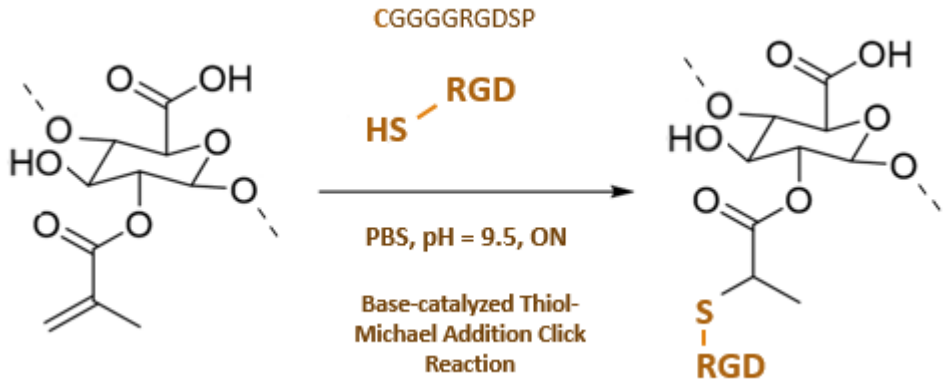


Figure 14 - Synthesis of RGD-modified methacrylated alginate (AlgMaRGD) - Grafting of a bioactive peptide containing the amino acid sequence RGD onto the methacrylated alginate through thiol-Michael addition click reaction

The success of the conjugation reaction was confirmed by ^{1}H-NMR, where it was possible to observe new peaks corresponding to the cell-adhesive peptide protons (Figure 15).

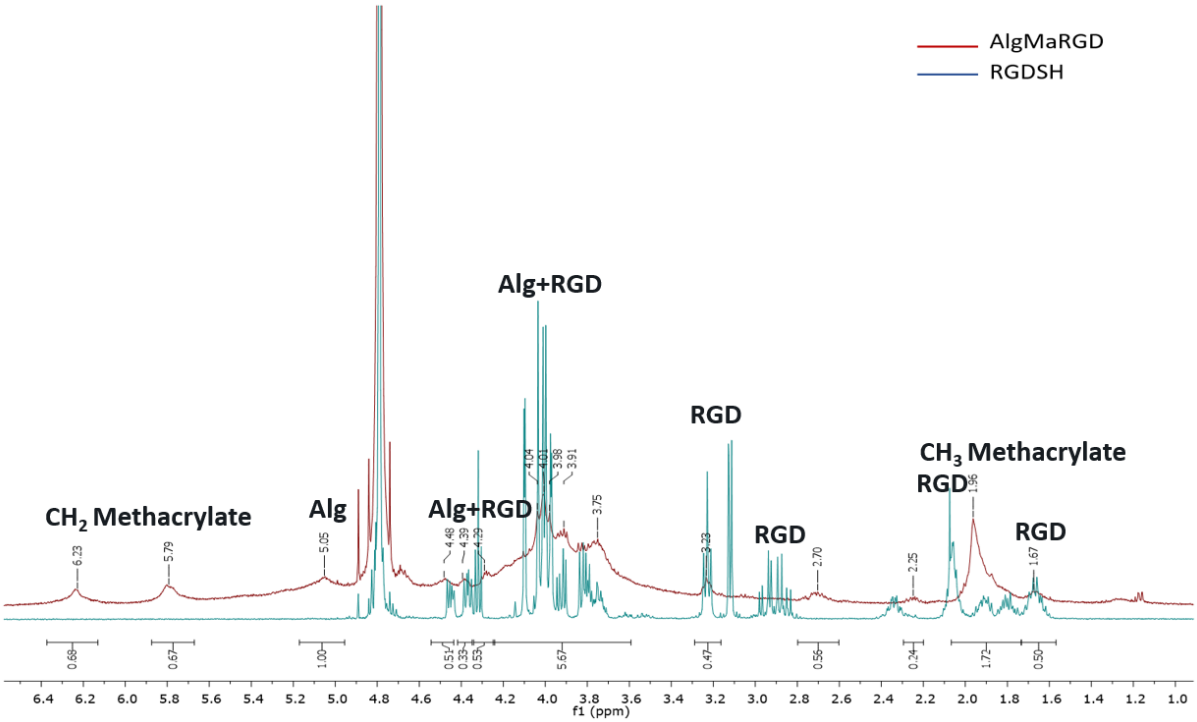


Figure 15 - ^{1}H-NMR spectrum of methacrylated alginate functionalized with the cell-adhesive peptide (AlgMaRGD)

ATR/FTIR spectra for high molecular weight alginate (AlgHMW), AlgMa, AlgMaRGD and the peptide containing the amino acid sequence RGD, were recorded (Figure 16). Few noticeable changes were found among the obtained spectra. Characteristic peaks at 1600 cm^{-1} and 1410 cm^{-1} were observed for AlgHMW and AlgMa samples. These peaks may be assigned to asymmetric and symmetric —C=O stretching vibrations of COO^- groups, respectively [139]. The coupling of methacrylate moieties to the alginate structure in AlgMa led to a sharpening within the broad range 3500-3000 cm^{-1}, when compared to the ATR/FTIR spectrum of AlgHMW. Such band may be assigned to O-H stretching of methacrylic moieties. Moreover, the spectrum of AlgMa also showed a sharpening at 1596 cm^{-1} due to stretching vibrations of carbonyl groups from the methacrylate moieties introduced. It was also possible to observe a characteristic peak at 1635 cm^{-1} for the ATR/FTIR spectrum of RGD-peptide, assigned to carbonyl stretching vibration in amide groups [140]. An amide II characteristic peak at 1532 cm^{-1} was also noticed regarding the peptide spectrum. Both these peaks were not found in any of the alginate-derived spectra probably due to the low concentration (200 μM) of RGD-peptide that is present in those polymers.

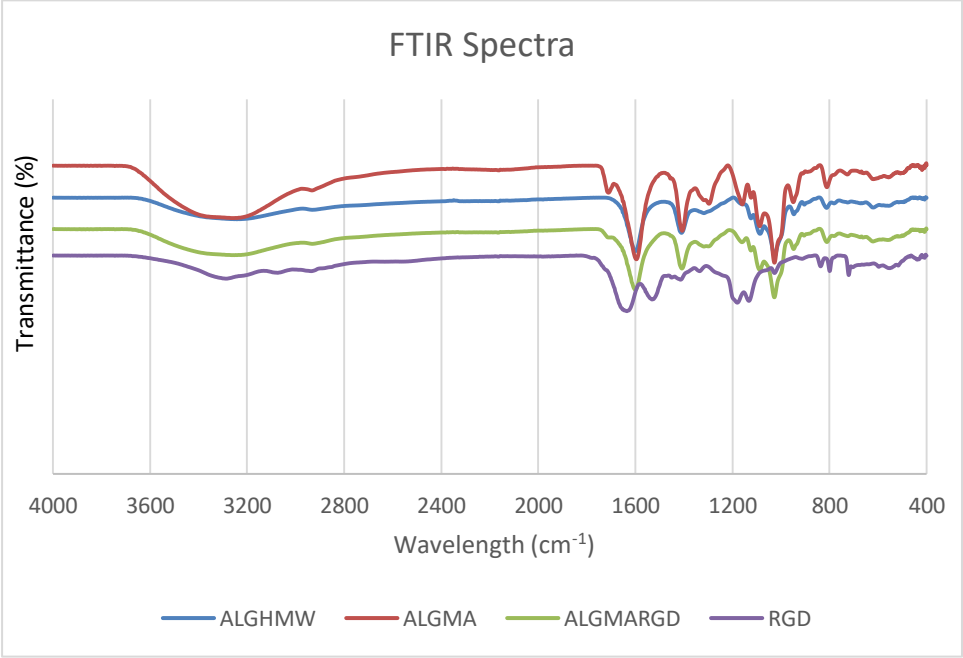


Figure 16 - ATR/FTIR spectra of high molecular weight alginate (AlgHMW), methacrylated alginate (AlgMa), RGD-modified methacrylated alginate (AlgMaRGD), and the RGD-containing peptide (RGD)

The amount of cell-adhesive peptide grafted onto AlgMa was 71 mg peptide/g AlgMa, as determined by the colorimetric DC protein assay. This represents an incorporation of 35% of the initial amount of peptide that participated in the coupling reaction. However, considering that the polymer presents a degree of methacrylation of, approximately, 50%, this means that the overall incorporation in respect to the available methacrylate groups was 70%.

3.3 Characterization of melanin particles

The structure of melanin particles was investigated by ATR-FTIR (Figure 17). The obtained spectrum presented strong peaks in the 3700-3000 cm^{-1} range, at 1582 cm^{-1} and 1358 cm^{-1}, and in the 780-596 cm^{-1} range. In the 3700-3000 cm^{-1} range, the broad peak may be due to νO-H and νN-H stretching vibration modes [141]. The peak at ca. 1582 is due to νC=O and νC=C stretching modes from carbonyl and conjugated double bonds, respectively, while the peak at ca. 1358 cm^{-1} is assigned to in-plane βC-H bending modes [141]. In the 780-596 cm^{-1} range, the wide band is assigned to the δO=C=O deformation mode of carboxyl groups [142].

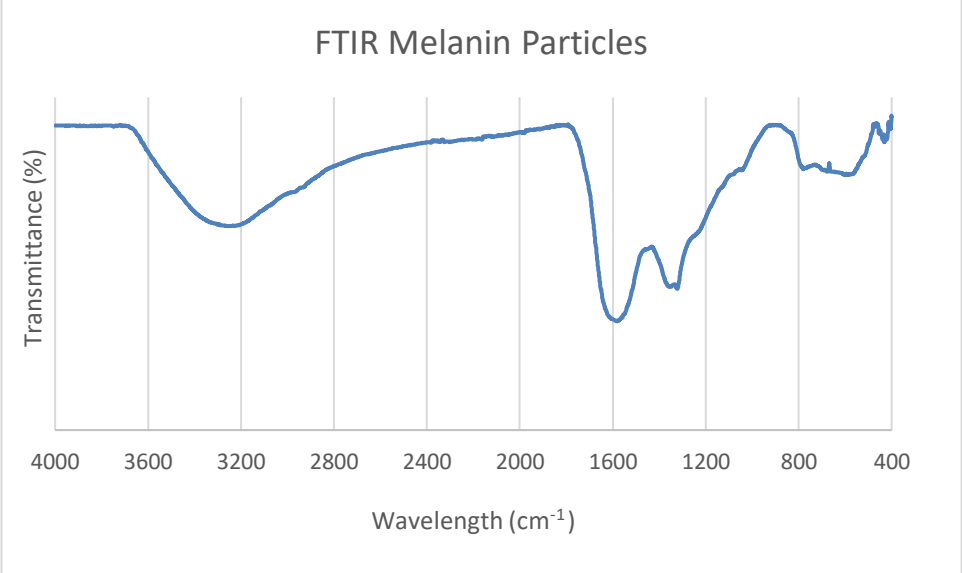


Figure 17 - ATR/FTIR spectrum of melanin particles

TEM images of melanin particles were kindly provided by Laura Marín Caba from the research group TeamNanotech at Universidad de Vigo (Figure 18).

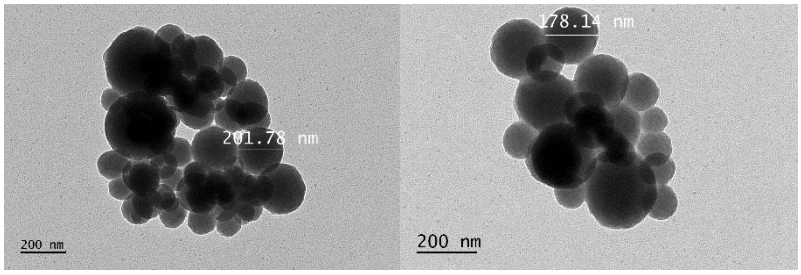


Figure 18 - TEM images of melanin particles

Through the analysis of the TEM images, it was possible to observe particles with spherical morphology exhibiting a dimension between 180 and 200 nm, which is in accordance with the shape and dimensions reported in the literature [143].

3.4 Development and characterization of the multi-functional alginate-based patch

3.4.1 Preparation of photocrosslinked alginate hydrogels

Alginate hydrogel discs were fabricated through photocrosslinking of a gel precursor solution in the presence of Irgacure 2959 as photoinitiator. A mixture of AlgMa and AlgMaRGD was adjusted in order to grant a final RGD concentration within the hydrogel of 200 μM, which is within the same range of that presented in ECM-derived biological matrices [144]. Free radicals generated upon exposure of the photoinitiator to UV radiation contributed to the alginate covalent crosslinking through both radical polymerization and radical-initiated thiol-ene photopolymerization. The presence of a peptide crosslinker allowed the latter covalent crosslinking strategy to occur due to its functionalization with terminal thiol groups of the amino acid cysteine at both ends. It is important to determine the amount of MMP-cleavable peptide that is covalently coupled to the polymer, since this peptide can affect the crosslinking density of the hydrogel network and, thus, the mechanical properties of the scaffold. Melanin nanoparticles were incorporated in the hydrogel structure during the gelation process.

Proof of MMP-sensitive peptide grafting was obtained through ATR/FTIR analysis of hydrogel formulations with no melanin nor MMP-cleavable peptide (Blank), no melanin and a peptide concentration of 4 mM (Pep4) and a melanin content of 0.3 wt% and a peptide concentration of 4 mM (Mel0.3Pep4) (Figure 19). The spectrum of the enzymatically degradable peptide was also recorded. New characteristic peaks in the Pep4 and Mel0.3Pep4 spectra were observed when compared to the Blank spectrum, at 1596 and 1410 cm^{-1}, due to the coupling of the peptide crosslinker. The first peak (1596 cm^{-1}) is assigned to amide I bonds from peptides [145]. The peak at 1410 cm^{-1} is due to amide III bonds [145], which are characteristic of proteins.

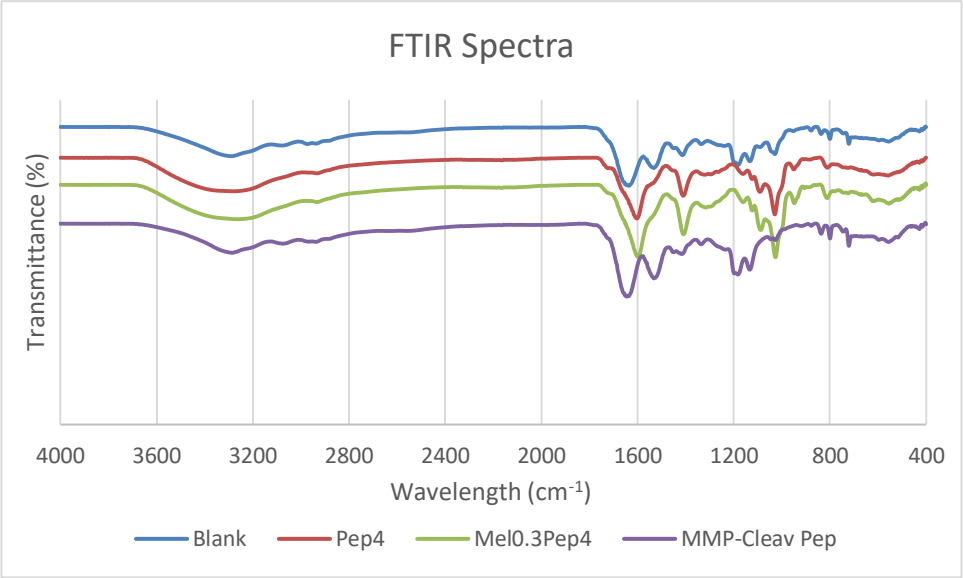


Figure 19 - ATR/FTIR spectra of the MMP-cleavable peptide and hydrogels with different composition. Blank hydrogels refer to constructs without melanin and MMP-sensitive peptide. Pep4 represent hydrogels without melanin and a peptide concentration of 4 mM. Mel0.3Pep4 refer to scaffolds with a melanin content of 0.3 wt% and a peptide molar concentration of 4 mM.

Influence of MMP-cleavable peptide and melanin quantities

Precursor gel solutions with different MMP-cleavable peptide concentration, namely 4 mM (Pep4) and 8 mM (Pep8), and different melanin content, such as 0.3 wt% (Mel0.3), 0.45 wt% (Mel0.45) and 0.6 wt% (Mel0.6) have been photocrosslinked by exposure to UV radiation. The first goal of this approach was to obtain stable hydrogel discs to evaluate their radical scavenging activity. Regarding this, it was interesting to change melanin concentration within the hydrogel in order to evaluate if the entrapment of a higher melanin content would result in higher radical scavenging ability. Furthermore, the amount of peptide crosslinker was changed in order to better promote hydrogel formation in the presence of higher concentrations of melanin particles. To fabricate such hydrogels, the precursor gel solutions were photopolymerized for 5 minutes (300 s). Formulations containing a melanin concentration of 0.6 wt% and without crosslinker failed to form stable constructs after 300 s. Consequently, as it was not possible to obtain the necessary controls to the assays to be carried out, the melanin concentration of 0.6 wt% was discarded. Regarding formulations without the peptide crosslinker and varying melanin content (0.0 wt%, 0.3 wt% and 0.45 wt%), the most stable hydrogel networks were fabricated after 300 s, so this was the time selected as reference for the majority of hydrogels to be analysed.

Furthermore, it was noticed that the incorporation of the peptide crosslinker allowed the formation of stable hydrogel networks after 300 s of photopolymerization (Figure 20). Hydrogels without the peptide crosslinker and with a melanin content of 0.3 wt% (Mel0.3 hydrogels) were more difficult to handle and less stable than hydrogels containing the same melanin content and a peptide crosslinker concentration of 4 mM (Mel0.3Pep4 hydrogels) or 8 mM (Mel0.3Pep8 hydrogels). Moreover,

noticeable changes were not found regarding the macroscopic appearance between Mel0.3Pep4 hydrogels and gels with the same amount of MMP-cleavable peptide and an increased melanin concentration of 0.45 wt% (Mel0.45Pep4 hydrogels) (Figure 20). This results show that the coupling of the peptide crosslinker induces a higher crosslinking density and, consequently, more stable hydrogel networks, allowing an efficient melanin incorporation. Increasing the peptide crosslinker concentration to 8 mM, while maintaining the melanin content at 0.3 wt% (Mel0.3Pep8 hydrogels) also did not produce significant changes regarding the overall handling and stability of the hydrogels, as no noticeable changes were found when compared to Mel0.3Pep4 hydrogels (Figure 20).

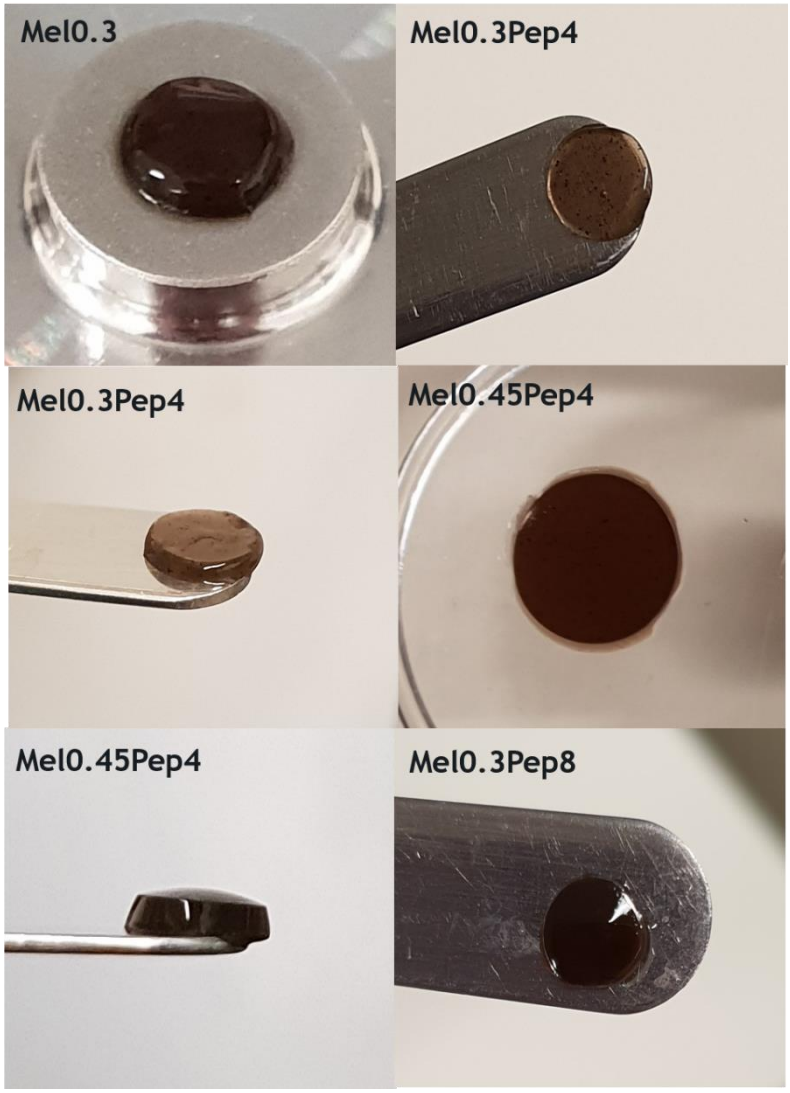


Figure 20 - Hydrogels formed after 300 s of photopolymerization, with varying concentrations of melanin and peptide crosslinker. Mel0.3 refer to scaffolds with a melanin content of 0.3 wt% and no MMP-cleavable peptide. Mel0.3Pep4 refer to scaffolds with a melanin content of 0.3 wt% and a peptide molar concentration of 4 mM. Mel0.45Pep4 refer to scaffolds with a melanin content of 0.45 wt% and a peptide molar concentration of 4 mM. Mel0.3Pep8 refer to scaffolds with a melanin content of 0.3 wt% and a peptide molar concentration of 8 mM.

Influence of photocrosslinking time

The photocrosslinking time was optimized using a formulation containing melanin and the MMP-cleavable peptide, namely Mel0.3Pep4. Hydrogels were photocrosslinked for different time periods (60 s, 70 s, 80 s, 90 s, 100 s, 140 s and 300 s) in order to achieve the minimum UV exposure time required to produce a stable hydrogel. It was found that, after 60 s, hydrogels did not acquire the structural stability needed in order to be easily handled without leaving gel-forming material in the glass slides. As this would prevent reproducible hydrogels to be obtained, the crosslinking time of 60 s was discarded. For the remaining gelation times, it was demonstrated that a higher photopolymerization time produces alginate-based constructs that present a more stable gel network (Figure 21). Therefore, Mel0.3Pep4 hydrogels fabricated after a higher UV exposure time of the precursor solution are easier to handle and present an enhanced structural stability.

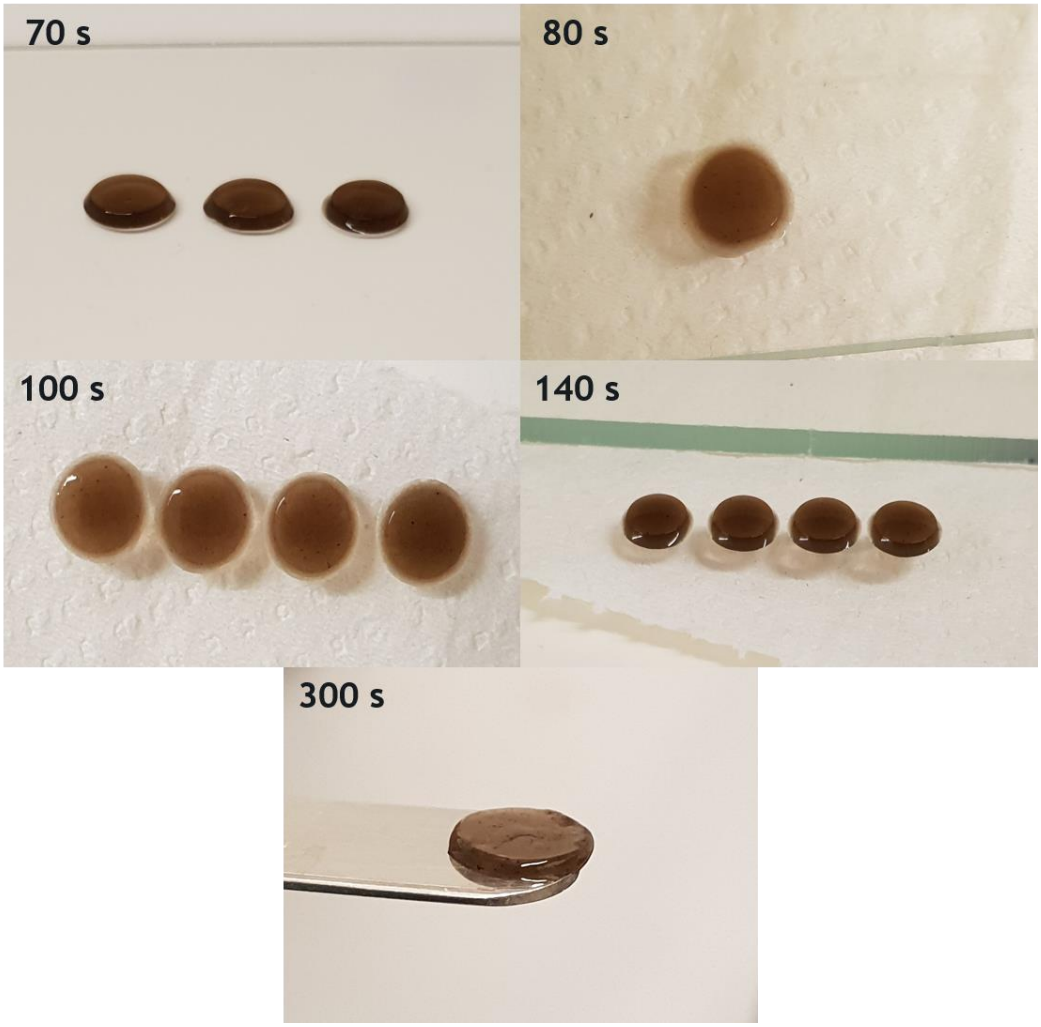


Figure 21 - Mel0.3Pep4 hydrogels were photocrosslinked for different time periods (70 s, 80 s, 100 s, 140 s and 300 s) to study the structural stability of the newly formed gel network. Mel0.3Pep4 refer to scaffolds with a melanin content of 0.3 wt% and a peptide molar concentration of 4 mM.

Influence of the freeze-drying process

Freeze-dried hydrogels were prepared, since the developed platform should be 1) adaptable, 2) easy to produce and ready-to-use, 3) present adequate mechanical properties, 4) easy to store and to handle. Therefore, it was important to study whether the freeze-drying process can affect the mechanical and biological properties of the designed patch, in order to validate the use of the platform as a lyophilized hydrogel construct, which would potentially show the versatility of the engineered biomaterial.

Differences in the macroscopic appearance between non-lyophilized and lyophilized hydrogels may be observed in formulations with no melanin and no MMP-cleavable peptide (Blank), as well as in Pep4 and Mel0.3Pep4 hydrogels (Figure 22).

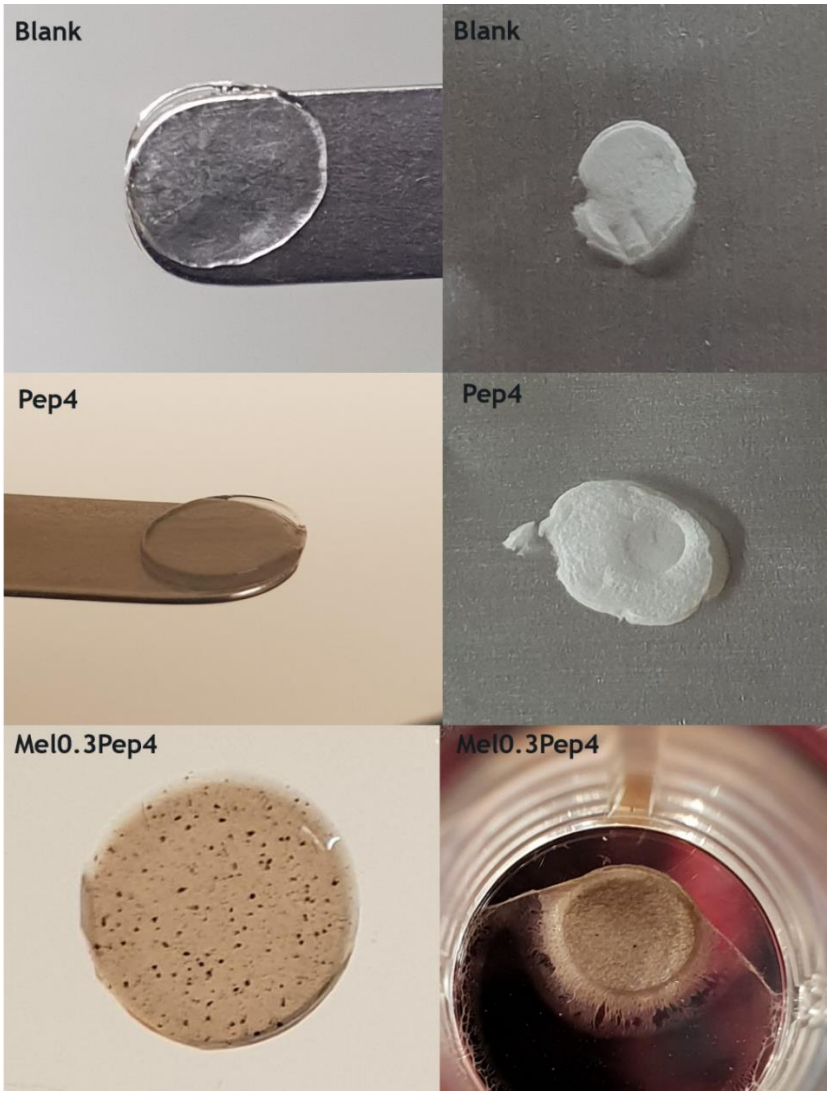


Figure 22 - Blank, Pep4 and Mel0.3Pep4 hydrogels before (left) and after (right) the freeze-drying process. All hydrogel samples were photocrosslinked for 300 s. Blank hydrogels refer to constructs without melanin and MMP-sensitive peptide. Pep4 refer to hydrogels without melanin and a peptide molar concentration of 4 mM. Mel0.3Pep4 refer to scaffolds with a melanin content of 0.3 wt% and a peptide molar concentration of 4 mM.

After the freeze-drying process, the hydrogel presents a sponge-like aspect and an interconnected porous structure for all the hydrogel samples evaluated.

Furthermore, alginate hydrogel fibers may be observed for the three formulations tested (Figure 23). The presence of melanin nanoparticles can be noticed for Mel0.3Pep4 hydrogels.

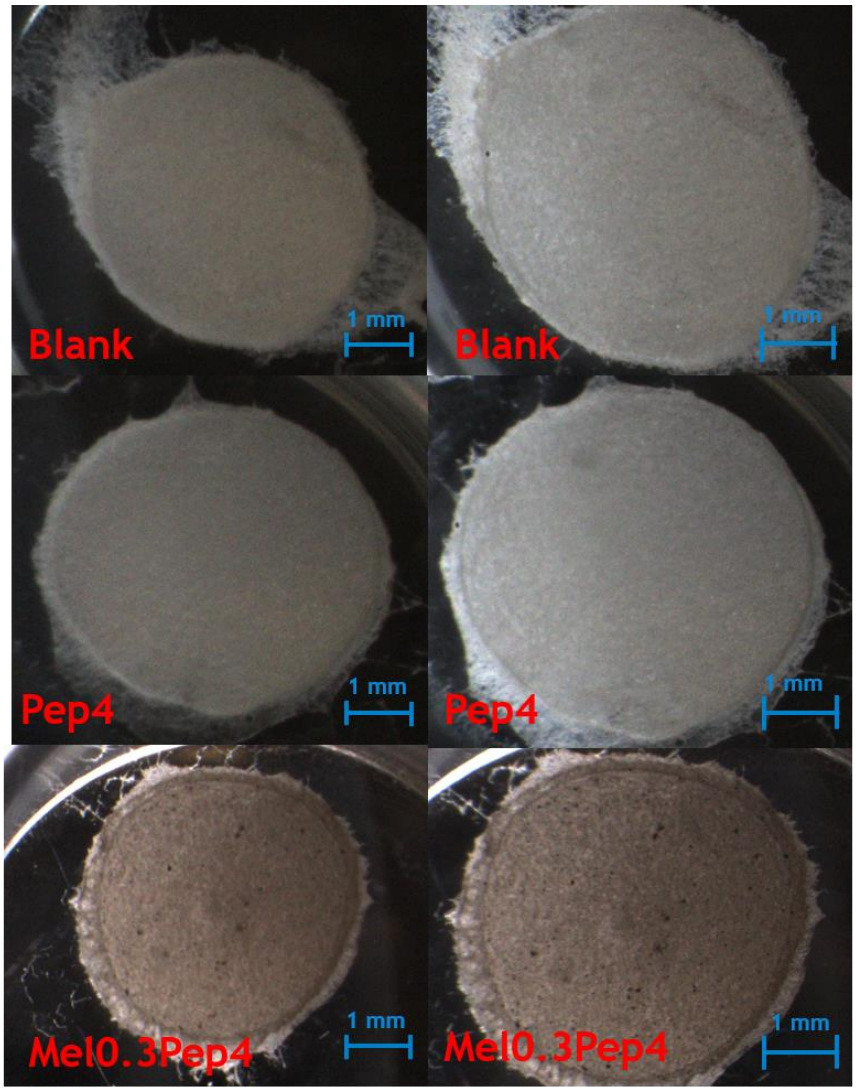


Figure 23 - Blank, Pep4 and Mel0.3Pep4 freeze-dried hydrogels. All hydrogel samples were photocrosslinked for 300 s. Blank hydrogels refer to constructs without melanin and MMP-sensitive peptide. Pep4 refer to hydrogels without melanin and a peptide molar concentration of 4 mM. Mel0.3Pep4 refer to scaffolds with a melanin content of 0.3 wt% and a peptide molar concentration of 4mM.

The aspect of freeze-dried Mel0.3Pep4 hydrogels before and after rehydration may also be observed (Figure 24). Upon rehydration, lyophilized hydrogels maintained their structural integrity and were easily handled.

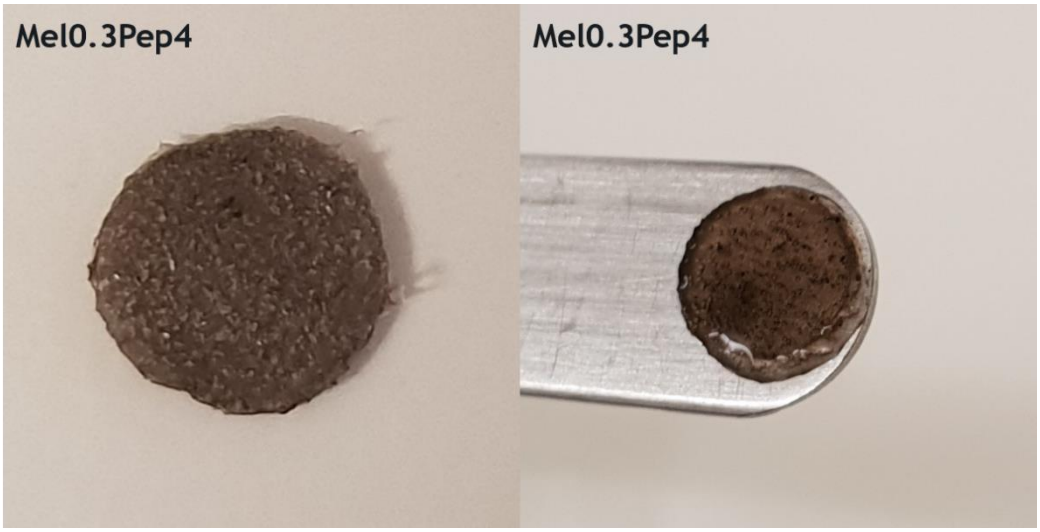


Figure 24 - Freeze-dried Mel0.3Pep4 hydrogels before (left) and after rehydration (right). Mel0.3Pep4 refer to scaffolds with a melanin content of 0.3 wt% and a peptide molar concentration of 4mM

3.4.2 Coupling efficiency of the MMP-cleavable peptide

The amount of MMP-cleavable peptide incorporated onto the alginate hydrogel network was evaluated through the Ellman's assay.

5,5′-dithiobis-(2-nitrobenzoic) acid (DTNB, Ellman's reagent) is a chromogenic reagent usually used for thiol detection, since it has a highly oxidizing disulfide bond. Therefore, free thiols in solution may stoichiometrically reduce this bond in an exchange reaction, leading to the formation of a mixed disulfide and the release of one molecule of 5-thio-2-nitrobenzoic acid (TNB) (Figure 25) [146]. As the MMP-cleavable peptide presents the amino acid cysteine (which contains a thiol group) at both ends, measuring the thiol content of a solution where hydrogel discs were immersed may indirectly estimate the extent of incorporation of the MMP-cleavable peptide.

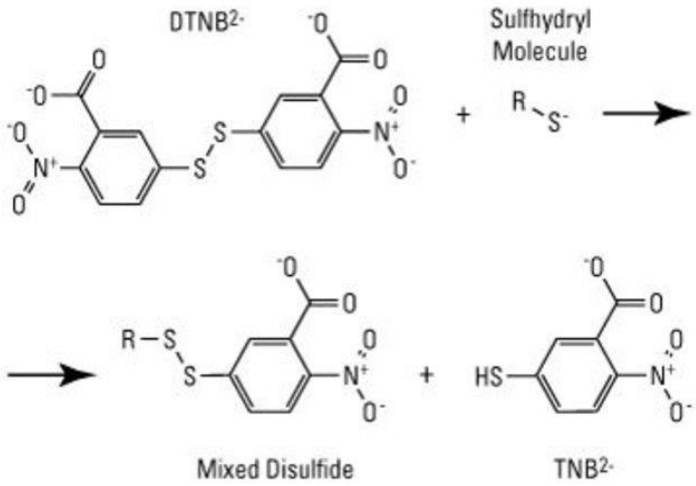


Figure 25 - Chemical reaction between the Ellman's reagent (DTNB) and free thiols in the DTNB assay [147]

Hydrogel samples with different compositions and the same photocrosslinking time (300 s) were tested (Figure 26 – A). Hydrogels were prepared with different MMP-cleavable peptide molar concentrations, namely 4 mM (Pep4) and 8 mM (Pep8), and varying melanin content (0 wt%, 0.3 wt% (Mel0.3) and 0.45 wt% (Mel 0.45)).

Results (Figure 26 - A) show that the incorporation percentage of both molar concentrations tested, Pep4 and Pep8, while maintaining the melanin content at a constant amount, were approximately the same. The coupling percentage varied between 93.67 ± 1.42 (Pep4) and 94.78 ± 0.71 (Pep8) for hydrogels with no melanin, 75.59 ± 4.27 (Pep4) and 76.70 ± 5.37 (Pep8) for Mel0.3 samples and 70.66 ± 6.52 (Pep4) and 68.07 ± 3.70 (Pep8) for Mel0.45 hydrogels.

Therefore, a variation on the peptide incorporation percentage was detected when altering the melanin concentration, while the MMP-cleavable peptide molar concentration was kept constant. In fact, a decrease of the coupling efficiency was noticed with an increase of melanin content.

Moreover, hydrogel samples with the same composition (Mel0.3Pep4), but different testing conditions, were also analysed. Freeze-dryed hydrogel samples (Liof) produced after 300 s of photocrosslinking and hydrogels fabricated after 100 s and 300 s of UV light exposure were analysed (Figure 26 – B). All hydrogel samples produced similar results, as the peptide incorporation percentage was determined as 75.59 ± 4.27 for Mel0.3Pep4, 82.43 ± 4.24 for Mel0.3Pep4Liof and 75.95 ± 7.34 for Mel0.3Pep4 100 s.

Importantly, the partial incorporation of the amount of MMP-cleavable peptide added to the hydrogel should be considered in order to more precisely estimate the actual peptide concentration within the hydrogel.

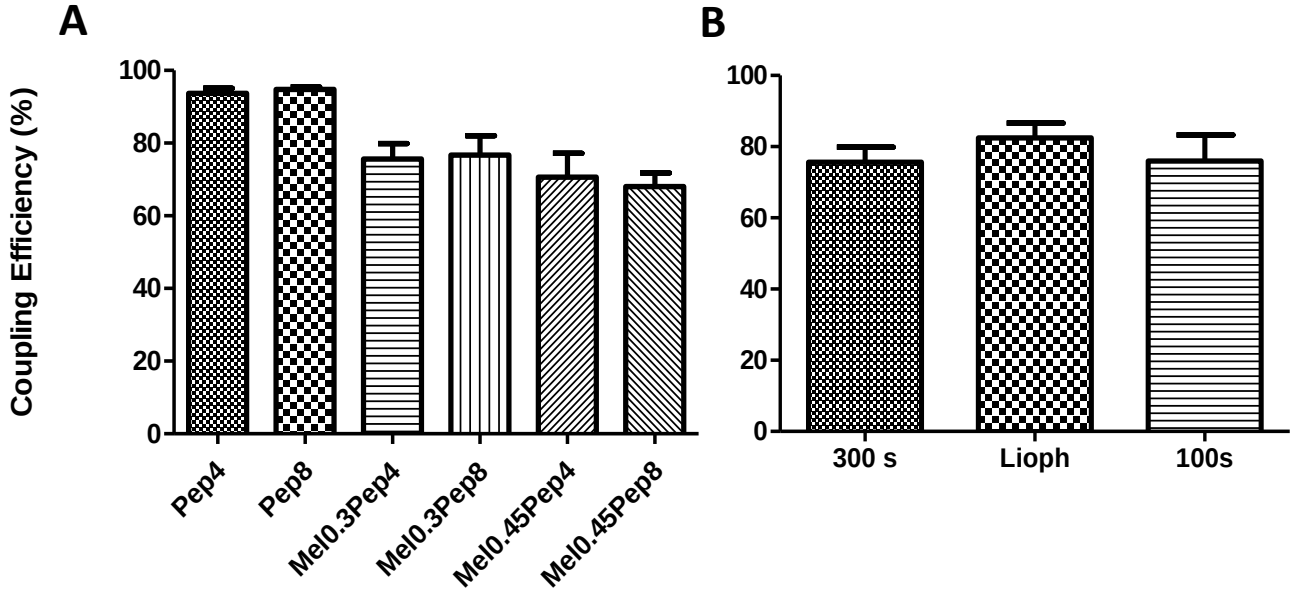


Figure 26 - Coupling Efficiency of the MMP-Sensitive Peptide was determined through a DTNB assay. (A) - All hydrogel samples present different compositions and were photocrosslinked after 300 s; Mel0.3 and Mel 0.45 refer to melanin concentrations within the hydrogel of 0.3 wt% and 0.45 wt%, respectively; Pep 4, Pep 8 refer to MMP-cleavable peptide molar concentrations of 4 mM and 8 mM, respectively. (B) - All hydrogel samples present the same composition (Mel0.3Pep4). The effect of the freeze-drying process and of the photocrosslinking time on the MMP-cleavable peptide incorporation was studied, since freeze-dryed hydrogel samples (Liof) and hydrogel samples fabricated after 100 s and 300 s of UV light exposure were analysed.

3.4.3 Free-radical scavenging activity

The radical scavenging activity of the hydrogel samples was assessed through the DPPH assay.

2,2-Diphenyl-1-picryl-hydrazyl (DPPH) is a purple-colored stable free radical that presents an unpaired valence electron at one nitrogen atom (Figure 27) [148]. The stability of the DPPH molecule is due to the delocalization of the spare electron over the entire molecule. Antioxidants can then donate a hydrogen atom and therefore reduce the stable DPPH radicals to the yellow compound diphenyl-picrylhydrazine (Figure 27) [149]. As free DPPH radicals present a maximum absorbance value at 517 nm, whenever these radicals interact with a proton donor substrate, they are removed and the absorbance at this particular wavelength decreases [149]. Therefore, the radical scavenging activity can be measured as a decrease in the absorbance of DPPH, since a lower absorbance of the reaction mixture means a higher free radical scavenging activity, as seen in the work of Kumar et al. [150].

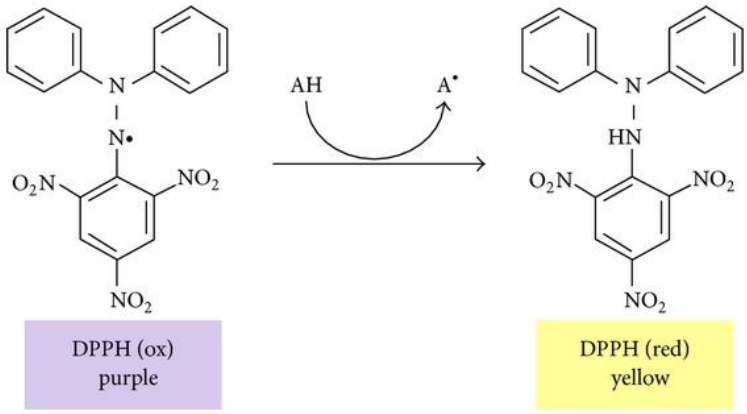


Figure 27 - Reaction mechanism of DPPH with an antioxidant. AH – antioxidant radical scavenger A˙ - antioxidant radical. Retrieved from [151].

The DPPH assay was performed on hydrogels with varying melanin concentrations (0 wt%, 0.3 wt% (Mel0.3) and 0.45 wt% (Mel0.45)). The possible influence of the peptide crosslinker on the radical scavenging ability of the hydrogels was also assessed by evaluating hydrogel formulations with 4 mM (Pep4) and 8 mM (Pep8) MMP-cleavable peptide. The kinetics of radical scavenging were evaluated for different time points, namely 2h, 3h, 6h, 9h and overnight (ON).

Results show a great variation on the radical scavenging activity from hydrogels with and without melanin nanoparticles, independently of the MMP-cleavable peptide concentration (Figures 28, 29 and 30).

The influence of a higher melanin content in the radical scavenging activity of the hydrogels was evaluated by varying the concentration of melanin in the hydrogel (0 wt%, 0.3 wt% and 0.45 wt%), while maintaining the MMP-sensitive peptide concentration constant (0 mM, 4 mM or 8mM).

Regarding hydrogels without the peptide crosslinker (Figure 28), the scaffolds without melanin (Blank hydrogels) presented low radical scavenging activity throughout all time points, with a peak of

radical scavenging activity at 6h (16.8 ± 2.0 %). Hydrogels with 0.3 wt% (Mel0.3) and 0.45 wt% melanin (Mel0.45) presented a higher free radical scavenging ability than Blank hydrogels. Overall, Mel0.3 and Mel0.45 samples presented a similar radical capture, with a peak of activity after being incubated overnight (Mel0.3 76.1 ± 1.8 % and Mel0.45 73.3 ± 3.9 %). Concerning earlier time points, Mel0.45 hydrogels (2h: 20.5 ± 0.4 %; 3h: 27.6 ± 1.1 %) presented higher scavenging activity than Mel0.3 hydrogels (2h: 14.5 ± 5.4 %; 3h: 21.1 ± 2.3 %), while at later time points, the opposite situation was observed (Mel0.3 – 6h: 35.2 ± 2.2 %; 9h: 46.1 ± 1.1 %; Mel0.45 – 6h: 31.7 ± 2.0 %; 9h: 36.7 ± 6.4 %).

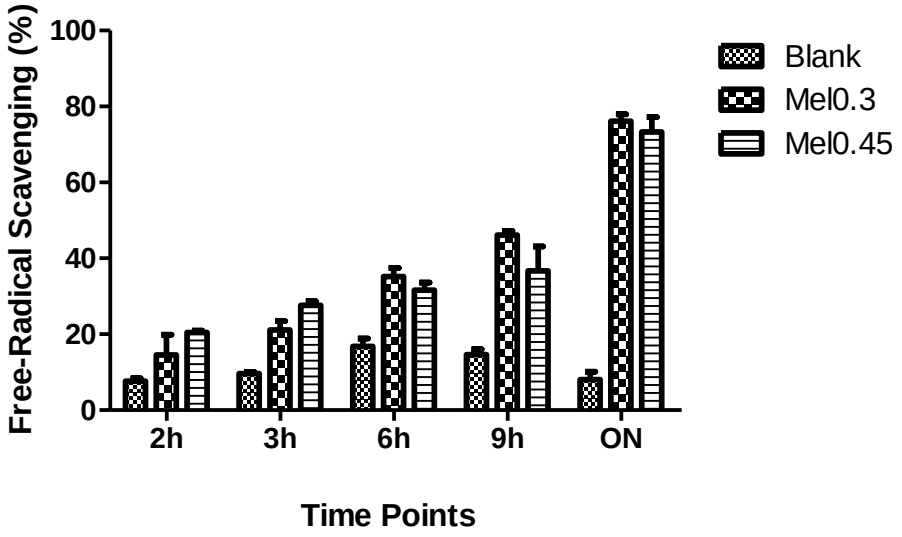


Figure 28 - Free-radical scavenging ability of the hydrogels through different time points, namely 2h, 3h, 6h, 9h and overnight (ON) was determined via the DPPH assay. All hydrogel samples present different composition and were photocrosslinked after 300 s. Although samples do not contain the MMP-cleavable peptide, they present varying melanin concentrations (0 wt% (Blank); 0.3 wt% (Mel 0.3); 0.45 wt% (Mel 0.45)).

For hydrogels with a MMP-cleavable peptide molar concentration of 4 mM (Figure 29), scaffolds without melanin (Pep4) were the hydrogels that showed lower radical scavenging activity after overnight incubation (48.5 ± 4.7 %).

However, for all the remaining time points, Pep4 hydrogels (2h: 9.7 ± 3.4 %; 3h: 22.9 ± 1.0 %; 6h: 28.8 ± 2.1 %; 9h: 38.7 ± 2.1 %) presented similar results when compared to melanin-containing hydrogels. Mel0.3Pep4 and Mel0.45Pep4 hydrogels showed similar DPPH scavenging ability for all time points, including a rather high radical scavenging activity after being incubated overnight (Mel0.3Pep4 – 87.8 ± 1.8 %; Mel0.45Pep4 – 87.0 ± 1.1 %).

Furthermore, radical scavenging activity was compared between hydrogels and free melanin nanoparticles at a similar concentration (0.3 wt% (MelNP0.3) and 0.45 wt% (MelNP0.45)). Results showed a higher DPPH radical scavenging activity of MelNP0.45 for the first time points (2h: 40.1 ± 5.8 %; 3h: 55.0 ± 2.6 %; 6h: 75.0 ± 1.0 %; 9h: 83.7 ± 0.9 %) when compared to the one of Mel0.3Pep4 and Mel0.45Pep4 hydrogels and of MelNP0.3 (2h: 24.0 ± 1.7 %; 3h: 27.3 ± 0.2 %; 6h: 39.0 ± 1.1 %; 9h: 45.7 ± 1.8 %). MelNP0.3 presented similar results to these two types of hydrogel samples, regardless the higher free radical scavenging activity for the first time point (2h).

Although free melanin nanoparticles presented a higher scavenging ability in the first time points, after overnight incubation, the free-radical scavenging activity of the hydrogels was similar to the free biopolymeric nanoparticles (MelNP0.3 – 71.4 ± 4.0 %; MelNP0.45 – 85.8 ± 4.7 %), with MelNP0.3 presenting lower DPPH scavenging activity than the hydrogels. This indicates that for a melanin concentration of 0.3 wt%, the kinetics of radical scavenging activity of free and entrapped melanin nanoparticles is, approximately, the same.

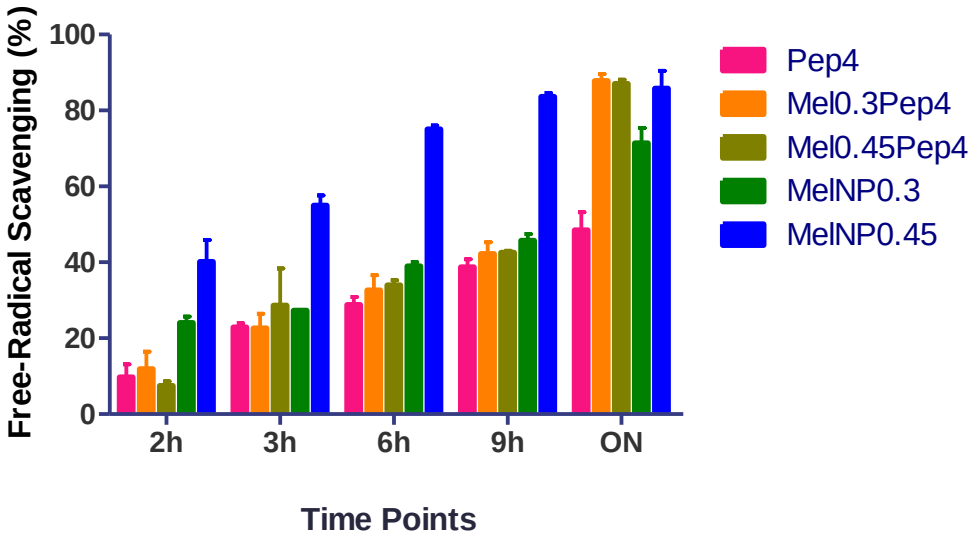


Figure 29 - Free-radical scavenging ability was assessed through different time points, namely 2h, 3h, 6h, 9h and overnight (ON). Hydrogels were prepared with a varying concentration of melanin (0 wt%; 0.3 wt% (Mel 0.3); 0.45 wt% (Mel 0.45)). All hydrogel samples contain a MMP-cleavable peptide molar concentration of 4 mM (Pep4) and were photocrosslinked for 300 s. Pep4 refers to a hydrogel without melanin. MelNP refers to free melanin nanoparticles

Regarding hydrogels with a peptide crosslinker concentration of 8 mM (Figure 30), scaffolds without melanin (Pep8) showed low free radical scavenging activity, as expected. The peak of activity for Pep8 hydrogels was observed at the last time point evaluated (overnight - 23.5 ± 5.3 %). Hydrogels with both 0.3 wt% (Mel0.3Pep8) and 0.45 wt% (Mel0.45Pep8) melanin concentrations presented similar DPPH scavenging activity at 3h and a rather high one after being incubated overnight (Mel 0.3Pep8 – 87.3 ± 0.3 %; Mel0.45Pep8 – 89.0 ± 0.7%). However, for the remaining time points Mel0.45Pep8 hydrogels showed a slightly higher free-radical scavenging ability (2h: 23.8 ± 4.7 %; 6h: 39.2 ± 3.1 %; 9h: 53.8 ± 1.3 %) than Mel0.3Pep8 constructs (2h: 11.7 ± 5.8 %; 6h: 33.0 ± 4.8 %; 9h: 43.6 ± 2.1 %).

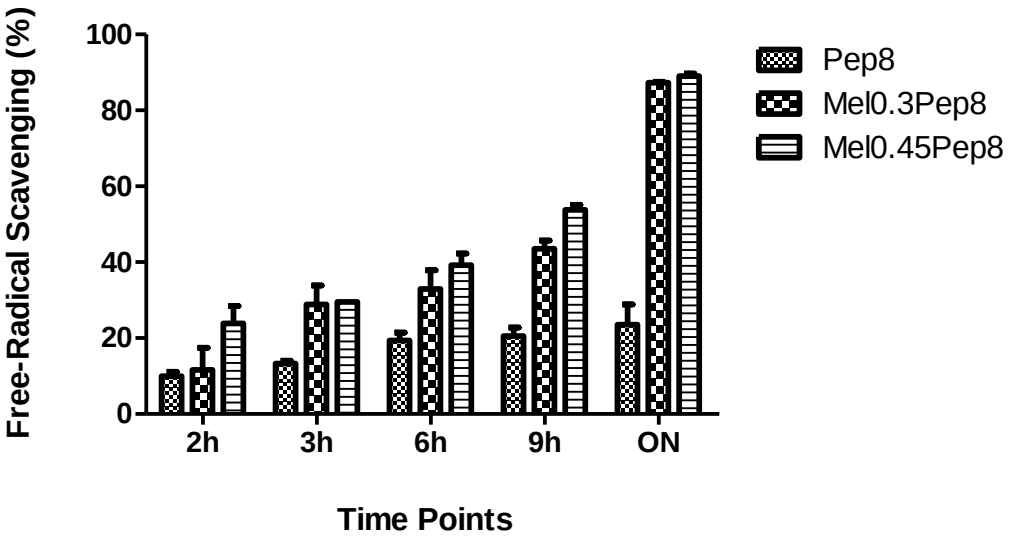


Figure 30 - Free-radical scavenging ability of hydrogels. All hydrogel samples present different composition and were photocrosslinked after 300 s. All samples contain a MMP-cleavable peptide molar concentration of 8 mM (Pep8). Pep8 refers to a hydrogel without melanin. Mel0.3 and Mel0.45 refer to a melanin content of 0.3 wt% and 0.45 wt%, respectively

Therefore, the hydrogel antioxidant activity was increased when adding melanin to the construct, comparing with samples containing no melanin. Furthermore, it was observed that increasing the melanin content from 0.3 wt% to 0.45 wt%, while maintaining the molar concentration of MMP-cleavable peptide constant, did not result in an increase of radical scavenging activity.

In addition, similar free-radical scavenging activity was observed for hydrogels with the same melanin content and varying peptide concentration, for all groups and all time points.

Moreover, the influence of the freeze-drying process and of the hydrogel photocrosslinking time on the free-radical scavenging activity of hydrogels was also tested with the Mel0.3Pep4 as the selected hydrogel formulation (Figure 31). For the first two time points, namely after 2h and 3h, all samples presented similar results. For the next two time points, Mel0.3Pep4 Liof hydrogels showed a slightly higher free-radical scavenging activity (6h: 44.3 ± 6.8 %; 9h: 62.1 ± 1.6 %) than Mel0.3Pep4 (6h: 32.6 ± 4.0 %; 9h: 42.2 ± 3.1 %) and Mel0.3Pep4 100 (6h: 33.9 ± 2.9 %; 9h: 37.4 ± 4.5 %). However, after being incubated overnight, Mel0.3Pep4 hydrogels presented the highest DPPH scavenging activity (87.8 ± 1.8 %), comparing with both Mel0.3Pep4 Liof (72.1 ± 1.7 %) and Mel0.3Pep4 100 (64.5 ± 8.1). Overall, all hydrogel samples presented similar free-radical scavenging activity, which means the freeze-drying process and different photopolymerization times may not affect the radical scavenging ability of the developed biomaterial.

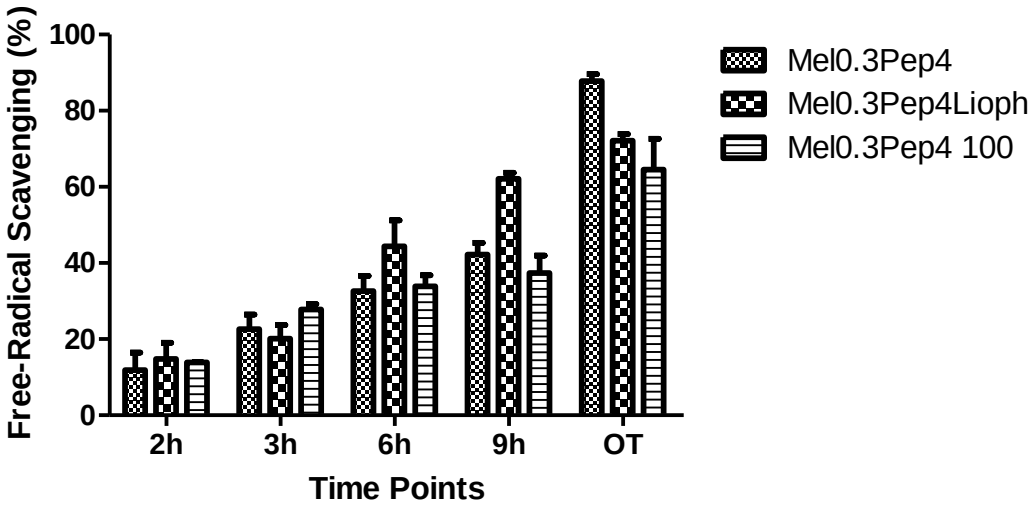


Figure 31 - Free-radical scavenging ability of the hydrogels. All hydrogel samples present the same composition (Mel0.3Pep4). Mel0.3Pep4 refer to scaffolds with a melanin content of 0.3 wt% and a peptide molar concentration of 4mM. The effect of the freeze-drying process and of the photocrosslinking time on the free-radical scavenging ability of the constructs was studied, since freeze-dryed hydrogel samples (Liof) and hydrogel samples fabricated after 100 s and 300 s of UV light exposure were analysed.

3.4.4 Rheological properties

The rheological properties of the fabricated hydrogel discs were evaluated by performing both strain-sweep and frequency-sweep (data not shown) analysis. All hydrogels show a higher shear elastic modulus (G') than shear viscous modulus (G''), which means all samples present a gel or solid-like behavior, as expected.

Viscoelastic properties of Mel0.3Pep4 hydrogels were determined for different gelation times, namely 70 s, 80 s, 100 s, 140 s and 300 s (Figure 32), in order to study the influence of the photocrosslinking time alone on the mechanical properties of the hydrogels with the same composition.

The elastic component of shear modulus (G') was tailored in a wide range (87.7 ± 3.9 Pa for the hydrogel formed after 70 s to 2886.7 ± 93.5 Pa for the hydrogel fabricated after 300 s of UV exposure) by simply varying the UV radiation exposure time (70 s, 80 s, 100 s, 140 s, 300 s). The viscous component of shear modulus (G'') was also tailored in a broad range (28.2 ± 2.6 Pa for a hydrogel formed after 70 s of UV exposure to 636.8 ± 26.0 Pa for hydrogels fabricated after 300 s of UV irradiation).

A higher UV exposure time led to higher values of both G' and G'', with hydrogels formed after 80 s (G': 110.5 ± 4.5 Pa; G'': 41.8 ± 8.7 Pa), 100 s (G': 279.5 ± 11.4 Pa; G'': 39.5 ± 2.9 Pa) and 140 s (G': 637.0 ± 26.4 Pa; G'': 58.3 ± 3.5 Pa) also showing continuously higher values for the shear modulus components.

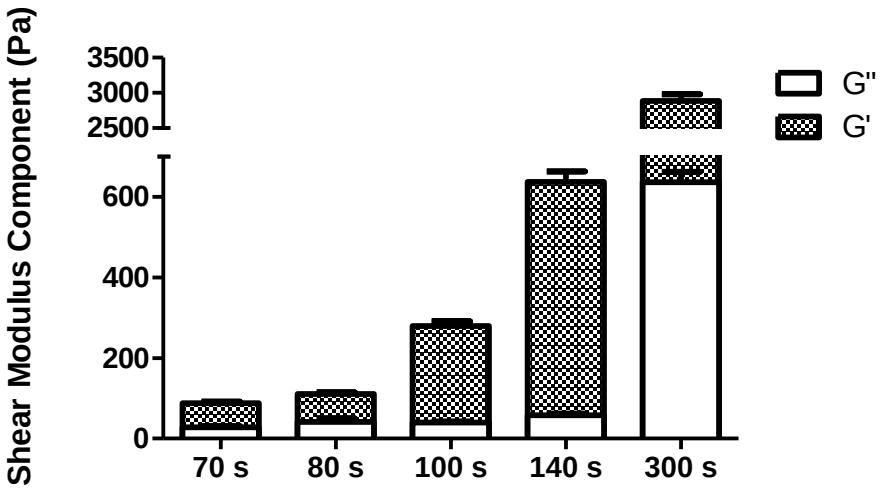


Figure 32 - Influence of crosslinking time on the rheological properties of Mel0.3Pep4 hydrogels. Results were obtained following amplitude sweep tests and the presented values are within the linear viscoelastic region. Mel0.3Pep4 refer to scaffolds with a melanin content of 0.3 wt% and a peptide molar concentration of 4mM

Therefore, it is concluded that increasing the photopolymerization time produces stiffer hydrogels due to an enhanced crosslinked network, as the G' of hydrogels was modulated from values lower than 100 Pa for hydrogels formed after 70 s of UV exposure to values around 3000 Pa for scaffolds fabricated after 300 s of UV irradiation.

The influence of melanin in the mechanical properties of the hydrogels was studied by varying the concentration of melanin in the hydrogel (0 wt%, 0.3 wt% and 0.45 wt%), while maintaining the MMP-sensitive peptide concentration constant at 4 mM (Figure 33). A photocrosslinking time of 300 s was established for all the hydrogel samples. The G' of the alginate-based hydrogels decreased with an increasing melanin content, ranging from 4302.5 ± 95.3 Pa for the Pep4 hydrogels to 2395 ± 63.7 Pa for the Mel0.45Pep4 scaffolds. The Mel0.3Pep4 constructs show an intermediate value for G' (2886.7 ± 93.5 Pa).

In addition, the influence of a lyophilization step on the mechanical properties of fabricated hydrogels was evaluated (Figure 33). Regarding Mel0.3Pep4 hydrogels, the G' measured for lyophilized (G': 3017.5 ± 34.5 Pa; G'': 174.7 ± 3.1 Pa) and non-lyophilized (G': 2886.7 ± 93.5 Pa; G'': 636.8 ± 26.0 Pa) scaffolds was relatively similar. These results show the independence of the biomechanical properties on the freeze-drying process. This is of the utmost importance regarding the delivery mode of the biomaterial, meaning that it can be used as a lyophilized patch that could be rehydrated in the wound site.

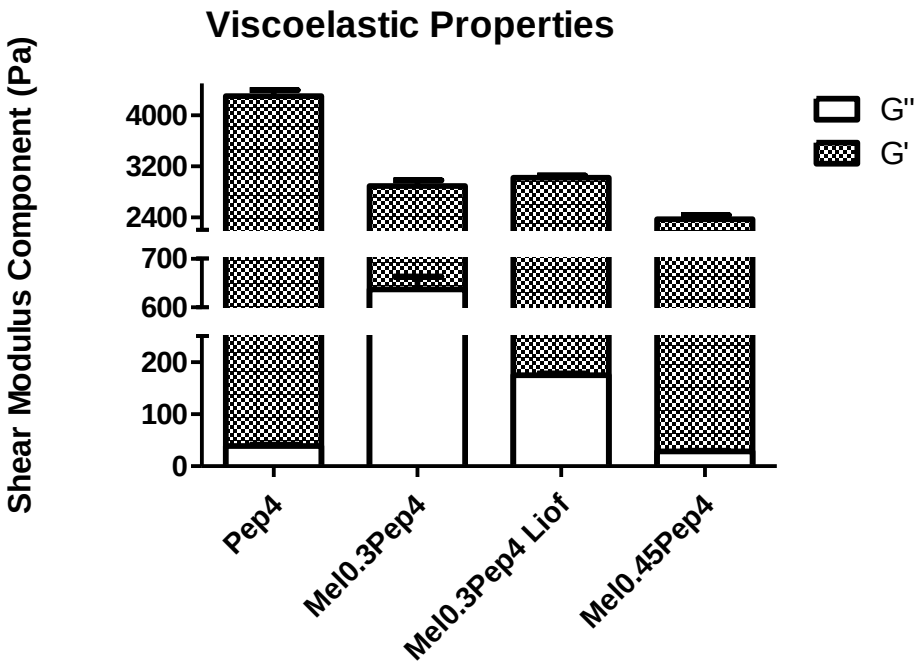


Figure 33 - Influence of a varying content of melanin on the rheological properties of hydrogels with a MMP-cleavable peptide molar concentration of 4 mM. All hydrogel samples were photocrosslinked for 300 s. Lyophilized Mel0.3Pep4 hydrogels show similar rheological properties than Mel0.3Pep4 hydrogels tested before the freeze-drying process. Results were obtained following amplitude sweep tests and the presented values are within the linear viscoelastic region. Pep4 refer to hydrogels with no melanin and a peptide molar concentration of 4 mM. Mel0.3Pep4 refer to scaffolds with a melanin content of 0.3 wt% and a peptide molar concentration of 4mM. Mel0.45Pep4 refer to scaffolds with a melanin content of 0.45 wt% and a peptide molar concentration of 4mM

The influence of the peptide crosslinker on the rheological properties of hydrogels with a melanin content of 0.3 wt% was also evaluated by varying the peptide concentration (0 mM, 4 mM and 8 mM) within the manufactured constructs (Figure 34). The shear modulus of Mel0.3Pep4 (G': 2886.7 ± 93.5 Pa; G'': 636.8 ± 26.0 Pa) and Mel0.3Pep8 (G': 1641.4 ± 90.4 Pa; G'': 300.1 ± 19.0 Pa) hydrogels was greater than the one of the scaffolds without the MMP-cleavable peptide, Blank (G': 1145.7 ± 43.5 Pa; G'': 120.8 ± 8.3 Pa) and Mel0.3 (G': 279.4 ± 44.9 Pa; G'': 108.9 ± 6.8 Pa). Therefore, the addition of the MMP-sensitive peptide promotes the formation of stiffer hydrogels. Nevertheless, when increasing the crosslinker peptide molar concentration from 4 mM to 8 mM, results show a decrease of the mechanical properties of the constructs, as Mel0.3Pep4 hydrogels are stiffer than Mel0.3Pep8 hydrogels. Moreover, the incorporation of melanin to hydrogels that do not contain the peptide crosslinker leads to a lower shear modulus, since both G' and G'' of Blank hydrogels are higher than the ones of Mel0.3 hydrogels.

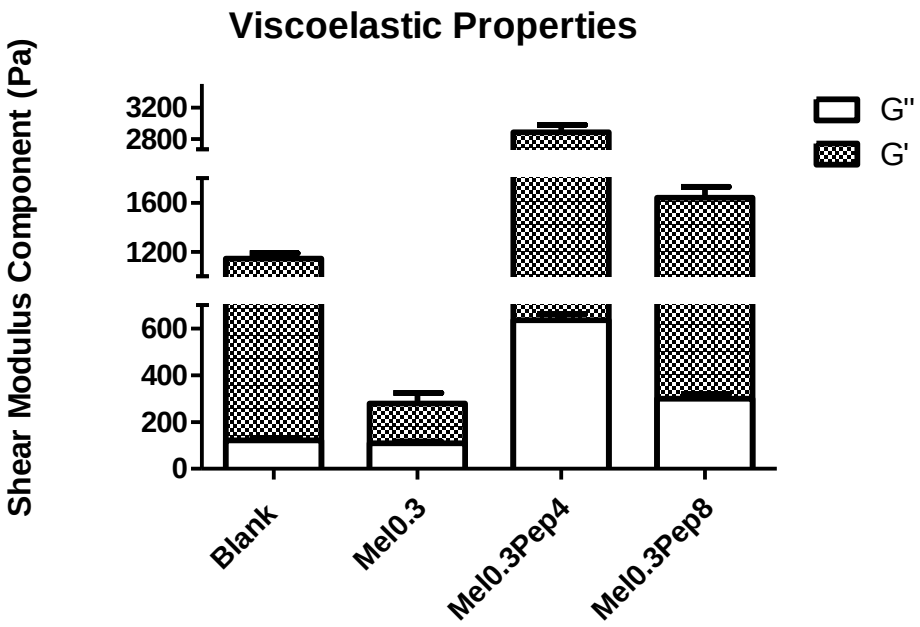


Figure 34 - Influence of the MMP-cleavable peptide concentration on the rheological properties of hydrogels with a melanin content of 0.3 wt%. Blank refer to hydrogels with no melanin nor MMP-cleavable peptide. Mel0.3 refer to scaffolds with a melanin content of 0.3 wt% and no peptide crosslinker. Mel0.3Pep4 refer to scaffolds with a melanin content of 0.3 wt% and a peptide molar concentration of 4mM. Mel0.3Pep8 refer to scaffolds with a melanin content of 0.3 wt% and a peptide molar concentration of 8mM. All hydrogel samples were photocrosslinked for 300 s. Results were obtained following amplitude sweep tests and the presented values are within the linear viscoelastic region

3.4.5 Swelling Ratio

The swelling ratio of hydrogel samples with various MMP-cleavable peptide concentration (0 mM, 4 mM and 8 mM) and melanin content (0 wt%, 0.3 wt% and 0.45 wt%) was determined. Hydrogel samples were freeze-dried and weighted to obtain their initial dry weight. Then, they were incubated in ultrapure water at 37 ºC for 24h, and the hydrated sample was weighted to determine the swollen weight. The swelling ratio was then calculated by dividing the weight after the hydration step of the hydrogel by its initial dry weight. Results (Figure 35) show that Blank hydrogels present a higher swelling ratio (95.4 ± 16.4) than any other sample tested. Pep4 hydrogels (48.4 ± 4.6) also show a higher swelling than melanin-containing hydrogels. Therefore, the incorporation of melanin within the alginate hydrogel structure leads to a decrease of the hydrogel swelling ratio. Furthermore, Mel0.3Pep4 hydrogels (23.2 ± 2.8) present a lower swelling ratio than Mel0.3Pep8 hydrogels (38.2 ± 5.3). Moreover, the influence of the photocrosslinking time on the swelling ratio was also evaluated, since Mel0.3Pep4 hydrogels were fabricated after 100 s and 300 s of UV exposure. Mel0.3Pep4 100 hydrogels (20.0 ± 2.2) produced a swelling ratio within the same range of the one related to Mel0.3Pep4 constructs, which indicates the absence of influence of the photocrosslinking time on this hydrogel property.

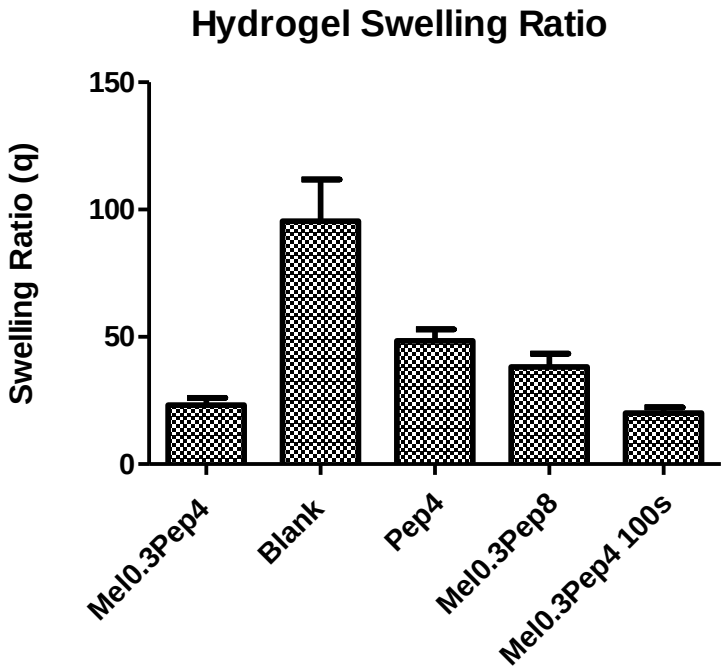


Figure 35 - Swelling ratio of hydrogels produced under different conditions. All hydrogel samples were photocrosslinked for 300 s, except Mel0.3Pep4 100 s, which was photopolymerized for 100 s. Blank refer to hydrogels with no melanin and no peptide crosslinker. Pep4 refer to hydrogels with no melanin and a peptide molar concentration of 4 mM. Mel0.3Pep4 refer to scaffolds with a melanin content of 0.3 wt% and a peptide molar concentration of 4mM. Mel0.3Pep8 refer to scaffolds with a melanin content of 0.3 wt% and a peptide molar concentration of 8mM

Chapter 4

4. Discussion

Over the past few years, several studies reported the development of photocrosslinked cell-instructive polymer-based hydrogels for tissue engineering applications [68], [74], [91], [137]. Much attention has been directed to the interactions established between the biomaterial and cells in order to design scaffolds with tailored biological properties [68], [137], [152]. In recent studies, 3D natural ECM-mimicking hydrogels have been designed with the appropriate physicochemical and biomechanical properties, working as scaffolds with improved cell-affinity that may provide the spatial support needed for cells to spread, grow, proliferate and differentiate, ultimately leading to tissue remodeling [68].

However, in the context of non-healing wounds and IBD, the construction of models that may resemble natural ECM may not be enough to attenuate the harsh conditions associated to chronic inflammation and prevent the progress of the injury or disease. Currently provided therapies in IBD are based on pharmacological agents, such as anti-inflammatory drugs and targeted biologic agents[153], and eventual surgical intervention, which in both cases does not allow an effective treatment of the disease [154]. As a result, there is a great and urgent need for new therapies that can provide better medical outcomes regarding IBD.

The present study aimed to develop and characterize an advanced multi-therapeutic bioactive platform, consisting on a biofunctionalized alginate hydrogel-based single patch, which could be potentially used for customized medical application in chronic wound healing. The new therapeutic biomaterial was designed to target the high levels of ROS that are present in general chronic wound environments, potentially leading to a better regulation of such local environments and a reverse of the chronicity of inflammation. The biochemical cues added to the scaffold would promote cell-biomaterial interactions, allowing cells to attach, spread, proliferate, differentiate, and eventually

induce tissue repair or regeneration. Thus, the main novelty of this project relies on the development of a multi-functional biomaterial single patch, which targets inflammation and, at the same time, promotes the regeneration of the local tissue.

Synthesis and characterization of functionalized alginate

The polymer of choice for the development of the multifunctional patch was alginate, a naturally derived anionic polysaccharide that has been widely used in the biomedical field. In its native structure, this polymer does not interact with cells, which constitutes a great advantage, since we can modify it in order to develop specific biological properties [66]–[68].

The first step to engineer such platform consisted on the functionalization of alginate with methacrylate groups through a nucleophilic substitution reaction. The success of functionalization was confirmed by ^{1}H-NMR, where new peaks in the spectrum of AlgMa, corresponding to methylene and methyl groups of the methacrylate functional group, were observed. ATR/FTIR analysis also confirmed the coupling of methacrylate moieties to the alginate structure, since the spectrum of AlgMa showed a sharpening within the broad range 3500-3000 cm^{-1} and at 1596 cm^{-1} when compared to the spectrum of AlgHMW. The first may be assigned to O-H stretching of methacrylic moieties, while the latter may be due to stretching vibrations of carbonyl groups from the methacrylate moieties introduced, thus confirming the functionalization of alginate.

The ratio between the peaks of methacrylate moieties and the protons corresponding to the alginate backbone allowed to determine the functionalization degree, which was 52%.

In order to improve cell-adhesion, a small cysteine-terminated peptide, containing the RGD adhesion motif (CGGGGRGDSP), was conjugated through base catalyzed thiol-Michael addition click reaction, yielding RGD-modified AlgMa (AlgMaRGD) as the reaction product. The coupling of this peptide was successfully confirmed by the appearance of new peaks on the ^{1}H-NMR spectrum of AlgMaRGD, corresponding to protons of the amino acids belonging to the peptide.

Results showed a cell-adhesive peptide incorporation of 35% for the thiol-Michael addition click reaction, which is higher than carbodiimide couplings that usually proceed with low yield owing to slow reaction kinetics under aqueous conditions [155].

However, since the polymer presents a degree of methacrylation of, approximately, 50%, the overall peptide incorporation in respect to the available methacrylate groups, was 70%. Thus, the coupling efficiency allows the estimation of the amount of RGD-containing peptide that is conjugated onto the hydrogel network.

Therefore, it becomes possible to tailor the physicochemical and biological properties of the constructs, which enables the development of cell-biomaterial interactions as required, according to the demands of the surrounding tissue.

Development and characterization of the multi-functional alginate-based patch

Preparation of alginate hydrogels

A mixture of AlgMa and AlgMaRGD was used for the design of 1.5 wt% alginate hydrogels, fabricated through photopolymerization. Their proportions were adjusted in order to grant a final constant RGD concentration within the hydrogel of 200 μM, which is within the same range of that presented in ECM-derived biological matrices [144].

These hydrogels were photocrosslinked in the presence of a MMP-sensitive bisfunctional peptide, containing the amino acid cysteine at each end (CGPQGIWGQC), which besides allowing matrix remodeling by cellular proteases, can also serve as a crosslinker. Melanin nanoparticles have also been introduced as a component of the final hydrogel network due to their radical scavenging ability. Photopolymerization was performed through exposure to UV light at a defined range of wavelengths (280-450 nm) with specific energy (7 mW/cm^2), using 0.05 wt% Irgacure 2959 as photoinitiator.

Proof of MMP-sensitive peptide grafting was evaluated by ATR/FTIR analysis of Blank, Pep4 and Mel0.3Pep4 hydrogel formulations, as well as the MMP-sensitive peptide. New characteristic peaks in the Pep4 and Mel0.3Pep4 spectra were noticed when compared to the Blank spectrum, at 1596 and 1410 cm^{-1}, due to the coupling of the peptide crosslinker. The first peak (1596 cm^{-1}) is assigned to amide I bonds from peptides. The peak at 1410 cm^{-1} is due to amide III bonds, which are typical of proteins. Therefore, the biofunctionalization of methacrylated alginate with a MMP-cleavable peptide was confirmed.

Influence of MMP-cleavable peptide and melanin quantities

The amount of melanin (0.3 wt%, 0.45 wt%, 0.6 wt%) and MMP-sensitive peptide (4mM and 8mM) in the precursor gel solution have been changed in order to study the influence of these components in hydrogel formation and in the radical scavenging ability of the final biomaterial. Furthermore, some hydrogels have been studied in the form of lyophilized scaffolds, since it provides an easier approach to handle and store the patch, granting a versatile biomaterial.

It was not possible to form stable hydrogels without the peptide crosslinker and with the highest concentration of melanin considered (0.6 wt%), even after 300 s of photopolymerization. Therefore, this melanin content was discarded, since it would be impossible to produce the necessary controls needed for the assays to be carried out. However, stable Mel0.3 and Mel0.45 hydrogels were fabricated after 300 s of UV light exposure. This indicates that the presence of melanin may hamper the photocrosslinking mechanism, as a decrease of melanin content enabled hydrogel formation, even without the MMP-cleavable moiety. Moreover, easier to handle and more stable hydrogels were produced after the incorporation of the peptide crosslinker, since Mel0.3Pep4, Mel0.45Pep4,

Mel0.3Pep8 and Mel0.45Pep8 constructs showed an enhanced structural integrity and stability when compared to Mel0.3 and Mel0.45 scaffolds. Furthermore, noticeable changes were not found regarding the macroscopic appearance between Mel0.3Pep4 and Mel0.45Pep4 hydrogels, which means that the coupling of the peptide crosslinker induces a higher crosslinking density and, consequently, more stable hydrogel networks, allowing an efficient melanin incorporation. Similar overall handling and stability was observed after increasing the enzymatically degradable peptide concentration, as Mel0.3Pep8 and Mel0.45Pep8 hydrogel structures seemed identical to the ones of Mel0.3Pep4 and Mel0.45Pep4.

Influence of photocrosslinking time

Optimization of the photocrosslinking time was achieved using Mel0.3Pep4 hydrogels, since it should be performed with hydrogels containing both melanin and the MMP-cleavable peptide. Mel0.3Pep4 hydrogels were photocrosslinked for different time periods (60 s, 70 s, 80 s, 90 s, 100 s, 140 s and 300 s) in order to obtain the minimum photopolymerization time needed to produce a stable hydrogel. After 60 s, hydrogels were not able to acquire the structural stability required to be easily handled without leaving considerable gel-forming material in the glass slides. The crosslinking time of 60 s was then discarded, since reproducible hydrogels would not be possible to obtain. For the remaining photocrosslinking times, it was noticed that a higher photopolymerization time generates more stable hydrogel networks, since a longer gelation time contributes to the development of an appropriate covalent crosslinking mechanism. Therefore, Mel0.3Pep4 hydrogels fabricated after a higher UV exposure time of the precursor solution were easier to handle and presented an enhanced structural stability.

Coupling efficiency of the MMP-cleavable peptide

The amount of MMP-sensitive peptide within the alginate hydrogel network was determined through the Ellman's assay.

For hydrogels produced after 300 s of photocrosslinking time, results show that the coupling efficiency of the proteolytically degradable peptide to alginate hydrogels is independent of the peptide crosslinker concentration in the gel precursor solution. In fact, hydrogels with no melanin presented a similar coupling percentage, 93.67 ± 1.42 for Pep4 and 94.78 ± 0.71 for Pep8 hydrogels. The incorporation of melanin led to the same conclusion, as the efficiency varied between 75.59 ± 4.27 (Mel0.3Pep4), 76.70 ± 5.37 (Mel0.3Pep8), 70.66 ± 6.52 (Mel0.45Pep4) and 68.07 ± 3.70 (Mel0.45Pep8). As shown, hydrogels with the same melanin content presented similar peptide incorporation, independently of the crosslinker molar concentration (4 mM or 8 mM). However, it should be noticed that the actual amount of MMP-cleavable peptide that is incorporated within the

hydrogel is higher for the scaffolds Pep8, Mel0.3Pep8 and Mel0.45Pep8, since it derives from the same percentage of a higher value.

Furthermore, a lower coupling efficiency was associated to an increased amount of melanin within the hydrogel structure. A possible explanation resides in the fact that melanin nanoparticles may physically hamper the crosslinking mechanism and prevent the formation of covalent crosslinked bonds, thus negatively affecting the coupling of the peptide crosslinker to the hydrogel.

The influence of the photopolymerization time and the freeze-drying process on the peptide incorporation in Mel0.3Pep4 scaffolds was also investigated. A similar coupling efficiency was obtained for scaffolds fabricated upon exposure to UV light during 100 s (75.95 ± 7.34) and 300 s (75.59 ± 4.27). Therefore, it was concluded that the variation of the photocrosslinking time does not interfere with the coupling efficiency of the MMP-cleavable peptide. This may reveal that differences between the crosslinking density of hydrogels of the same formulation, but with different photopolymerization time, should rely mostly on the crosslinking mechanism via free radical polymerization using the methacrylate moieties, as the peptide crosslinker concentration is the same. Moreover, Mel0.3Pep4 scaffolds before (75.59 ± 4.27) and after (82.43 ± 4.24) lyophilization presented a similar coupling efficiency. This constitutes an important result regarding the physicochemical and biological properties of freeze-dried hydrogels, as the amount of MMP-cleavable peptide incorporated by both lyophilized and non-lyophilized hydrogels was, approximately, the same.

As a result, it becomes possible to more precisely estimate and adjust the amount of MMP-sensitive peptide incorporated onto the manufactured alginate hydrogels and, therefore, elicit different biological responses.

Free-radical scavenging activity

Melanin nanoparticles were entrapped within the hydrogel network in order to provide an enhanced radical scavenging ability to the fabricated scaffolds. Such feature was assessed for different time points, namely 2h, 3h, 6h, 9h and overnight, through the DPPH assay.

In general, almost all samples presented a continuously higher radical scavenging activity throughout all time points, since a longer sample incubation leads to a higher absorbance decrease of the DPPH radical.

The influence of melanin on the radical scavenging activity of the hydrogels was evaluated by maintaining the MMP-sensitive peptide concentration constant (0 mM, 4 mM or 8mM), while varying the melanin content (0 wt%, 0.3 wt% and 0.45 wt%) of the constructs.

The obtained results show that the addition of melanin to the hydrogel structure increases the free radical scavenging activity of the alginate-based constructs, since hydrogels with melanin nanoparticles in their composition capture a considerably higher amount of free radicals than hydrogels without this biopolymer in their structure. This fact was observed independently of the MMP-cleavable peptide concentration, although for the 4 mM concentration, Pep4 hydrogels showed

similar free radical scavenging activity than Mel0.3Pep4 and Mel0.45Pep4 for all time points, except after overnight incubation (Pep4: 48.5 ± 4.7 %; Mel0.3Pep4: 87.8 ± 1.8 %; Mel0.45Pep4: 87.0 ± 1.1 %). Mel0.3Pep4 and Mel0.45Pep4 hydrogels produced the same radical scavenging ability for all time points, including a rather high capture of free radicals after being incubated overnight (Mel0.3Pep4 – 87.8 ± 1.8 %; Mel0.45Pep4 – 87.0 ± 1.1 %).

For scaffolds without the peptide crosslinker, Blank hydrogels showed rather low capture of free radicals for all time points, with a peak of radical scavenging activity at 6h (16.8 ± 2.0 %). Mel0.3 and Mel0.45 hydrogels produced similar results between them, with Mel0.45 presenting higher scavenging activity for the first two time points (Mel0.3 - 2h: 14.5 ± 5.4 %; 3h: 21.1 ± 2.3 %; Mel0.45 - 2h: 20.5 ± 0.4 %; 3h: 27.6 ± 1.1 %) and lower capture of free radicals for the next two time points (Mel0.3 - 6h: 35.2 ± 2.2 %; 9h: 46.1 ± 1.1 %; Mel0.45 - 6h: 31.7 ± 2.0 %; 9h: 36.7 ± 6.4 %). After overnight incubation, the two constructs showed approximately the same scavenging activity (Mel0.3 - 76.1 ± 1.8 %; Mel0.45 - 73.3 ± 3.9 %).

Therefore, increasing melanin concentration in the hydrogels failed to produce an enhanced free radical scavenging, as hydrogels with different melanin contents, namely 0.3 wt% and 0.45 wt%, presented a similar radical scavenging ability.

Concerning hydrogels with a peptide crosslinker concentration of 8 mM, Pep8 scaffolds showed low free radical scavenging activity with a peak of activity after being incubated overnight (23.5 ± 5.3 %). Mel0.3Pep8 and Mel0.45Pep8 produced similar capture of free radicals after 3h and a rather high activity after being incubated overnight (Mel 0.3Pep8 – 87.3 ± 0.3 %; Mel0.45Pep8 – 89.0 ± 0.7%). However, for the remaining time points Mel0.45Pep8 hydrogels showed a slightly higher free-radical scavenging ability (2h: 23.8 ± 4.7 %; 6h: 39.2 ± 3.1 %; 9h: 53.8 ± 1.3 %) than Mel0.3Pep8 constructs (2h: 11.7 ± 5.8 %; 6h: 33.0 ± 4.8 %; 9h: 43.6 ± 2.1).

When comparing hydrogels with different peptide crosslinker concentrations (4 mM and 8 mM), but an equal melanin content, such as Mel0.3Pep4 and Mel0.3Pep8 or Mel0.45Pep4 and Mel0.45Pep8 scaffolds, free radical scavenging activity kinetics that were found, for all groups and all time points, were, approximately, the same.

Thus, a fixed melanin concentration of 0.3 wt% was selected as preferred, since there was no relevant advantage in using 0.45 wt% melanin, regarding the free-radical scavenging activity. It also should be taken into consideration that melanin is a biopolymer that physically hampers the crosslinking mechanism, so it is essential to have just the minimum required amount of melanin that can provide a good radical scavenging ability to the photocrosslinked hydrogel. Moreover, the final molar concentration of MMP-cleavable peptide was decided to be 4 mM, since, as expected, there were no noticeable changes in the radical scavenging ability when using 8 mM crosslinker in the hydrogel formulation.

Furthermore, the radical scavenging activity of hydrogels and free melanin nanoparticles at a similar concentration was studied. A higher DPPH radical scavenging activity was presented by MelNP0.45 for the first time points (2h: 40.1 ± 5.8 %; 3h: 55.0 ± 2.6 %; 6h: 75.0 ± 1.0 %; 9h: 83.7 ± 0.9

%) when compared to Mel0.3Pep4 and Mel0.45Pep4 hydrogels and MelNP0.3 (2h: 24.0 ± 1.7 %; 3h: 27.3 ± 0.2 %; 6h: 39.0 ± 1.1 %; 9h: 45.7 ± 1.8 %). These two hydrogel samples and MelNP0.3 presented similar results, regardless the higher free radical scavenging activity of MelNP0.3 for the first time point (2h). Nevertheless, after overnight incubation, the free-radical scavenging activity of the hydrogels was similar to the free biopolymeric nanoparticles (MelNP0.3 – 71.4 ± 4.0 %; MelNP0.45 – 85.8 ± 4.7 %), with MelNP0.3 presenting lower DPPH scavenging activity than the hydrogels.

As a result, it may be concluded that, for a melanin concentration of 0.3 wt%, the entrapment of this biopolymer within the alginate hydrogel structure does not affect its radical scavenging performance.

Furthermore, results show that the photocrosslinking time does not considerably influence the radical scavenging ability of the constructs, since Mel0.3Pep4 100 hydrogels present a similar capture of free radicals in the first four time points when compared to Mel0.3Pep4 hydrogels, photocrosslinked for 300 s. However, after overnight incubation, Mel0.3Pep4 hydrogels (87.8 ± 1.8 %) presented a higher capture of free radicals than Mel0.3Pep4 100 (64.5 ± 8.1).

Finally, the radical scavenging ability of the Mel0.3Pep4 Liof scaffold upon rehydration was similar to the one of the non-lyophilized Mel0.3Pep4 hydrogel. For the two earliest time points, the two samples showed similar results, while for the next two time points, Mel0.3Pep4 Liof (6h: 44.3 ± 6.8 %; 9h: 62.1 ± 1.6 %) hydrogels presented a higher scavenging activity than Mel0.3Pep4 (6h: 32.6 ± 4.0 %; 9h: 42.2 ± 3.1 %) constructs. However, for the last time point, Mel0.3Pep4 (87.8 ± 1.8 %) showed a higher ability to capture free radicals when compared to Mel0.3Pep4 Liof (72.1 ± 1.7 %).

Moreover, no release of melanin particles were observed from the lyophilized scaffold after rehydration, meaning that melanin remains incorporated within the polymeric network. These results demonstrate the versatility of the material, which can be used either as a hydrogel or as a lyophilized patch with similar efficiency regarding the free radical scavenging activity.

Rheological properties

The fact that the biological behaviour of cells in a scaffold is highly dependent on the matrix stiffness, combined with the need of fabricating a scaffold that matches the biomechanical properties of the target tissue, motivated the rheological study of the obtained hydrogel formulations.

The influence of gelation time on the mechanical properties of the scaffolds was evaluated in Mel0.3Pep4 hydrogel formulations photocrosslinked for several time periods (70 s, 80 s, 100 s, 140 s and 300 s). Results showed that a higher photopolymerization time leads to an increased hydrogel stiffness. Hydrogels with tailored mechanical properties were obtained by simply varying the photopolymerization time, with the elastic component of the shear modulus varying from G' = 87.7 ± 3.9 Pa (for hydrogels fabricated after 70 s of UV exposure) to G'= 2886.7 ± 93.5 Pa (for scaffolds manufactured after 300 s of photocrosslinking). Moreover, hydrogels formed after 80 s (G': 110.5 ±

4.5 Pa; G'': 41.8 ± 8.7 Pa), 100 s (G': 279.5 ± 11.4 Pa; G'': 39.5 ± 2.9 Pa) and 140 s (G': 637.0 ± 26.4 Pa; G'': 58.3 ± 3.5 Pa) also showed continuously higher values for the shear modulus components.

This was in line with similar strategies described in the literature [101], since higher UV exposure time leads to the generation of a greater amount of photoinitiator-derived free radicals that actively participate in the crosslinking mechanism, resulting in a greater crosslinking density. Therefore, stiffer alginate hydrogels may be produced with exactly the same composition.

The effect of the presence of melanin nanoparticles in the mechanical properties of the alginate-based hydrogels was also investigated by varying the melanin content of the hydrogels (0 wt%, 0.3 wt% and 0.45 wt%), while the MMP-cleavable peptide concentration was kept constant (4 mM). All hydrogel samples were fabricated with a photocrosslinking time of 300 s. The G' of the alginate-based hydrogels decreased with a higher melanin content, ranging from 4302.5 ± 95.3 Pa for the Pep4 hydrogels to 2395 ± 63.7 Pa for the Mel0.45Pep4 scaffolds. The Mel0.3Pep4 constructs showed an intermediate value for G' (2886.7 ± 93.5 Pa).

The obtained results demonstrate that an increase of the melanin nanoparticles concentration within the hydrogel leads to a decrease of the shear modulus of the construct. Therefore, the incorporation of melanin generates hydrogels with a lower stiffness, since melanin may constitute a physical hurdle to the dual hydrogel crosslinking mechanism, hampering the formation of new covalent bonds between alginate polymer chains.

Moreover, the influence of the freeze-drying process on the mechanical properties of Mel0.3Pep4 hydrogels was evaluated. Similar values for G' were measured for lyophilized (G': 3017.5 ± 34.5 Pa; G'': 174.7 ± 3.1 Pa) and non-lyophilized (G': 2886.7 ± 93.5 Pa; G'': 636.8 ± 26.0 Pa) scaffolds. These results show the independence of the biomechanical properties of the hydrogels on the freeze-drying process. This is extremely important regarding the delivery mode of the biomaterial, meaning that it can be used as a lyophilized patch that may undergo rehydration at the wound site without changing its mechanical properties, showing the biomaterial versatility.

Furthermore, mechanical tests were also conducted on hydrogels with a varying MMP-cleavable peptide content (none, 4 mM and 8 mM) and a constant melanin content (0.3 wt%) to study the influence of the peptide crosslinker on the final rheological properties of the constructs. Hydrogel mechanical properties were enhanced when adding the enzymatically degradable peptide, as stiffer hydrogels were produced upon coupling of the peptide. The shear modulus of Mel0.3Pep4 (G': 2886.7 ± 93.5 Pa; G'': 636.8 ± 26.0 Pa) and Mel0.3Pep8 (G': 1641.4 ± 90.4 Pa; G'': 300.1 ± 19.0 Pa) hydrogels was greater than the one of the scaffolds without the MMP-cleavable peptide, Blank (G': 1145.7 ± 43.5 Pa; G'': 120.8 ± 8.3 Pa) and Mel0.3 (G': 279.4 ± 44.9 Pa; G'': 108.9 ± 6.8 Pa). With the incorporation of the crosslinker onto the alginate hydrogel structure, a higher crosslinking density was expected due to the occurrence of a dual crosslinking mechanism, one between methacrylate moieties of several alginate chains and another between methacrylate groups of polymer chains and thiol groups of the bisfunctional cysteine terminated MMP-sensitive peptide. Nevertheless, when increasing the crosslinker peptide molar concentration from 4 mM to 8 mM, results did not show the

predicted increase of the shear modulus, but a decrease of the mechanical properties of the hydrogels, as Mel0.3Pep4 hydrogels are stiffer than Mel0.3Pep8 hydrogels. This may be explained since hydrogels were manufactured through a dual crosslinking mechanism. Therefore, a higher peptide crosslinker concentration may lead, to a certain extent, to a higher crosslinking density of the hydrogel and, consequently, to an increased shear modulus, as stiffer hydrogels are produced. In such cases, both crosslinking mechanisms coexist in an appropriate manner. As demonstrated in the results of the Ellman's assay, the MMP-cleavable peptide incorporation of Mel0.3Pep4 hydrogels with different photocrosslinking times, namely 100 s and 300 s, was the same. Therefore, the amount of peptide crosslinker in both hydrogels is equal. However, as abovementioned, substantially different mechanical properties may be found between these two conditions, as Mel0.3Pep4 hydrogels are stiffer than Mel0.3Pep4 100s. This difference is related not to the newly formed covalent bonds induced by the peptide crosslinker, since the amount is the same, but to the traditional radical polymerization mechanism, between the methacrylate groups of different polymer chains, which is the type of crosslinking that prevails in this case. A higher crosslinking density is generated and, thus, hydrogels present improved mechanical properties. However, a higher incorporation of peptide crosslinker, from 4 mM to 8 mM, may somehow promote the peptide-mediated covalent crosslinking, while reducing the effect of the radical polymerization process between methacrylate moieties, even knowing both Mel0.3Pep4 and Mel0.3Pep8 hydrogels were formed after 300 s of UV light exposure. It was also proved that Mel0.3Pep8 hydrogels present twice the concentration of the crosslinker peptide than Mel0.3Pep4 constructs, as they present the same MMP-cleavable peptide incorporation percentage. As the peptide-mediated covalent crosslinking is not as effective as the traditional radical polymerization mechanism involving methacrylate groups, a higher peptide crosslinker concentration, within some range, may lead to a less crosslinked hydrogel network, thus showing decreased mechanical properties and explaining this result.

Besides, the incorporation of melanin to hydrogels that do not contain the peptide crosslinker leads to a lower shear modulus, since both G' and G'' of Blank hydrogels are higher than the ones of Mel0.3 hydrogels. This fact confirms the influence of the presence of this biopolymer on the rheological properties of the fabricated hydrogels.

The fact that the hydrogel mechanical properties may be tailored through a variation of the photopolymerization time, MMP-cleavable peptide crosslinker concentration, or melanin content, constitutes an important finding. The fabricated hydrogels may, then, present different crosslinking densities and, consequently, different mechanical strength. In fact, manufacturing alginate hydrogels with tunable degradation rates is extremely relevant for tissue engineering applications, since the degradation rate should match the rate at which new tissue formation occurs in chronic wound healing. Moreover, the inherently poor mechanical properties of alginate hydrogels [156] may be enhanced in order to produce stiffer constructs, with an adequate initial mechanical strength to undergo cell-mediated degradation. These represent important developments concerning the design of hydrogels to be employed as scaffolds for tissue engineering in chronic wound healing, as it

becomes possible to tailor the viscoelastic properties of the developed platform in order to match the biomechanical requirements of the target tissue. Such ability is significantly relevant when engineering a patch to be applied on different tissues, and, consequently, that should be adapted to interact with different cell types [68].

Swelling ratio

The swelling ratio of hydrogel samples with varying MMP-cleavable peptide (0 mM, 4 mM and 8 mM) and melanin (0 wt%, 0.3 wt% and 0.45 wt%) content was assessed.

Results showed that Blank hydrogels present the highest swelling ratio (95.4 ± 16.4) among the tested samples. The swelling ratio is intrinsically related with the hydrophilicity of the construct [157]. Since alginate hydrogels are inherently hydrophilic, Blank hydrogels present a higher swelling ratio. Furthermore, the addition of the peptide crosslinker in the Pep4 (48.4 ± 4.6) constructs leads to a loss of hydrophilic character of the hydrogel during the crosslinking reaction between hydrophilic groups in the backbone [157] and, thus, to a lower swelling ratio than the one of Blank hydrogels. Furthermore, Pep4 showed a higher swelling than melanin-containing hydrogels. Therefore, it may be concluded that the incorporation of melanin within the alginate hydrogel structure leads to a decrease of the hydrogel swelling ratio, as melanin is a hydrophobic biopolymer, thus decreasing the overall hydrophilic character of the alginate hydrogel. Another explanation may be related to the fact that the presence of melanin nanoparticles may decrease the available free volume within the hydrogel structure, thus reducing the amount of water that can be absorbed by the biomaterial.

Moreover, Mel0.3Pep4 hydrogels (23.2 ± 2.8) presented a lower swelling ratio than Mel0.3Pep8 hydrogels (38.2 ± 5.3), since this hydrogel property may also be related to the crosslinking density of the constructs [157]. As previously seen, Mel0.3Pep8 hydrogels present a lower crosslinking density and stiffness than Mel0.3Pep4 constructs, which means Mel0.3Pep8 network chains are weakly stretched when compared to Mel0.3Pep4. This allows, then, a higher swelling degree for the Mel0.3Pep8 hydrogels as they are able to retain greater amounts of water.

In addition, the influence of the photocrosslinking time on the swelling ratio was also investigated, since Mel0.3Pep4 hydrogels were fabricated after 100 s and 300 s of UV exposure. Mel0.3Pep4 100 hydrogels (20.0 ± 2.2) produced a swelling ratio within the same range of the one related to Mel0.3Pep4 constructs, which indicates the absence of influence of the photocrosslinking time on this hydrogel property, even knowing both hydrogel samples present different crosslinking densities, as previously reported.

Further biological assays that may more closely resemble physiologically relevant *in vitro* and *in vivo* conditions to test the real hydrogel antioxidant activity regarding the capture of ROS are needed. Such studies should grant a biological validation of the developed platform as an efficient free radical scavenger biomaterial.

Chapter 5

5. Conclusion and Future Perspectives

A multi-therapeutic hydrogel single patch based on methacrylated alginate was developed through a rapid, straightforward and highly efficient dual crosslinking strategy, via both radical polymerization using methacrylate moieties and peptide-mediated covalent crosslinking.

The obtained multifunctional biomaterial contains in its structure bioactive cues that allow the scaffold to be recognized and remodeled by cells. Bioactive ligands with cell-adhesion motifs and MMP-cleavable moieties were successfully incorporated in the scaffold, potentially granting enhanced cell-biomaterial interactions. Moreover, the bioactive scaffold may adhere to the neighboring biological tissues, since the biofunctionalization with an integrin binding peptide promotes the formation of chemical bonds between the hydrogel and the tissue surface, granting a better integration of the construct [158]. The developed MMP-sensitive alginate hydrogel may then present the ability to induce cell growth and proliferation, ECM deposition and neo-tissue formation, promoting tissue repair and regeneration.

The entrapment of melanin nanoparticles within the hydrogel network allowed the design of scaffolds with radical scavenging ability, capable of capturing free radicals that may be present in solution. The additional free radical scavenging activity granted by the melanin nanoparticles may potentially protect tissues from eventual oxidative damage in an IBD situation, thus constituting a possible approach to reverse the chronicity of non-healing wounds and ameliorate the harsh existing conditions in such environments. Consequently, the platform may provide a targeted effect in chronic wound healing, and its tunable biochemical composition may induce the local tissue regeneration.

Depending on the amount of MMP-cleavable peptide incorporated, amount of melanin loaded and photopolymerization time, scaffolds with tunable mechanical properties may be obtained. This versatility is an important feature when engineering a multimodal platform that can potentially be applied to chronic wounds occurring in different types of tissues. Therefore, it is important to tailor

the mechanical properties of the scaffold to match the biomechanical properties of the target tissue, in order to induce appropriate biological responses.

More importantly, it was observed that the radical scavenging ability and mechanical properties of the obtained hydrogels were similar to the ones of corresponding freeze-dried scaffolds. This is of great importance as it gives high versatility to the biomaterial, which can be efficiently applied either as a hydrogel for cell delivery or as a lyophilized scaffold that could be rehydrated at the wound site. In a clinical point of view, the use of a lyophilized scaffold is more attractive since it would be easier to store and to handle. Such lyophilized scaffold could be administered by colonoscopy and rehydrated *in situ* in a situation of IBD.

Overall, the best alginate hydrogel formulation obtained includes a melanin content of 0.3 wt% and a peptide crosslinker concentration of 4mM (Mel0.3Pep4). This is due to the fact that there was not found any relevant advantage in using 0.45 wt% melanin, regarding the free-radical scavenging activity of the hydrogels. Moreover, as melanin may hamper the photocrosslinking mechanism, it is essential to have just the minimum required amount of melanin that can provide a good radical scavenging ability to the hydrogel. Additionally, the final molar concentration of MMP-cleavable peptide was decided to be 4 mM, since using 8 mM crosslinker in the hydrogel formulation produced similar results when compared to hydrogels with MMP-cleavable peptide at 4 mM, regarding the radical scavenging activity of constructs with a constant melanin content.

Although additional biological assessment of the biomaterial needs to be performed, the developed platform may potentially be used for tissue engineering applications regarding chronic wound healing. Nevertheless, biological validation of the hydrogel in well-established wound healing models is required to test the biomaterial efficacy in an environment that may more closely resemble actual *in vivo* conditions.

Several tests need to be conducted in order to obtain biological validation of the biomaterial and prove its multi-therapeutic effect of attenuating oxidative stress that typically characterize chronic wounds in IBD, and promote new tissue formation. Moreover, further biological studies may contribute for a better understanding of the underlying biological mechanisms regarding chronic wounds, namely in terms of oxidative stress induced tissue damage.

Hopefully, this project may provide a better insight into the development of a material that is able to positively influence the chronic wound environment, promoting tissue repair and regeneration, as well as wound closure, thus granting quality of life to patients affected.

Future perspectives

The next step in the development of the presented platform is to obtain biological validation of the biomaterial under physiologically relevant conditions. Therefore, cytotoxicity assessment of the patch is required, in order to understand if the hydrogel does not disturb the normal biological functions when in contact with cells, which can be evaluated by the well-established resazurin or MTT

assays [159]. Moreover, cytocompatibility may also be investigated via the cell viability LIVE/DEAD kit, as reported by Pereira et al. [137]. The developed platform is based on naturally derived polymers, such as alginate and melanin, and other components at extremely low quantities and, thus, it should not elicit any potentially deleterious effects on cells. Therefore, although it is expected that the hydrogel system does not produce cytotoxic effects, since all its constituents have already been used with proved efficacy in contact with cells, evaluation of the biocompatibility of the patch is still required. Cell seeding on top of the biomaterial can also be performed to assess if cells are able to spread, proliferate and migrate in contact with the platform. ECM production may also be evaluated to better understand the regenerative potential of the biomaterial.

Furthermore, the H_2DCFDA/DCFDA assay may also be carried out in order to monitor intracellular ROS production, providing a direct measure of overall oxidative stress. Briefly, 2',7'-dichlorodihydrofluorescein diacetate (H_2DCFDA) freely passes the cytoplasmic membrane and is deacetylated to H_2DCF by intracellular esterases. Then, ROS species may promote the oxidation of H_2DCF, resulting in the formation of a fluorescent product (DCF) (Figure 36) [160].

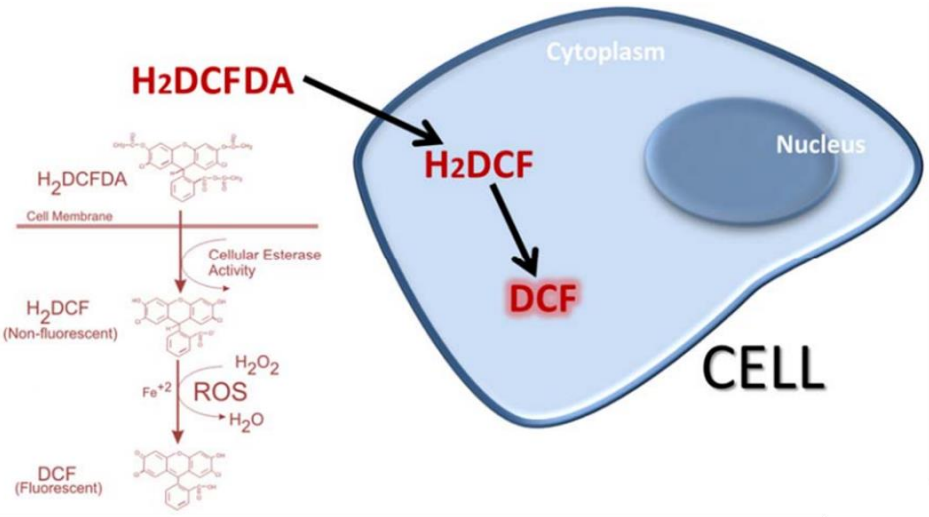


Figure 36 - Mechanism of the H_2DCFDA/DCFDA assay. H_2DCFDA is taken up by the cells, deacetylated by intracellular esterases and oxidized by ROS, yielding a fluorescent product (DCF). Retrieved from [160]

Therefore, this assay may grant preliminary insights into the antioxidant activity of the developed biomaterial.

Moreover, the mucosal adhesion of the patch may also be tested using *ex vivo* models to see if the platform is able to adhere to *post-mortem* intestinal tissue.

Further biological studies may also include testing the platform in well-established wound healing models to determine the biomaterial efficacy in an environment that may more closely resemble actual *in vivo* conditions. Regarding IBD, a possible approach to test the patch under such conditions would require the use of an *in vitro* cellular model that precisely mimics the intestinal epithelial

layer. To achieve that, triple co-culture models may be used, as previously reported with human colon carcinoma Caco-2, mucus-producing HT29, and Raji B cells [161]. The addition of acrylamide to the model may induce oxidative stress [162], allowing the antioxidant activity of the biomaterial to be tested under biologically relevant conditions.

References

[1] K. Järbrink *et al.*, "The humanistic and economic burden of chronic wounds: a protocol for a systematic review," *Syst. Rev.*, vol. 6, no. 1, p. 15, Dec. 2017.

[2] M. Sasaki *et al.*, "D-2-hydroxyglutarate produced by mutant IDH1 perturbs collagen maturation and basement membrane function," *GENES Dev.*, vol. 26, no. 18, pp. 2038–2049, 2012.

[3] H. Brem and M. Tomic-Canic, "Cellular and molecular basis of wound healing in diabetes," *J. Clin. Invest.*, vol. 117, no. 5, pp. 1219–1222, May 2007.

[4] N. A. Richmond *et al.*, "US-National Institutes of Health-funded research for cutaneous wounds in 2012," *Wound Repair Regen.*, vol. 21, no. 6, pp. 789–792, Nov. 2013.

[5] S. A. Eming, P. Martin, and M. Tomic-Canic, "Wound repair and regeneration: Mechanisms, signaling, and translation," *Sci. Transl. Med.*, vol. 6, no. 265, pp. 265sr6-265sr6, Dec. 2014.

[6] S. Mandla, L. Davenport Huyer, and M. Radisic, "Review: Multimodal bioactive material approaches for wound healing," 2013.

[7] Y. Xiao *et al.*, "Diabetic wound regeneration using peptide-modified hydrogels to target re-epithelialization," *Proc. Natl. Acad. Sci.*, vol. 113, no. 40, pp. E5792–E5801, Oct. 2016.

[8] J. D. Stroncek and W. M. Reichert, *Overview of Wound Healing in Different Tissue Types*. CRC Press/Taylor & Francis, 2008.

[9] S. Enoch and P. Price, "Cellular, molecular and biochemical differences in the pathophysiology of healing between acute wounds, chronic wounds and wounds in the aged." [Online]. Available: http://www.worldwidewounds.com/2004/august/Enoch/Pathophysiology-Of-Healing.html. [Accessed: 19-Jun-2019].

[10] G. Han and R. Ceilley, "Chronic Wound Healing: A Review of Current Management and Treatments," *Adv. Ther.*, vol. 34, no. 3, pp. 599–610, Mar. 2017.

[11] R. G. Frykberg and J. Banks, "Challenges in the Treatment of Chronic Wounds," *Adv. Wound Care*, vol. 4, no. 9, pp. 560–582, 2015.

[12] J. Todoric, L. Antonucci, and M. Karin, "Targeting Inflammation in Cancer Prevention and Therapy," *Cancer Prev. Res.*, vol. 9, no. 12, pp. 895–905, Dec. 2016.

[13] T. Wynn and L. Barron, "Macrophages: Master Regulators of Inflammation and Fibrosis," *Semin. Liver Dis.*, vol. 30, no. 03, pp. 245–257, Aug. 2010.

[14] J. S. Duffield, "The inflammatory macrophage: a story of Jekyll and Hyde.," *Clin. Sci. (Lond).*, vol. 104, no. 1, pp. 27–38, Jan. 2003.

[15] D. M. Mosser and J. P. Edwards, "Exploring the full spectrum of macrophage activation," *Nat. Rev. Immunol.*, vol. 8, no. 12, pp. 958–969, Dec. 2008.

[16] A. Mantovani, C. Garlanda, and M. Locati, "Macrophage Diversity and Polarization in Atherosclerosis," *Arterioscler. Thromb. Vasc. Biol.*, vol. 29, no. 10, pp. 1419–1423, Oct. 2009.

[17] S. F. Badylak and T. W. Gilbert, "Immune response to biologic scaffold materials," *Semin. Immunol.*, vol. 20, no. 2, pp. 109–116, Apr. 2008.

[18] A. Mantovani, A. Vecchi, and P. Allavena, "Pharmacological modulation of monocytes and macrophages," *Curr. Opin. Pharmacol.*, vol. 17, pp. 38–44, Aug. 2014.

[19] T. C. King, "Inflammation, Inflammatory Mediators, and Immune-Mediated Disease," in *Elsevier's Integrated Pathology*, Elsevier, 2007, pp. 50–51.

[20] M. P. Caley, V. L. C. Martins, and E. A. O'toole, "Metalloproteinases and Wound Healing," *Adv. WOUND CARE*, vol. 4, no. 4.

[21] S. M. Mccarty and S. L. Percival, "CRITICAL REVIEWS Proteases and Delayed Wound Healing."

[22] M. Mittal, M. R. Siddiqui, K. Tran, S. P. Reddy, and A. B. Malik, "Reactive Oxygen Species in

Inflammation and Tissue Injury," *Antioxid. Redox Signal.*, vol. 20, no. 7, pp. 1126–1167, Mar. 2014.

[23] W. Hou, G. Xu, H. Wang, and J. Gould, *Treating autoimmune disease with Chinese medicine*. Churchill Livingstone, 2011.

[24] S. Reuter, S. C. Gupta, M. M. Chaturvedi, and B. B. Aggarwal, "Oxidative stress, inflammation, and cancer: How are they linked?," *Free Radic. Biol. Med.*, vol. 49, no. 11, pp. 1603–1616, Dec. 2010.

[25] A. Geremia, P. Biancheri, P. Allan, G. R. Corazza, and A. Di Sabatino, "Innate and adaptive immunity in inflammatory bowel disease," *Autoimmun. Rev.*, vol. 13, no. 1, pp. 3–10, Jan. 2014.

[26] I. Balmus, A. Ciobica, A. Trifan, and C. Stanciu, "The implications of oxidative stress and antioxidant therapies in Inflammatory Bowel Disease: Clinical aspects and animal models," *Saudi J. Gastroenterol.*, vol. 22, no. 1, p. 3, 2016.

[27] "Inflammatory Bowel Disease (IBD) Diagnosis and Treatment Options | Johns Hopkins Inflammatory Bowel Disease Center." [Online]. Available: https://www.hopkinsmedicine.org/inflammatory_bowel_disease_center/about_ibd/index.html. [Accessed: 11-Apr-2019].

[28] B. E. Wendland *et al.*, "Lipid peroxidation and plasma antioxidant micronutrients in Crohn disease," *Am. J. Clin. Nutr.*, vol. 74, no. 2, pp. 259–264, Aug. 2001.

[29] N. I. Krinsky, "Mechanism of action of biological antioxidants.," *Proc. Soc. Exp. Biol. Med.*, vol. 200, no. 2, pp. 248–54, Jun. 1992.

[30] T. Tian, Z. Wang, and J. Zhang, "Pathomechanisms of Oxidative Stress in Inflammatory Bowel Disease and Potential Antioxidant Therapies," 2017.

[31] B. Halliwell, "Antioxidants and Human Disease: A General Introduction," *Nutr. Rev.*, vol. 55, no. 1, pp. S44–S49, Apr. 2009.

[32] D. N. Seril, J. Liao, G.-Y. Yang, and C. S. Yang, "Oxidative stress and ulcerative colitis-associated carcinogenesis: studies in humans and animal models," *Carcinogenesis*, vol. 24, no. 3, pp. 353–362, Mar. 2003.

[33] M. A. Odenwald and J. R. Turner, "The intestinal epithelial barrier: a therapeutic target?," *Nat. Rev. Gastroenterol. Hepatol.*, vol. 14, no. 1, pp. 9–21, Jan. 2017.

[34] G. D. Buffinton and W. F. Doe, "Altered ascorbic acid status in the mucosa from inflammatory bowel disease patients.," *Free Radic. Res.*, vol. 22, no. 2, pp. 131–43, Feb. 1995.

[35] R. A. Floyd, "Role of oxygen free radicals in carcinogenesis and brain ischemia.," *FASEB J.*, vol. 4, no. 9, pp. 2587–97, Jun. 1990.

[36] A. Di Sabatino, M. V. Lenti, P. Giuffrida, A. Vanoli, and G. R. Corazza, "New insights into immune mechanisms underlying autoimmune diseases of the gastrointestinal tract," *Autoimmun. Rev.*, vol. 14, no. 12, pp. 1161–1169, Dec. 2015.

[37] J. Beisner, E. F. Stange, and J. Wehkamp, "Innate antimicrobial immunity in inflammatory bowel diseases," *Expert Rev. Clin. Immunol.*, vol. 6, no. 5, pp. 809–818, Sep. 2010.

[38] M. A. McGuckin, R. Eri, L. A. Simms, T. H. J. Florin, and G. Radford-Smith, "Intestinal barrier dysfunction in inflammatory bowel diseases," *Inflamm. Bowel Dis.*, vol. 15, no. 1, pp. 100–113, Jan. 2009.

[39] L. Pastorelli, C. De Salvo, J. R. Mercado, M. Vecchi, and T. T. Pizarro, "Central Role of the Gut Epithelial Barrier in the Pathogenesis of Chronic Intestinal Inflammation: Lessons Learned from Animal Models and Human Genetics," *Front. Immunol.*, vol. 4, p. 280, Sep. 2013.

[40] D. C. Baumgart and S. R. Carding, "Inflammatory bowel disease: cause and immunobiology," *Lancet*, vol. 369, no. 9573, pp. 1627–1640, May 2007.

[41] S. O'Sullivan, J. F. Gilmer, and C. Medina, "Matrix Metalloproteinases in Inflammatory Bowel Disease: An Update," *Mediators Inflamm.*, vol. 2015, pp. 1–19, 2015.

[42] M. Coskun, S. Vermeire, and O. H. Nielsen, "Novel Targeted Therapies for Inflammatory Bowel Disease," *Trends Pharmacol. Sci.*, vol. 38, no. 2, pp. 127–142, Feb. 2017.

[43] M. Perše and A. Unkovič, "The Role of TNF in the Pathogenesis of Inflammatory Bowel Disease," in *Gastroenteritis [Working Title]*, IntechOpen, 2019.

[44] C. M. Olesen, M. Coskun, L. Peyrin-Biroulet, and O. H. Nielsen, "Mechanisms behind efficacy of tumor necrosis factor inhibitors in inflammatory bowel diseases," *Pharmacol. Ther.*, vol. 159, pp. 110–119, Mar. 2016.

[45] S. Lega and M. C. Dubinsky, "What Are the Targets of Inflammatory Bowel Disease Management," *Inflamm. Bowel Dis.*, vol. 24, no. 8, pp. 1670–1675, Jul. 2018.

[46] G. Pineton de Chambrun, L. Peyrin-Biroulet, M. Lémann, and J.-F. Colombel, “Clinical implications of mucosal healing for the management of IBD,” *Nat. Rev. Gastroenterol. Hepatol.*, vol. 7, no. 1, pp. 15–29, Jan. 2010.

[47] L. Peyrin-Biroulet *et al.*, “Results from the 2nd Scientific Workshop of the ECCO (I): Impact of mucosal healing on the course of inflammatory bowel disease,” *J. Crohn’s Colitis*, vol. 5, no. 5, pp. 477–483, Oct. 2011.

[48] S. Zhang *et al.*, “An inflammation-targeting hydrogel for local drug delivery in inflammatory bowel disease,” *Sci. Transl. Med.*, vol. 7, no. 300, 2015.

[49] J. M. Rosiak and F. Yoshii, “Hydrogels and their medical applications,” *Nucl. Instruments Methods Phys. Res. Sect. B Beam Interact. with Mater. Atoms*, vol. 151, no. 1–4, pp. 56–64, May 1999.

[50] O. Jeon, C. Powell, S. M. Ahmed, and E. Alsberg, “Biodegradable, photocrosslinked alginate hydrogels with independently tailorable physical properties and cell adhesivity.,” *Tissue Eng. Part A*, vol. 16, no. 9, pp. 2915–25, Sep. 2010.

[51] B. Ozcelik, “Degradable hydrogel systems for biomedical applications,” *Biosynthetic Polym. Med. Appl.*, pp. 173–188, Jan. 2016.

[52] Y. Dahman, *Nanotechnology and functional materials for engineers*. .

[53] P. B. Malafaya, G. A. Silva, and R. L. Reis, “Natural–origin polymers as carriers and scaffolds for biomolecules and cell delivery in tissue engineering applications,” *Adv. Drug Deliv. Rev.*, vol. 59, no. 4–5, pp. 207–233, May 2007.

[54] F. T. Bosman and I. Stamenkovic, “Functional structure and composition of the extracellular matrix,” *J. Pathol.*, vol. 200, no. 4, pp. 423–428, Jul. 2003.

[55] J. L. Drury and D. J. Mooney, “Hydrogels for tissue engineering: scaffold design variables and applications,” *Biomaterials*, vol. 24, no. 24, pp. 4337–4351, Nov. 2003.

[56] F. Brandl, F. Sommer, and A. Goepferich, “Rational design of hydrogels for tissue engineering: Impact of physical factors on cell behavior,” *Biomaterials*, vol. 28, no. 2, pp. 134–146, Jan. 2007.

[57] D. Seliktar, “Designing Cell-Compatible Hydrogels for Biomedical Applications,” *Science (80-.).*, vol. 336, no. 6085, pp. 1124–1128, Jun. 2012.

[58] G. M. Beattie *et al.*, “A Novel Approach to Increase Human Islet Cell Mass While Preserving - Cell Function,” *Diabetes*, vol. 51, no. 12, pp. 3435–3439, Dec. 2002.

[59] J. W. Weisel and R. I. Litvinov, “Mechanisms of fibrin polymerization and clinical implications,” *Blood*, vol. 121, no. 10, pp. 1712–1719, Mar. 2013.

[60] U. Hersel, C. Dahmen, and H. Kessler, “RGD modified polymers: biomaterials for stimulated cell adhesion and beyond,” *Biomaterials*, vol. 24, no. 24, pp. 4385–4415, Nov. 2003.

[61] M. P. Lutolf, G. P. Raeber, A. H. Zisch, N. Tirelli, and J. A. Hubbell, “Cell-Responsive Synthetic Hydrogels,” *Adv. Mater.*, vol. 15, no. 11, pp. 888–892, Jun. 2003.

[62] K. Y. Lee and D. J. Mooney, “Alginate: Properties and biomedical applications,” *Prog. Polym. Sci.*, vol. 37, no. 1, pp. 106–126, Jan. 2012.

[63] M. George and T. E. Abraham, “Polyionic hydrocolloids for the intestinal delivery of protein drugs: Alginate and chitosan — a review,” *J. Control. Release*, vol. 114, no. 1, pp. 1–14, Aug. 2006.

[64] J. A. BURDICK and M. M. STEVENS, “Biomedical hydrogels,” *Biomater. Artif. Organs Tissue Eng.*, pp. 107–115, Jan. 2005.

[65] T. Jiang, B. Singh, Y.-J. Choi, T. Akaike, and C.-S. Cho, “Liver tissue engineering using functional marine biomaterials,” *Funct. Mar. Biomater.*, pp. 91–106, Jan. 2015.

[66] S. N. Pawar and K. J. Edgar, “Alginate derivatization: A review of chemistry, properties and applications,” *Biomaterials*, vol. 33, no. 11, pp. 3279–3305, Apr. 2012.

[67] J.-S. Yang, Y.-J. Xie, and W. He, “Research progress on chemical modification of alginate: A review,” *Carbohydr. Polym.*, vol. 84, no. 1, pp. 33–39, Feb. 2011.

[68] J. Sun *et al.*, “The development of cell-initiated degradable hydrogel based on methacrylated alginate applicable to multiple microfabrication technologies,” *J. Mater. Chem. B*, vol. 5, no. 40, pp. 8060–8069, Oct. 2017.

[69] D. E. Chickering and E. Mathiowitz, “Bioadhesive microspheres: I. A novel electrobalance-based method to study adhesive interactions between individual microspheres and intestinal mucosa,” *J. Control. Release*, vol. 34, no. 3, pp. 251–262, Jun. 1995.

[70] H. S. Ch’ng, H. Park, P. Kelly, and J. R. Robinson, “Bioadhesive polymers as platforms for oral controlled drug delivery II: synthesis and evaluation of some swelling, water-insoluble

bioadhesive polymers.," *J. Pharm. Sci.*, vol. 74, no. 4, pp. 399–405, Apr. 1985.
[71] J. L. Drury, R. G. Dennis, and D. J. Mooney, "The tensile properties of alginate hydrogels," *Biomaterials*, vol. 25, no. 16, pp. 3187–3199, Jul. 2004.
[72] Y. Suzuki *et al.*, "Evaluation of a novel alginate gel dressing: cytotoxicity to fibroblasts in vitro and foreign-body reaction in pig skin in vivo.," *J. Biomed. Mater. Res.*, vol. 39, no. 2, pp. 317–22, Feb. 1998.
[73] K. T. Nguyen and J. L. West, "Photopolymerizable hydrogels for tissue engineering applications," *Biomaterials*, vol. 23, no. 22, pp. 4307–4314, Nov. 2002.
[74] O. Jeon, K. H. Bouhadir, J. M. Mansour, and E. Alsberg, "Photocrosslinked alginate hydrogels with tunable biodegradation rates and mechanical properties," *Biomaterials*, vol. 30, no. 14, pp. 2724–2734, May 2009.
[75] A. I. Chou and S. B. Nicoll, "Characterization of photocrosslinked alginate hydrogels for nucleus pulposus cell encapsulation," *J. Biomed. Mater. Res. Part A*, vol. 91A, no. 1, pp. 187–194, Oct. 2009.
[76] J. P. Fisher, D. Dean, P. S. Engel, and A. G. Mikos, "Photoinitiated Polymerization of Biomaterials," *Annu. Rev. Mater. Res.*, vol. 31, no. 1, pp. 171–181, Aug. 2001.
[77] K. A. Smeds *et al.*, "Photocrosslinkable polysaccharides forin situ hydrogel formation," *J. Biomed. Mater. Res.*, vol. 55, no. 2, pp. 254–255, May 2001.
[78] R. H. Schmedlen, K. S. Masters, and J. L. West, "Photocrosslinkable polyvinyl alcohol hydrogels that can be modified with cell adhesion peptides for use in tissue engineering," *Biomaterials*, vol. 23, no. 22, pp. 4325–4332, Nov. 2002.
[79] J. L. Ifkovits and J. A. Burdick, "Review: Photopolymerizable and Degradable Biomaterials for Tissue Engineering Applications," *Tissue Eng.*, vol. 13, no. 10, pp. 2369–2385, Oct. 2007.
[80] P. Coimbra, D. Fernandes, P. Ferreira, M. H. Gil, and H. C. de Sousa, "Solubility of Irgacure® 2959 photoinitiator in supercritical carbon dioxide: Experimental determination and correlation," *J. Supercrit. Fluids*, vol. 45, no. 3, pp. 272–281, Jul. 2008.
[81] C. G. Williams, A. N. Malik, T. K. Kim, P. N. Manson, and J. H. Elisseeff, "Variable cytocompatibility of six cell lines with photoinitiators used for polymerizing hydrogels and cell encapsulation," *Biomaterials*, vol. 26, no. 11, pp. 1211–1218, Apr. 2005.
[82] J. Sun and H. Tan, "Alginate-Based Biomaterials for Regenerative Medicine Applications," *Materials (Basel).*, vol. 6, no. 4, pp. 1285–1309, Mar. 2013.
[83] K. B. Fonseca, S. J. Bidarra, M. J. Oliveira, P. L. Granja, and C. C. Barrias, "Molecularly designed alginate hydrogels susceptible to local proteolysis as three-dimensional cellular microenvironments," *Acta Biomater.*, vol. 7, no. 4, pp. 1674–1682, Apr. 2011.
[84] M. P. Lutolf, P. M. Gilbert, and H. M. Blau, "Designing materials to direct stem-cell fate," *Nature*, vol. 462, no. 7272, pp. 433–441, Nov. 2009.
[85] P. P. Lehenkari and M. A. Horton, "Single Integrin Molecule Adhesion Forces in Intact Cells Measured by Atomic Force Microscopy," *Biochem. Biophys. Res. Commun.*, vol. 259, no. 3, pp. 645–650, Jun. 1999.
[86] L. Y. Koo, D. J. Irvine, A. M. Mayes, D. A. Lauffenburger, and L. G. Griffith, "Co-regulation of cell adhesion by nanoscale RGD organization and mechanical stimulus.," *J. Cell Sci.*, vol. 115, no. Pt 7, pp. 1423–33, Apr. 2002.
[87] S. J. Bidarra, C. C. Barrias, K. B. Fonseca, M. A. Barbosa, R. A. Soares, and P. L. Granja, "Injectable in situ crosslinkable RGD-modified alginate matrix for endothelial cells delivery," *Biomaterials*, vol. 32, no. 31, pp. 7897–7904, Nov. 2011.
[88] M. Ø. Dalheim, J. Vanacker, M. A. Najmi, F. L. Aachmann, B. L. Strand, and B. E. Christensen, "Efficient functionalization of alginate biomaterials," *Biomaterials*, vol. 80, pp. 146–156, Feb. 2016.
[89] M. B. Evangelista *et al.*, "Upregulation of bone cell differentiation through immobilization within a synthetic extracellular matrix," *Biomaterials*, vol. 28, no. 25, pp. 3644–3655, 2007.
[90] A. Page-McCaw, A. J. Ewald, and Z. Werb, "Matrix metalloproteinases and the regulation of tissue remodelling," *Nat. Rev. Mol. Cell Biol.*, vol. 8, no. 3, pp. 221–233, Mar. 2007.
[91] R. F. Pereira, C. C. Barrias, P. J. Bártolo, and P. L. Granja, "Cell-instructive pectin hydrogels crosslinked via thiol-norbornene photo-click chemistry for skin tissue engineering," *Acta Biomater.*, vol. 66, pp. 282–293, Jan. 2018.
[92] S. Varghese and J. H. Elisseeff, "Hydrogels for Musculoskeletal Tissue Engineering," Springer, Berlin, Heidelberg, 2006, pp. 95–144.
[93] S. C. Neves, R. F. Pereira, M. Araújo, and C. C. Barrias, "Bioengineered peptide-functionalized

hydrogels for tissue regeneration and repair," *Pept. Proteins as Biomater. Tissue Regen. Repair*, pp. 101–125, Jan. 2018.

[94] C. E. Hoyle and C. N. Bowman, "Thiol-Ene Click Chemistry," *Angew. Chemie Int. Ed.*, vol. 49, no. 9, pp. 1540–1573, Feb. 2010.

[95] C. Desai, S. T. Koshy, S. A. Hilderbrand, D. J. Mooney, and N. S. Joshi, "Versatile Click Alginate Hydrogels Crosslinked via Tetrazine-norbornene Chemistry," *Biomaterials*, vol. 50, pp. 30–37, 2015.

[96] L. Liang and D. Astruc, "The copper(I)-catalyzed alkyne-azide cycloaddition (CuAAC) 'click' reaction and its applications. An overview," *Coord. Chem. Rev.*, vol. 255, no. 23–24, pp. 2933–2945, Dec. 2011.

[97] A. E. Rydholm, C. N. Bowman, and K. S. Anseth, "Degradable thiol-acrylate photopolymers: polymerization and degradation behavior of an in situ forming biomaterial," *Biomaterials*, vol. 26, no. 22, pp. 4495–4506, Aug. 2005.

[98] A. B. Lowe, "Thiol-ene 'click' reactions and recent applications in polymer and materials synthesis," *Polym. Chem.*, vol. 1, no. 1, pp. 17–36, Feb. 2010.

[99] K. Y. Lee, H. J. Kong, and D. J. Mooney, "Quantifying Interactions between Cell Receptors and Adhesion Ligand-Modified Polymers in Solution," *Macromol. Biosci.*, vol. 8, no. 2, pp. 140–145, Feb. 2008.

[100] D. P. Nair *et al.*, "The Thiol-Michael Addition Click Reaction: A Powerful and Widely Used Tool in Materials Chemistry," *Chem. Mater.*, vol. 26, no. 1, pp. 724–744, Jan. 2014.

[101] B. D. Fairbanks, M. P. Schwartz, A. E. Halevi, C. R. Nuttelman, C. N. Bowman, and K. S. Anseth, "A Versatile Synthetic Extracellular Matrix Mimic via Thiol-Norbornene Photopolymerization," *Adv. Mater.*, vol. 21, no. 48, pp. 5005–5010, Dec. 2009.

[102] B. D. Polizzotti, B. D. Fairbanks, and K. S. Anseth, "Three-Dimensional Biochemical Patterning of Click-Based Composite Hydrogels via Thiolene Photopolymerization," *Biomacromolecules*, vol. 9, no. 4, pp. 1084–1087, Apr. 2008.

[103] Z. Xu and K. M. Bratlie, "Click Chemistry and Material Selection for *in Situ* Fabrication of Hydrogels in Tissue Engineering Applications," *ACS Biomater. Sci. Eng.*, vol. 4, no. 7, pp. 2276–2291, Jul. 2018.

[104] Y. Zou *et al.*, "'Click' chemistry in polymeric scaffolds: Bioactive materials for tissue engineering," *J. Control. Release*, vol. 273, pp. 160–179, Mar. 2018.

[105] C. Qi, L.-H. Fu, H. Xu, T.-F. Wang, J. Lin, and P. Huang, "Melanin/polydopamine-based nanomaterials for biomedical applications," *Sci. China Chem.*, vol. 62, no. 2, pp. 162–188, Feb. 2019.

[106] J. M. Henson, M. J. Butler, and A. W. Day, "T HE D ARK S IDE OF THE M YCELIUM : Melanins of Phytopathogenic Fungi," *Annu. Rev. Phytopathol.*, vol. 37, no. 1, pp. 447–471, Sep. 1999.

[107] A. Casadevall, A. L. Rosas, and J. D. Nosanchuk, "Melanin and virulence in Cryptococcus neoformans.," *Curr. Opin. Microbiol.*, vol. 3, no. 4, pp. 354–8, Aug. 2000.

[108] M. d'Ischia, A. Napolitano, V. Ball, C.-T. Chen, and M. J. Buehler, "Polydopamine and Eumelanin: From Structure–Property Relationships to a Unified Tailoring Strategy," *Acc. Chem. Res.*, vol. 47, no. 12, pp. 3541–3550, Dec. 2014.

[109] A. Napolitano, L. Panzella, G. Monfrecola, and M. d'Ischia, "Pheomelanin-induced oxidative stress: bright and dark chemistry bridging red hair phenotype and melanoma," *Pigment Cell Melanoma Res.*, vol. 27, no. 5, pp. 721–733, Sep. 2014.

[110] J. D. Simon and D. N. Peles, "The Red and the Black," *Acc. Chem. Res.*, vol. 43, no. 11, pp. 1452–1460, Nov. 2010.

[111] C. D. Derby, "Cephalopod ink: production, chemistry, functions and applications.," *Mar. Drugs*, vol. 12, no. 5, pp. 2700–30, May 2014.

[112] S. Ito, "A Chemist's View of Melanogenesis," *Pigment Cell Res.*, vol. 16, no. 3, pp. 230–236, Jun. 2003.

[113] P. Meredith, B. J. Powell, J. Riesz, S. P. Nighswander-Rempel, M. R. Pederson, and E. G. Moore, "Towards structure–property–function relationships for eumelanin," *Soft Matter*, vol. 2, no. 1, pp. 37–44, Dec. 2006.

[114] M. Araujo, J. R. Xavier, C. D. Nunes, P. D. Vaz, and M. Humanes, "Marine sponge melanin: a new source of an old biopolymer," *Struct. Chem.*, vol. 23, no. 1, pp. 115–122, Feb. 2012.

[115] C. M. R. C. and and ‡,§ John D. Simon*, "Ultrastructural Organization of Eumelanin from Sepia officinalis Measured by Atomic Force Microscopy†," 2001.

[116] M. Araújo *et al.*, "Natural melanin: A potential pH-responsive drug release device," *Int. J.*

Pharm., vol. 469, no. 1, pp. 140–145, Jul. 2014.
[117] Y. Liu, K. Ai, and L. Lu, "Polydopamine and Its Derivative Materials: Synthesis and Promising Applications in Energy, Environmental, and Biomedical Fields," *Chem. Rev.*, vol. 114, no. 9, pp. 5057–5115, May 2014.
[118] N. F. della Vecchia *et al.*, "Artificial Biomelanin: Highly Light-Absorbing Nano-Sized Eumelanin by Biomimetic Synthesis in Chicken Egg White," *Biomacromolecules*, vol. 15, no. 10, pp. 3811–3816, Oct. 2014.
[119] P. Meredith and T. Sarna, "The physical and chemical properties of eumelanin," *Pigment Cell Res.*, vol. 19, no. 6, pp. 572–594, Dec. 2006.
[120] A. Lampel *et al.*, "Polymeric peptide pigments with sequence-encoded properties.," *Science*, vol. 356, no. 6342, pp. 1064–1068, Jun. 2017.
[121] M. d'Ischia *et al.*, "Melanins and melanogenesis: from pigment cells to human health and technological applications," *Pigment Cell Melanoma Res.*, vol. 28, no. 5, pp. 520–544, Sep. 2015.
[122] Y. Liu *et al.*, "Comprehensive Insights into the Multi-Antioxidative Mechanisms of Melanin Nanoparticles and Their Application To Protect Brain from Injury in Ischemic Stroke," *J. Am. Chem. Soc.*, vol. 139, no. 2, pp. 856–862, Jan. 2017.
[123] L. F. Burbulla *et al.*, "Dopamine oxidation mediates mitochondrial and lysosomal dysfunction in Parkinson's disease," *Science (80-.).*, vol. 357, no. 6357, pp. 1255–1261, Sep. 2017.
[124] K.-Y. Ju, Y. Lee, S. Lee, S. B. Park, and J.-K. Lee, "Bioinspired Polymerization of Dopamine to Generate Melanin-Like Nanoparticles Having an Excellent Free-Radical-Scavenging Property," *Biomacromolecules*, vol. 12, no. 3, pp. 625–632, Mar. 2011.
[125] L. Panzella *et al.*, "Atypical Structural and π-Electron Features of a Melanin Polymer That Lead to Superior Free-Radical-Scavenging Properties," *Angew. Chemie Int. Ed.*, vol. 52, no. 48, pp. 12684–12687, Nov. 2013.
[126] F. E. Barr, "Melanin: the organizing molecule.," *Med. Hypotheses*, vol. 11, no. 1, pp. 1–139, May 1983.
[127] D. L. Longo, R. Stefania, S. Aime, and A. Oraevsky, "Melanin-Based Contrast Agents for Biomedical Optoacoustic Imaging and Theranostic Applications," *Int. J. Mol. Sci.*, vol. 18, no. 8, p. 1719, Aug. 2017.
[128] Y. Liu, K. Ai, J. Liu, M. Deng, Y. He, and L. Lu, "Dopamine-Melanin Colloidal Nanospheres: An Efficient Near-Infrared Photothermal Therapeutic Agent for In Vivo Cancer Therapy," *Adv. Mater.*, vol. 25, no. 9, pp. 1353–1359, Mar. 2013.
[129] K.-Y. Ju, J. Kang, J. Pyo, J. Lim, J. H. Chang, and J.-K. Lee, "pH-Induced aggregated melanin nanoparticles for photoacoustic signal amplification," *Nanoscale*, vol. 8, no. 30, pp. 14448–14456, Jul. 2016.
[130] Y. Shi *et al.*, "Recent progress and development on polymeric nanomaterials for photothermal therapy: a brief overview," *J. Mater. Chem. B*, vol. 5, no. 2, pp. 194–206, Jan. 2017.
[131] S. Cho, W. Park, and D.-H. Kim, "Silica-Coated Metal Chelating-Melanin Nanoparticles as a Dual-Modal Contrast Enhancement Imaging and Therapeutic Agent," *ACS Appl. Mater. Interfaces*, vol. 9, no. 1, pp. 101–111, Jan. 2017.
[132] Q. Fan *et al.*, "Transferring Biomarker into Molecular Probe: Melanin Nanoparticle as a Naturally Active Platform for Multimodality Imaging," *J. Am. Chem. Soc.*, vol. 136, no. 43, pp. 15185–15194, Oct. 2014.
[133] S. H. Hong *et al.*, "Chelator-Free and Biocompatible Melanin Nanoplatform with Facile-Loading Gadolinium and Copper-64 for Bioimaging," *Bioconjug. Chem.*, vol. 28, no. 7, pp. 1925–1930, Jul. 2017.
[134] K.-Y. Ju *et al.*, "Bio-Inspired, Melanin-Like Nanoparticles as a Highly Efficient Contrast Agent for T_1 -Weighted Magnetic Resonance Imaging," *Biomacromolecules*, vol. 14, no. 10, pp. 3491–3497, Oct. 2013.
[135] X. Bao, J. Zhao, J. Sun, M. Hu, and X. Yang, "Polydopamine Nanoparticles as Efficient Scavengers for Reactive Oxygen Species in Periodontal Disease," *ACS Nano*, vol. 12, no. 9, pp. 8882–8892, Sep. 2018.
[136] M. Araújo, M. Miola, E. Bertone, G. Baldi, J. Perez, and E. Verné, "On the mechanism of apatite-induced precipitation on 45S5 glass pellets coated with a natural-derived polymer," *Appl. Surf. Sci.*, vol. 353, pp. 137–149, Oct. 2015.
[137] R. F. Pereira, A. Sousa, C. C. Barrias, P. J. Bártolo, and P. L. Granja, "A single-component hydrogel bioink for bioprinting of bioengineered 3D constructs for dermal tissue engineering,"

Mater. Horizons, vol. 5, no. 6, pp. 1100–1111, Oct. 2018.
[138] A. D. Rouillard *et al.*, "Methods for photocrosslinking alginate hydrogel scaffolds with high cell viability.," *Tissue Eng. Part C. Methods*, vol. 17, no. 2, pp. 173–9, Feb. 2011.
[139] S. Jana, A. Samanta, A. K. Nayak, K. K. Sen, and S. Jana, "Novel alginate hydrogel core–shell systems for combination delivery of ranitidine HCl and aceclofenac," *Int. J. Biol. Macromol.*, vol. 74, pp. 85–92, Mar. 2015.
[140] H.-Q. Yin, D.-S. Mai, F. Gan, and X.-J. Chen, "One-step synthesis of linear and cyclic RGD conjugated gold nanoparticles for tumour targeting and imaging," *RSC Adv.*, vol. 4, no. 18, p. 9078, Jan. 2014.
[141] M. Araujo, J. R. Xavier, C. D. Nunes, P. D. Vaz, and M. Humanes, "Marine sponge melanin: A new source of an old biopolymer," *Struct. Chem.*, vol. 23, no. 1, pp. 115–122, 2012.
[142] S. A. Centeno and J. Shamir, "Surface enhanced Raman scattering (SERS) and FTIR characterization of the sepia melanin pigment used in works of art," *J. Mol. Struct.*, vol. 873, no. 1–3, pp. 149–159, Feb. 2008.
[143] M. Araújo *et al.*, "Natural melanin: A potential pH-responsive drug release device," *Int. J. Pharm.*, vol. 469, no. 1, pp. 140–145, 2014.
[144] N. Huebsch *et al.*, "Harnessing traction-mediated manipulation of the cell/matrix interface to control stem-cell fate," *Nat. Mater.*, vol. 9, no. 6, pp. 518–526, Jun. 2010.
[145] A. Barth, "Infrared spectroscopy of proteins," *Biochim. Biophys. Acta - Bioenerg.*, vol. 1767, no. 9, pp. 1073–1101, Sep. 2007.
[146] P. W. Riddles, R. L. Blakeley, and B. Zerner, "[8] Reassessment of Ellman's reagent," *Methods Enzymol.*, vol. 91, pp. 49–60, Jan. 1983.
[147] "User Guide: Ellman's Reagent." [Online]. Available: https://www.thermofisher.com/document-connect/document-connect.html?url=https%3A%2F%2Fassets.thermofisher.com%2FTFS-Assets%2FLSG%2Fmanuals%2FMAN0011216_Ellmans_Reag_UG.pdf&title=VXNlciBHdWlkZTogIEVsbG1hbiZyc3F1bztzIFJlYWdlbnQ=. [Accessed: 14-Jun-2019].
[148] P. C. Eklund, O. K. Långvik, J. P. Wärnå, T. O. Salmi, S. M. Willför, and R. E. Sjöholm, "Chemical studies on antioxidant mechanisms and free radical scavenging properties of lignans," *Org. Biomol. Chem.*, vol. 3, no. 18, p. 3336, Sep. 2005.
[149] S. B. Kedare and R. P. Singh, "Genesis and development of DPPH method of antioxidant assay.," *J. Food Sci. Technol.*, vol. 48, no. 4, pp. 412–22, Aug. 2011.
[150] C. G. Kumar, P. Mongolla, S. Pombala, A. Kamle, and J. Joseph, "Physicochemical characterization and antioxidant activity of melanin from a novel strain of Aspergillus bridgeri ICTF-201," *Lett. Appl. Microbiol.*, vol. 53, no. 3, pp. 350–358, Sep. 2011.
[151] J. Teixeira, A. Gaspar, E. M. Garrido, J. Garrido, and F. Borges, "Hydroxycinnamic acid antioxidants: an electrochemical overview.," *Biomed Res. Int.*, vol. 2013, p. 251754, Jul. 2013.
[152] R. F. Pereira, C. C. Barrias, P. J. Bártolo, and P. L. Granja, "Cell-instructive pectin hydrogels crosslinked via thiol-norbornene photo-click chemistry for skin tissue engineering," *Acta Biomater.*, vol. 66, pp. 282–293, 2018.
[153] R. C. Ungaro and J.-F. Colombel, "Editorial: biologics in inflammatory bowel disease—time for direct comparisons," *Aliment. Pharmacol. Ther.*, vol. 46, no. 1, pp. 68–69, Jul. 2017.
[154] K. Bodger, "Cost Effectiveness of Treatments for Inflammatory Bowel Disease," *Pharmacoeconomics*, vol. 29, no. 5, pp. 387–401, May 2011.
[155] J. A. Rowley, G. Madlambayan, and D. J. Mooney, "Alginate hydrogels as synthetic extracellular matrix materials.," *Biomaterials*, vol. 20, no. 1, pp. 45–53, Jan. 1999.
[156] M. Ahearne, Y. Yang, and K.-K. Liu, "Mechanical Characterisation of Hydrogels for Tissue Engineering Applications Hydrogels for Tissue Engineering," 2008.
[157] †,‡,§ Kuen Yong Lee, † Jon A. Rowley, ‡ Petra Eiselt, ⊥ Erick M. Moy, †,‡,§ and Kamal H. Bouhadir, and †,‡,§ David J. Mooney*, "Controlling Mechanical and Swelling Properties of Alginate Hydrogels Independently by Cross-Linker Type and Cross-Linking Density," 2000.
[158] Y. Yang *et al.*, "Tissue-Integratable and Biocompatible Photogelation by the Imine Crosslinking Reaction," *Adv. Mater.*, vol. 28, no. 14, pp. 2724–2730, Apr. 2016.
[159] T. L. Riss *et al.*, *Cell Viability Assays*. Eli Lilly & Company and the National Center for Advancing Translational Sciences, 2004.
[160] "ROS Detection Assay Kit (DCFDA / H2DCFDA) Biotrend." [Online]. Available: https://www.biotrend.com/-186/ros-detection-assay-kit-dcfda-h2dcfda-681001185.html. [Accessed: 22-Jun-2019].

[161] F. Antunes, F. Andrade, F. Araújo, D. Ferreira, and B. Sarmento, “Establishment of a triple co-culture in vitro cell models to study intestinal absorption of peptide drugs,” *Eur. J. Pharm. Biopharm.*, vol. 83, no. 3, pp. 427–435, Apr. 2013.

[162] B. Catalgol, G. Özhan, and B. Alpertunga, “Acrylamide-induced oxidative stress in human erythrocytes,” *Hum. Exp. Toxicol.*, vol. 28, no. 10, pp. 611–617, Oct. 2009.